UNIVERSITA' DEGLI STUDI DI PARMA

Dottorato di ricerca in Scienza e Tecnologia dei Materiali Innovativi

Ciclo XXVII (2012-2014)

Phosphonate and quinoxaline cavitands for molecular recognition and sensing

Coordinatore:
Prof. Enrico Dalcanale

Tutor:
Prof. Enrico Dalcanale
Dr. Roberta Pinalli

Dottoranda
Tahnie BARBOZA

2016

Università degli studi di Parma
Parma, Italy

CONTENTS

Chapter 1

GENERAL INTRODUCTION

1.1 SUPRAMOLECULAR CHEMISTRY

As defined by Jean-Marie Lehn in 1988, supramolecular chemistry refers to *chemistry beyond the molecule*, and focuses on organized architectures made of several chemical entities, held together by intermolecular, weak interactions.[1] Mastering non-covalent forces is key requirement for the development of highly sophisticated supramolecular systems. The recognition of a substrate (guest) by a molecular receptor (host), is driven by a combination of shape complementarity and non-covalent forces, ranging from Van der Waals contacts to electrostatic interactions.

Cavitands, defined as synthetic organic compounds with enforced cavities of molecular dimensions, are particularly interesting and versatile molecular receptors.[2] Among molecular platforms suitable for the formation of cavitands, macrocycles, and especially resorcinarenes are substrates of choice, thanks to their synthetic versatility. Prepared by the condensation of resorcinol with an aldehyde (R-CHO) under acidic conditions,[3] they are constituted by four aromatic units, with eight OH groups forming the upper rim, and the R chain from the aldehyde, forming the lower rim. Reactions of the eight OH residues with bridging units leads to the formation of the cavitand. The bridging units at the upper rim will define the complexation properties of the receptor, through shape shape and dimensions of the resulting cavity, and the nature of the interactions with the guest.

1.1.1 PHOSPHONATE CAVITANDS

Phosphonate cavitands are a class of concave molecular receptors presenting one to four phosphonate moieties P=O at the upper rim of the cavity. P=O groups are known to be good H-Bond acceptor, and can make ion-dipole interactions with cationic species. Therefore, these receptors are prone to complex positively charged species, and H-bond donors.[4] The bridging of the phenolic hydroxyl of the resorcinarene with the phosphine reagent leads to the formation of $P^{(V)}$ stereocenters, which can have two possible configurations, namely *i* when the P=O moiety is pointing *inward* the

cavity, and *o* when pointing *outward*. In mixed-bridged diphosphonate cavitands, the relative positioning of the P=O moieties, namely vicinal or distal, is defined by respectively AB or AC configuration.[5]

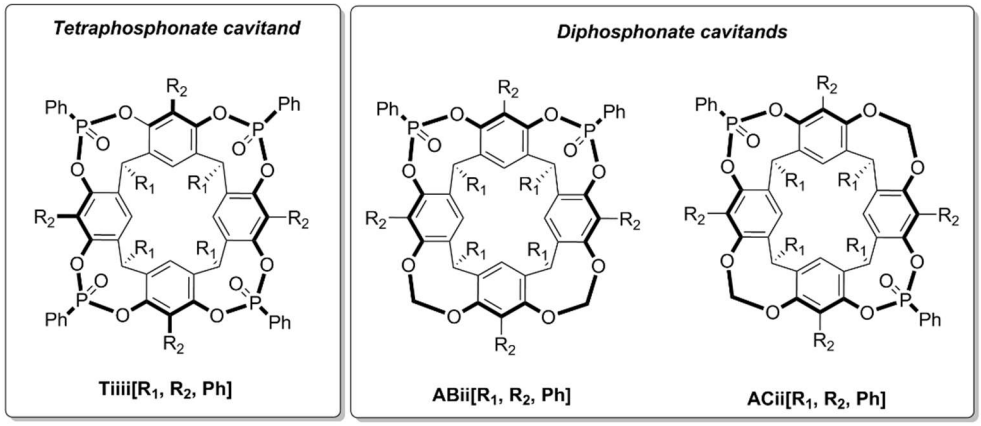

Scheme 1.2 – *General structures of the phosphonate cavitands used in this thesis. a) Tetraphosphonate cavitand Tiiii. b) diphosphonate cavitands ABii and ACii.*

The recognition features of the receptor are driven by the stereochemistry of the bridging units: maximizing the number of inward P=O enhances the recognition properties.[6,7] Indeed, the cavitand bearing four inward P=O moieties pointing inward the cavity, namely **Tiiii**, displayed outstanding complexation properties towards N-methyl ammonium salts, N-methyl-pyridinium salts, and short alkyl chain alcohols.[8] The recognition is mediated by a synergistic combination of weak interactions, namely H-bond between the P=O of the cavitand and the OH or NH residue of the guest, cation-dipole interactions between the P=O and the positively charged N^+ of the ammonium salts, and CH-π interaction with either the CH_3-N^+ of the ammonium or the terminal methyl of the short alkyl chain alcohol. NMR and ITC studies showed that at least two P=O moieties are necessary to provide the complexation properties.[9]

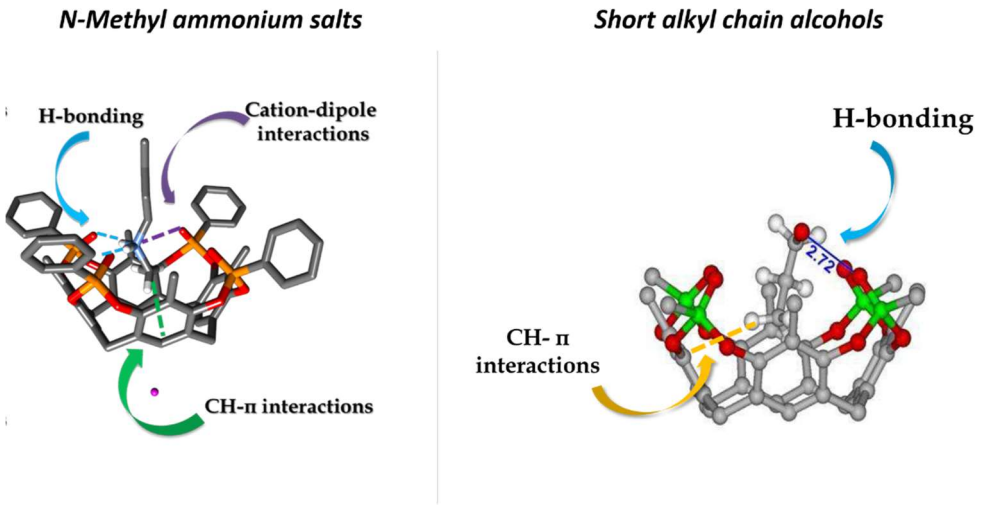

Figure 1.1 *– Complexation mode of Tiiii with a) N-Methyl butyl ammonium and b) n-propanol*

1.1.2 QUINOXALINE CAVITANDS

Tetraquinoxaline cavitands (QxCav) are prepared by reacting the phenolic OH residues of a resorcinarene with dichloroquinoxaline moieties.[10] The resulting cavitand presents a deep, hydrophobic, π-enriched cavity, thanks to the four aromatic quinoxaline units, which also confer a conformational freedom to the receptor. Indeed, quinoxaline walls can adopt an axial or an equatorial position with respect to the vertical axis of the molecule, leading to respectively *vase* and *kite* conformations.[11] In the *vase* conformation, the molecule presents a 7Å wide, 8Å deep, box-shaped cavity, opened at the top, and prone to the formation of inclusion complexes. In the *kite* conformation, the quinoxaline moieties in equatorial position are almost coplanar.

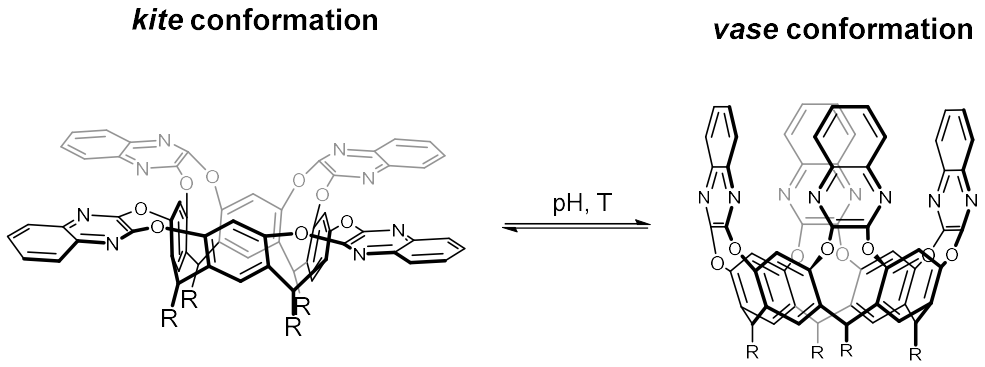

Scheme 1.3 *- General structure of QxCav in kite conformation (left) and vase conformation (right)*

The switch between the *vase* and *kite* conformations is driven by several parameters. The presence of a methyl in the apical position of the resorcinarene forces the *kite* conformation, due to the steric hindrance. Otherwise, *vase* and *kite* conformations are in equilibrium, which can be controlled by temperature[12] and pH.[13] QxCav are a promising class of synthetic receptors for the complexation of aromatic compounds. Solution and gas phase studies demonstrated the interesting complexation properties of QxCav towards aromatic hydrocarbons. The non-covalent complexation involved in the molecular recognition are mainly π-π stacking between the electron rich cavity and the aromatic guest, and CH-π interactions, at the solid state and in solution.[14] In particular, QxCav displayed exceptional affinity for the BTEX family (benzene, toluene, ethylbenzene, xylenes), an extremely important class of volatile organic compounds (VOCs) for air quality control.[13f]

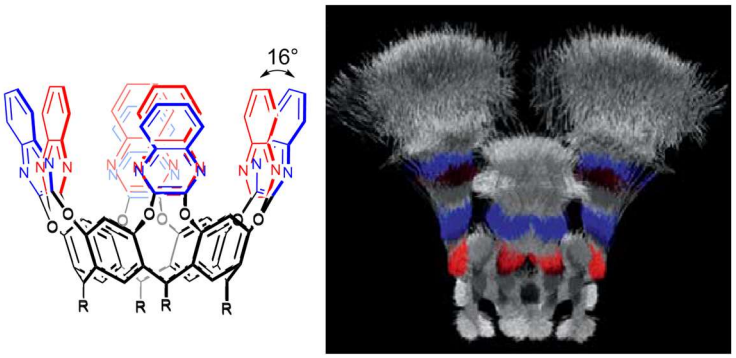

Figure 1.3 *– Left: Schematic representation of the quinoxaline moieties mobility in the solid state. Right: Overlays of 1000 structures of the vase forms of a QxCav derivative, sampled from molecular dynamics simulations.*

The mobility of the quinoxaline moieties was also investigated in the solid state. Indeed, molecular models realized by *Diedrich et al*. showed that the aromatic walls have an average opening angle of 16° with respect to the axis of the cavitand.[15] The dynamic behavior of the cavity is promoted by heating, and adversely impacts the molecular recognition properties: upon opening, the non-covalent forces driving the complexation are weakened by the increasing distance between the aromatic walls and the guest. To overcome this drawback, our group designed and synthesized new conformationnally blocked quinoxaline cavitands, reported in figure 4. The insertion of ethylenoxy bridges joining the quinoxaline walls, prevents the motion of the cavity, and therefore strengthens the weak interactions between the cavitand and its guests. The entrance of the cavity is also reduced, which was expected to increase the selectivity towards benzene by steric hindrance. EtQxBox and MeQxBox displayed better performances towards BTEX compounds, with respect to QxCav. SPME-GC experiments highlighted the exceptional performances of QxBox towards BTEX. A patent application has been deposited for these results.[16]

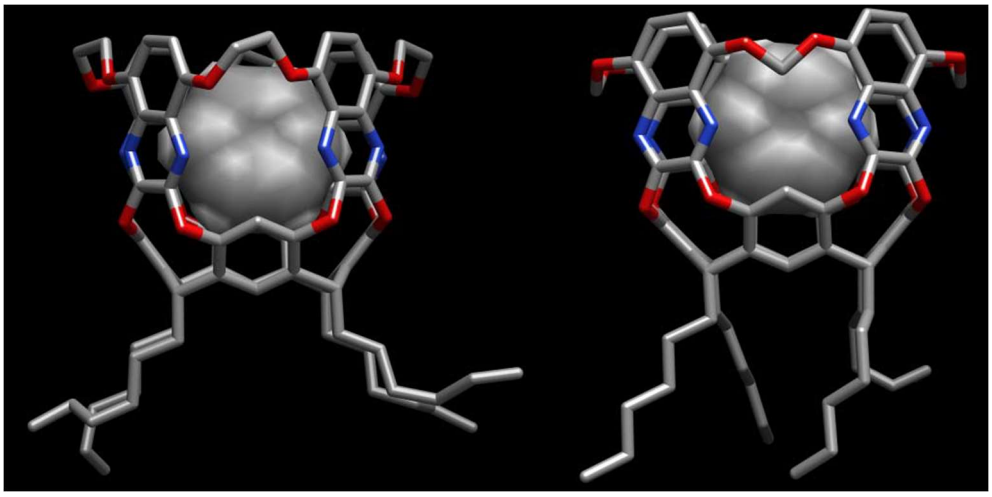

Figure 1.4 *– Molecular structures of EtQxBox@Benzene (left) and MeEtQxBox (right)*

1.2 SUPRAMOLECULAR RECEPTORS IN SENSING

1.2.1 SUPRAMOLECULAR SENSING

As defined by IUPAC, a chemical sensor is *a device that transforms a chemical information, ranging from the concentration of a specific sample component to total composition analysis, into an analytically useful signal*. The process of chemical sensing relies on the recognition of one or a set of relevant analytes. The choice of the sensing material, responsible of the recognition, is pivotal. Indeed, it must satisfy requirements of sensitivity, selectivity and reversibility. Furthermore, the sensitivity to interferents (low-cross sensitivity), must be minimized. In this context, supramolecular receptors offer remarkable features matching the sensing requests: the weak interactions driving the recognition allow a reversible process, while selectivity and sensitivity can be tuned by an appropriate design of the receptor. The design of selective receptors is mostly based on the Nature's *lock-and-key* approach:[17] the shape complementarity and the weak interactions leading to the specific molecular recognition event is a successful strategy in solution. However, sensing of gaseous analytes cannot be directly transferred from recognition in

solution. Indeed, upon host-guest complexation the entropic contribution of the solvent release is absent in the solid phase.[18] Moreover, non-specific interactions, negligible in solution, are dramatically increased in the solid-gas interface, and have a potential adverse effect on the recognition.[19]

1.2.2 PRECONCENTRATION PROCESS IN SENSING DEVICES

To face the growing threat of terrorism, human and drugs traffics, Police and custom services exploit the exceptional dogs' olfactory properties to detect illicit substances and hidden persons.[20,21,22] However, the use of dogs requires intensive training, and their limited operability time reduces the effectiveness of controls. In this context, the development of sniffing systems mimicking canine skills but overcoming their drawbacks appears a challenging matter. The DOGGIES project aims at developing an operational movable stand-alone sensor for an efficient detection of (i) hidden persons, (ii) drugs & (iii) explosives. The detection relies on the combination of two orthogonal physical methods, namely Ion Mobility Spectroscopy[23] (IMS) and Mid-Infrared/Photo Acoustic cell Spectroscopy (MIRPAS).[24] The three different classes of VOCs substances, namely volatile fatty acids for hidden persons, safrole and derivatives for drugs precursors, and volatile nitroaromatics for explosives, are present in air at trace levels, and must be collected, concentrated and revealed. In order to decrease the limit of detection of the device, the target VOCs require a preconcentration step which rely on high flow rate sampling of a large volume of air into the functionalized preconcentration cartridge, which adsorbs the target chemicals. After sampling, a heat pulse applied to the cartridge allows the desorption of the chemicals into a much smaller volume of carrier gas, thus increasing the concentration of the sample.

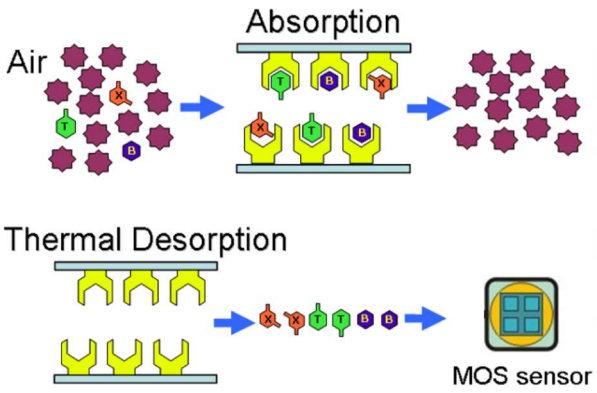

Figure 1.5 *– Schematic pre-concentration process.*

At the laboratory scale, one analytical technique for probing the preconcentration is the Solid Phase Micro-extraction.[25] Coupled with an analytical system, typically GC-MS, this technique allows to extract and concentrate volatile compounds at trace level. The SPME support is a fiber made in fused silica and coated with a stationary phase (sorbent material, either a polymer or a molecular receptor) of which the extraction capacity is investigated.

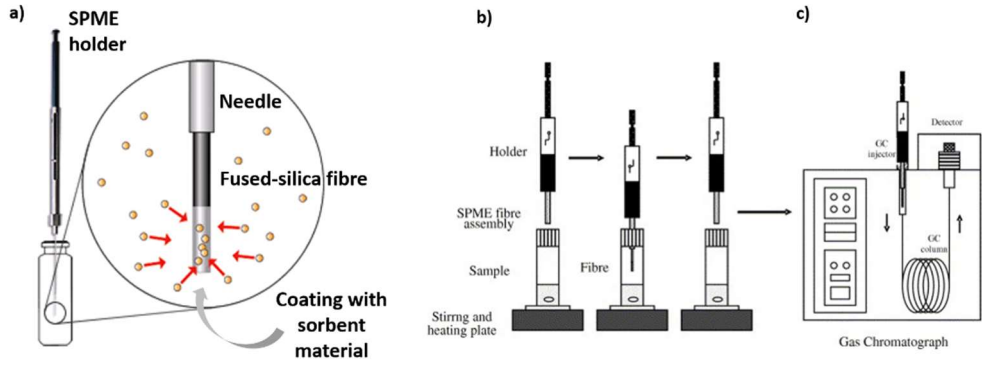

Figure 1.6 *– Schematic setup of SPME-GC experiment. a) Adsorption process; b) Headspace adsorption setup; c) GC desorption.*

This fast and simple analytical method allows to identify and quantify volatile compounds at very low concentrations, with very low limit of detection (ppt). Using

molecular receptors as stationary phase, this technique characterizes the extraction properties of the receptor, and consequently its selectivity towards one or a class of analytes. Our group successfully exploited this technique to evaluate the recognition properties of our cavitands at the solid-gas interface.[26] In sensing devices, the preconcentration can be achieved by the use of functionalized MEMs preconcentrators. In collaboration with Dr. S. Zampolli (CNR Bologna, Italy), our group developed a stand-alone mini GC device, based on the QxCav recognition properties, for the monitoring of BTEX in air. The key components of the sensing device are the preconcentration unit, and the miniaturized GC column. The preconcentrator is a silicon MEMs cartridge, filled with raw powder of the QxCav. The receptor being selective for BTEX but not benzene, the GC column separates the analytes, for further identification by photoionisation (PID) or MOX (metal oxide) detectors.

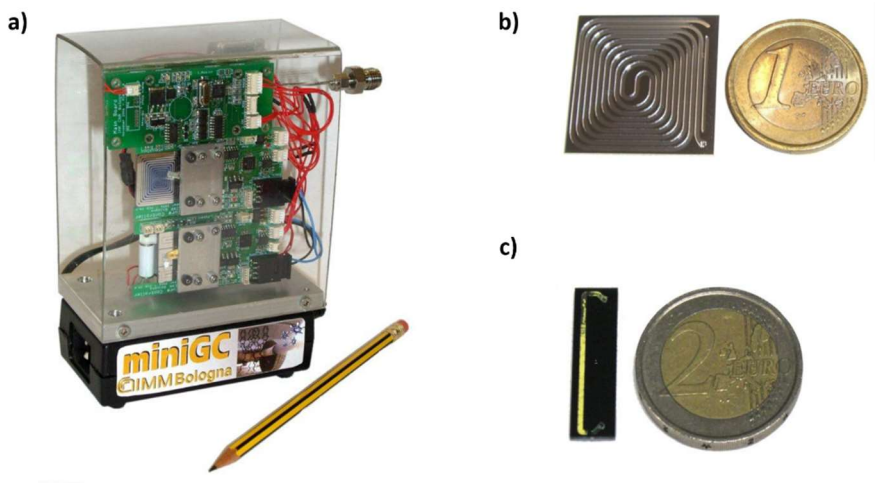

Figure 1.7 *– stand-alone mini GC device, a) full device, b) miniaturized GC column, c) preconcentration cartridge.*

1.3 REFERENCES

[1] J.M. Lehn, *Angew. Chem. Int. Ed. Engl*. **1988**, 27, 89-112.

[2] a) D. J. Cram, *Science*, **1983**, *219*, 1177–1183. b) D. J. Cram, J. M. Cram, *Container Molecules and Their Guests.* (ED.:J. F. Stoddart), The Royal Society of Chemistry, Cambridge, **1994**, Chapter 5.

[3] a) A. G. S. Hogberg, *J. Org. Chem*. **1980**, *45*, 4498–4500. b) A. G. S. Hogberg, *J. Am. Chem. Soc.* **1980**, *102*, 6046–6050.

[4] B. Bibal, B. Tinant, J.-P. Declercq and J.-P. Dutasta, *Chem. Commun. (Camb).* **2002**, *6*, 432-433. b) P. Delangle, J.-C. Mulatier, B. Tinant, J.-P Declercq, J.-P. Dutasta, *Eur. J. Org. Chem*. **2001**, 3695-3704; c) J.-P. Dutasta, *Top. Curr. Chem*. **2004**, *232*, 55-91.

[5] R. Pinalli, M. Suman, E. Dalcanale, *Eur. J. Org. Chem.* **2004**, 451-462

[6] R. Pinalli, F. F. Nachtigall, F. Ugozzoli, E. Dalcanale, *Angew. Chemie Int. Ed.* **1999**, *38*, 2377–2380.

[7] M. Melegari, M. Suman, L. Pirondini, D. Moiani, C. Massera, F. Ugozzoli, E. Kalenius, P. Vainiotalo, J. Mulatier, J. Dutasta and E. Dalcanale, *Chem. Eur. J.* **2008**, *14*, 5772–5779.

[8] E. Biavardi, M. Favazza, A. Motta, I. L. Fragalà, C. Massera, L. Prodi, M. Montalti, M. Melegari, G. C. Condorelli, E. Dalcanale, *J. Am. Chem. Soc*. **2009**, *131*, 7447-7455.

[9] D. Menozzi, R. Pinalli, C. Massera, F. Maffei and E. Dalcanale, *Molecules*, **2015**, *20*, 4460–4472.

[10] a) J. R. Moran, S. Karbach, D. J. Cram, *J. Am. Chem. Soc*. **1982**, *104*, 5826-5828; b) J. A. Bryant, J. L. Ericson, D. J. Cram, *J. Am. Chem. Soc.* **1990**, *112*, 1255-1256;

c) D. J. Cram, H. J. Choi, J. A. Bryant, C. B. Knobler, *J. Am. Chem. Soc*. **1992**, *114*, 7748-7765.

[11] P. Roncucci, L. Pirondini, G. Paderni, C. Massera, E. Dalcanale, V. A. Azov and F. Diederich, *Chem. Eur. J.* **2006**, *12*, 4775–4784.

[12] V. A. Azov, B. Jaun, F. Diederich, *Helv. Chim. Acta,* **2004**, *87*, 449- 462.

[13] P. J. Skinner, A. G. Cheetham, A. Beeby, V. Gramlich, F. Diederich, *Helv. Chim. Acta,* **2001**, *84*, 2146-2153.

[14] a) D. J. Cram, S. Karbach, H. E. Kim, C. B. Knobler, E. F. Maverick, J. L. Ericson, R. C. Helgeson, *J. Am. Chem. Soc.* **1988**, *110*, 2229-2237; b) J. A. Tucker, C. B. Knobler, K. N. Trueblood, D. J. Cram, *J. Am. Chem. Soc.* **1989**, *111*, 3688-3689; d) J. R. Moran, J. L. Ericson, E. Dalcanale, J. A. Bryant, C. B. Knobler and D. J. Cram, *J. Am. Chem. Soc*. **1991**, *113*, 5707-5714; e) P. Soncini, S. Bonsignore, E. Dalcanale and F. Ugozzoli, *J. Org. Chem*., **1992**, *57*, 4608-4612; f) F. Bianchi, R. Pinalli, F. Ugozzoli, S. Spera, M. Careri and E. Dalcanale, *New J. Chem.,* **2003**, *27*, 502–509; g) P. Clément, S. Korom, C. Struzzi, E. J. Parra, C. Bittencourt, P. Ballester and E. Llobet, *Adv. Funct. Mater.* **2015**, *25*, 4011–4020.

[15] L. D. Shirtcliff, H. Xu and F. Diederich, *Eur. J. Org. Chem*. **2010**, 846–855.

[16] J. W. Trzcinski, F. Bianchi, R. Pinalli, C. Massera, E. Dalcanale, Patent EP2924041, September 30th, 2015.

[17] E. Fischer, *Ber. Dtsch. Chem. Ges*. **1894**, 27, 2985-2993.

[18] J. Janata, *Principles of Chemical Sensors*, Plenum press, New York, USA, **1989.**

[19] J.W. Grate, G.C. Frye, *Sensors Update*, **1996**, Vol. 2, 37-83.

[20] H. Kalmus, *Anim. Behav*. **1953**, 3, 25-31.

[21] P. G. Hepper, *Perception*, **1988**, 17, 549-554

[22] G. A. A. Schoon, J. C. De Bruin, *Forensic Sci. Int*. **1994**, 69, 111-118.

[23] a) Y. A. Zolotov, *J. Anal. Chem.* **2006**, *61*, 519–519; b) A. B. Kanu, P. Dwivedi, M. Tam, L. Matz and H. H. Hill, *J. Mass Spectrom*. **2008**, *43*, 1–22.

[24]a) A. G. Bell, *Philos. Mag. J. Sci.*, 1881, **11**, 510–530; b) F. J. M. Harren, G. Cotti, J. Oomens and L. Hekkert, *Encycl. Anal. Chem.* **2000**, 2203–2226.

[25] a) V. N. Zaitsev and M. F. Zui, *J. Anal. Chem.* **2014**, *69*, 715–727. b) A. Spietelun, M. Pilarczyk, A. Kloskowski and J. Namieśnik, *Chem. Soc. Rev.* **2010**, *39*, 4524-4537. c) G. Vas and K. Vékey, *J. Mass Spectrom*. **2004**, 39, 233–254.

[26] F. Bianchi, M. Mattarozzi, P. Betti, F. Bisceglie, M. Careri, A. Mangia, L. Sidisky, S. Ongarato, E. Dalcanale, *Anal. Chem,* **2008**, *80*, 6423-6430.

Chapter 2

ENANTIOSELECTIVE RECOGNITION WITH AN INHERENTLY CHIRAL CAVITAND[1]

This chapter reports the design and the synthesis of a new, inherently chiral receptor, based on a mixed-bridges phosphonate cavitand. Three different bridging units, namely phosphonate, thiophosphonate and methylene bridges have been introduced, in AABC configuration. The enantioselectivity was explored for both chiral alcohol 2-butanol, and enantiopure N-methyl-leucine. After resolution of the racemic mixture, the enantiopure cR cavitand afforded crystals of the diastereomeric complex by co-crystallization with a racemic mixture of 2-butanol. The single crystal X-ray diffraction analysis provides insights on the stereodifferentiation, revealing that the cR-cavitand hosts enantioselectively the R-2-butanol. Used as a racemate, the receptors displayed complete enantioselectivity towards N-methyl-L-leucine in the solid state and partial enantioselectivity in solution.

[1]Part of this work has been submitted for publication to *Chem. Comm.:* "Enantioselective discrimination of 2-butanol by an inh erently chiral cavitand" by C. Nicosia, T. Barboza, R. Pinalli, G. Brancatelli, L. Guy, J. P. Dutasta, S. Geremia and E. Dalcanale.

2.1 INTRODUCTION

Discrimination of enantiomers plays a key role in many biological processes, involving chiral biomolecules. The design of artificial chiral receptors capable of enantioselective recognition constitutes a major challenge, regarding its potential applications in chiral separation[1,2], enantioselective sensing[3,4,5], or asymmetric catalysis[6,7]. For this purpose, concave macrocycles like calixarenes and resorcinarenes have emerged as a popular class of receptors, due to their rigid, highly tunable cavity scaffold[8,9,10]. As defined by Zhang, Izatt and Bradshow, the ideal enantioselective receptor forms stable complexes with the guest, and presents a high chiral barrier, enhanced by structural complementarity between the host and the congruent guest[11]. The typical way to introduce chirality is to include a stereogenic center close to the binding site. An alternative approach is to induce inherent chirality. Inherent chirality arises from the introduction of a curvature in an ideal planar structure that is devoid of a perpendicular symmetry plan in its bidimensional representation[12]. Applied to C_4-symmetry scaffolds, this strategy requires to use at least three different bridging units at the upper rim, namely A, B and C, and arrange them in a non-symmetric pattern (AABC)[13]. Combined with the curvature of the cavity, this structure deprives the receptor of its symmetry plan.

Several examples of inherently chiral calixarenes and resorcinarenes were reported[14,15]. Dutasta *et al.* introduced a series of inherently chiral phosphonate cavitands[16] in which two vicinal P=O groups confer the complexation properties, and are combined with one or two additional bridging units in AAB(C) configuration, to promote the inherent chirality. One of these cavitands, bearing two P=O bridges, one methylene bridge and one free position with two OH left unreacted, showed interesting enantioselectivity towards pseudoephedrine in solution[17]. In this context, we designed and synthesized a new, inherently chiral phosphonate cavitand, with mixed bridges, in AABC configuration, reported in scheme 1. The cavitand presents two P=O groups, one P=S moiety and one methylene bridge. The introduction of a

methylene bridge rigidifies the cavity, and increases the difference in shape between the left and the right-handed enantiomers.

Phosphonate cavitands have high affinity for short alkyl chains alcohols and *N*-methyl ammonium salts[18],[19]. The non-covalent interactions involved in the complexation are hydrogen bonding and CH-π interactions. Furthermore, in the case of *N*-methyl ammonium cations, a cation-dipole interaction (P=O···N^+) strengthens the recognition. Only two P=O units are necessary to promote the complexation of *N*-methyl-ammonium ions, as already demonstrated by Dalcanale *et al*.[20]

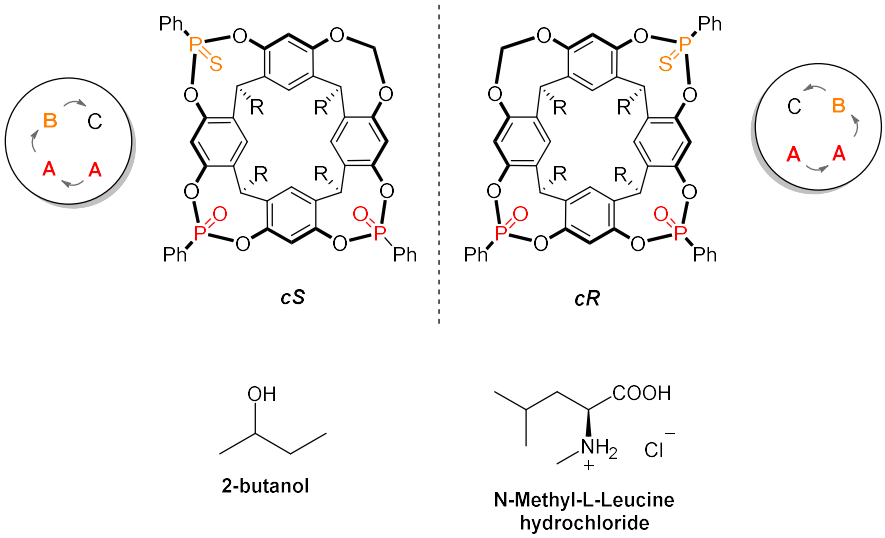

Scheme 2.1 *– Structures of the inherently chiral cavitands* ***cR*** *and* ***cS****. (R = C_2H_5), 2-butanol and N-Methyl-Leucine hydrochloride.*

N-methyl amino acids are another interesting class of chiral molecules, worth exploring[21]. In this framework, we studied the enantioselectivity of our cavitand towards (D/L)-*N*-methyl-leucine, in the solid state and in solution.

2.2 SYNTHESIS

The synthesis of racemic **cS** and **cR** cavitands was achieved in four steps starting from resorcinarene **1**, already reported in literature.[22] Reaction of **1** with $PPhCl_2$ and S_8 affords cavitand **2**, with all P=S bridged oriented inward the cavity.

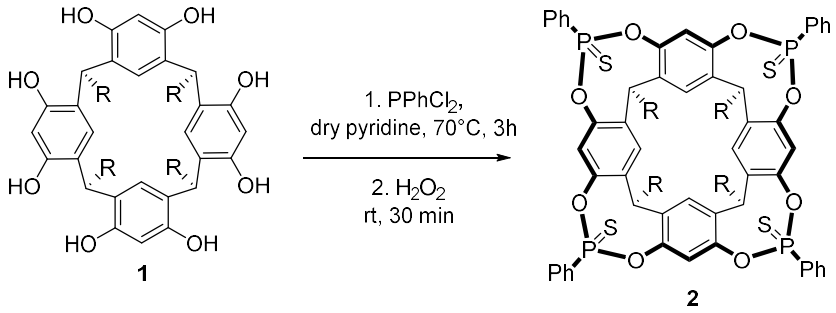

Scheme 2.2 *– Synthesis of tetrathiophosphonate cavitand **2**. (R = C_2H_5)*

One P=S bridge is selectively excised by a stoichiometric amount of catechol affording the trithiophosphonate resorcinarene **3**.[23]

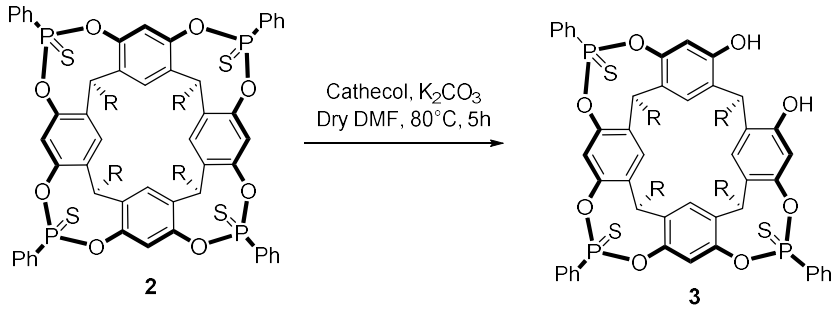

Scheme 2.3 *– Synthesis of trithiophosphonate resorcinarene **3**. (R = C_2H_5)*

Further reaction of the generated free OHs with CH_2BrCl leads to the introduction of the methylene bridge in cavitand **4**.

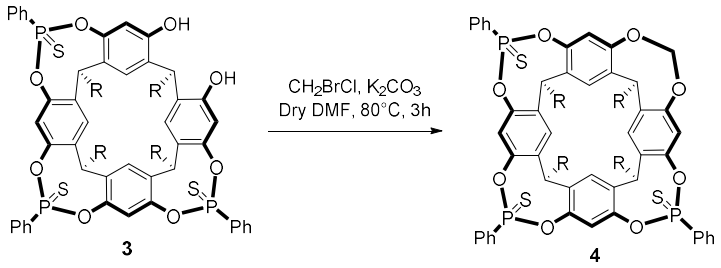

Scheme 2.4 *– Synthesis of cavitand **4**. (R = C_2H_5)*

The last step consists in introducing the chirality by reacting **4** with 2.5 eq of m-chloroperbenzoic acid (m-CPBA). During this reaction, the exchange P=S/P=O, leads to the formation of the racemic mixture **cR/cS** in AABC configuration, and its achiral isomer in ABAC configuration (cavitand **5**). The configuration of the phosphorous is retained. Compounds resulting from only one P=S/P=O exchange were reacted again with m-CPBA. The racemic mixture was characterized by ^{1}H and ^{31}P NMR.

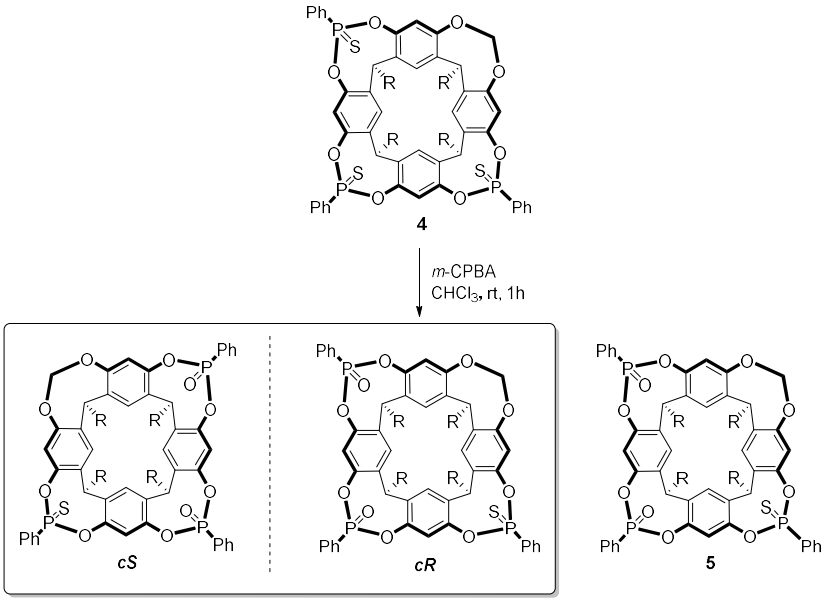

Scheme 2.5 *– Synthesis of the racemic mixture **cR/cS** and achiral cavitand **5** (R = C_2H_5).*

The ^{31}P NMR analysis shows the presence of two singlets at 8.69 and 8.60 ppm corresponding to the phosphorous groups, which are chemically different due to the chirality. The ^{1}H NMR spectrum shows four different signals for the apical protons at 7.04, 6.84, 6.80 and 6.68 ppm.

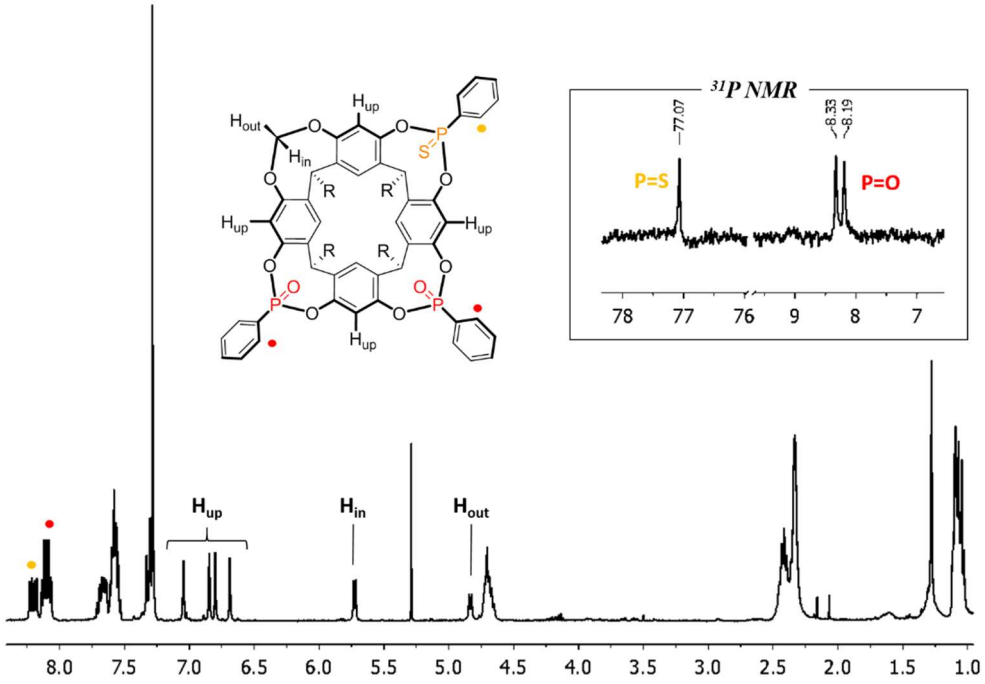

Figure 2.1** – ^{1}H NMR and ^{31}P NMR spectra of racemic **cR/cS

2.3 CHIRAL SEPARATION

The racemic mixture of cavitands **cR** and **cS** (figure 2.2) was separated by semi-preparative chiral HPLC Chiralpak IC, using CH_3CN/Acetone/H_2O (8:2:2) as eluent in isocratic conditions. As observed in figure 2.2, the two isomers are well separated, and it was possible to perform several cycle of purification, while maintaining a good solubility. The first enantiomer was eluted at 7.50 min, while the second one was eluted at 9.75 min. The enantiopurity of the two fractions was controlled by circular dichroism (figure 2.3): the main mirrored Cotton effects observed at 233, 250, and

265 nm, confirmed the enantiomeric relationship and the enantiopurity of the two fractions. The attribution of the absolute configurations was deduced from the X-ray molecular structures described in paragraph 4.

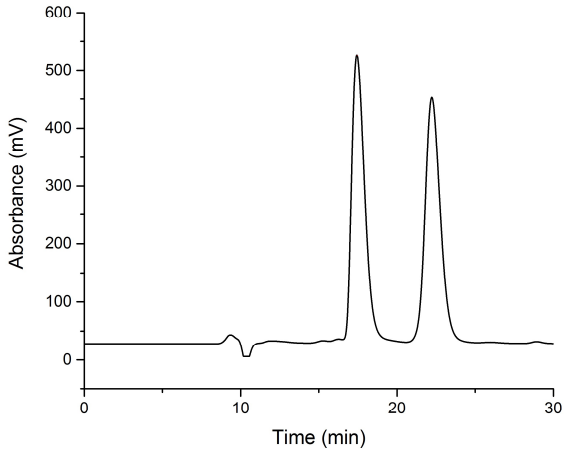

Figure 2.2 *– Chromatogram of the chiral resolution performed by semi-preparative HPLC. First peak:* ***cS****; second peak:* ***cR****.*

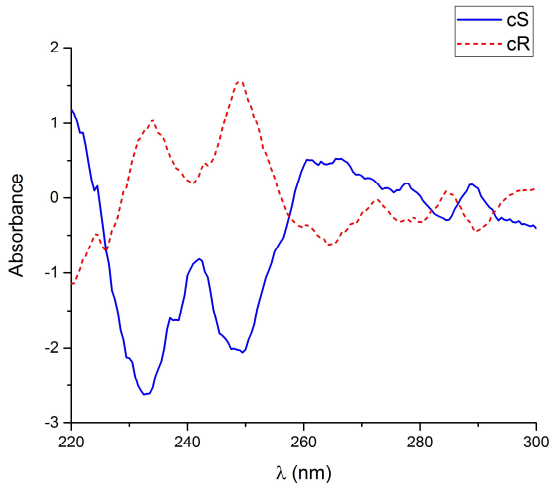

Figure 2.3 *– Circular dichroism spectra of* ***cR*** *and* ***cS*** *in CH_3CN.*

2.4 RECOGNITION OF 2-BUTANOL IN THE SOLID STATE

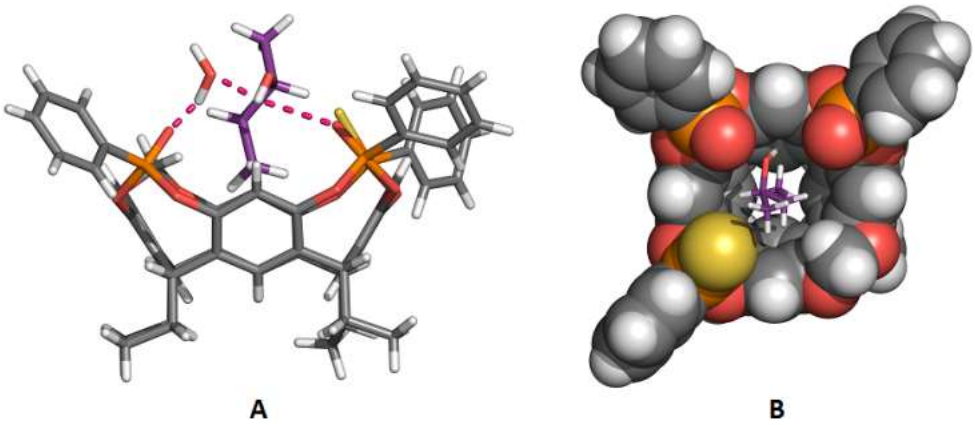

Figure 2.4 *– Side (A) and top (B) view of the molecular structure of the complex* ***cR@2-(R)-butanol****. Hydrogen bonds are represented as red dotted lines.*

The co-crystallization experiment of the **cR** cavitand with 2-(±)-butanol, performed by slow solvent evaporation method, lead to the formation of crystals of the diastereoisomeric complex reported in figure 2.4, namely **cR@2-(R)-butanol**, demonstrating that the enantiopure receptor successfully discriminated the two enantiomers of 2-butanol in the solid state. The guest is included with its ethyl moiety inside the cavity, which maximizes the Van der Waals interactions with the aromatic walls. **2-(R)-butanol** interacts with the cavitand forming a H-bond between the OH group and the P=O moiety at the upper rim [OH···O=P 2.685(8) Å], and a CH-π interaction between the terminal methyl group and the π-basic aromatic cavity. A further weak H-bond is observed between the chiral CH group of the butanol and the P=S moiety (CH···S=P 3.47(1) Å).

The **2-(R)-butanol** guest shows the ethyl group oriented towards the interior of the cavity (Figure 2.5) as already observed also in the crystallographic model of the analogue complex with the achiral **Tiiii[H, CH_3, CH_3]** cavitand.[24] The degree of penetration of the guest in both complexes is slightly different: in the **cR@2-(R)-**

butanol complex the terminal methyl group is placed at -1.29(1) Å below the mean plane defined by the two oxygen and the sulfur atoms (OOSp), with distances from the centroids of the aromatic rings in the range 3.74(1)−3.965(9) Å, whereas in the ***n*-BuOH@Tiiii[H, CH_3, CH_3]** complex the terminal methyl group is found at -1.43(1) Å below the mean plane defined by the four oxygen atoms (OOp), with distances from the centroids of the aromatic rings in the range 3.47(1)−3.87(1) Å.

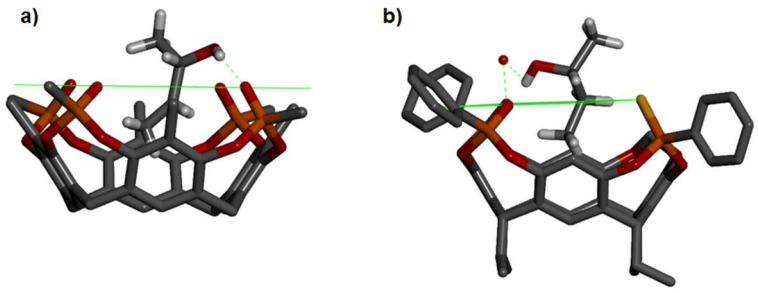

***Figure 2.5** - Orientations of the guests in cavity for a)**n-BuOH@Tiiii[H, CH_3, CH_3]** and b) **cR@2-(R)-butanol** cavitands.*

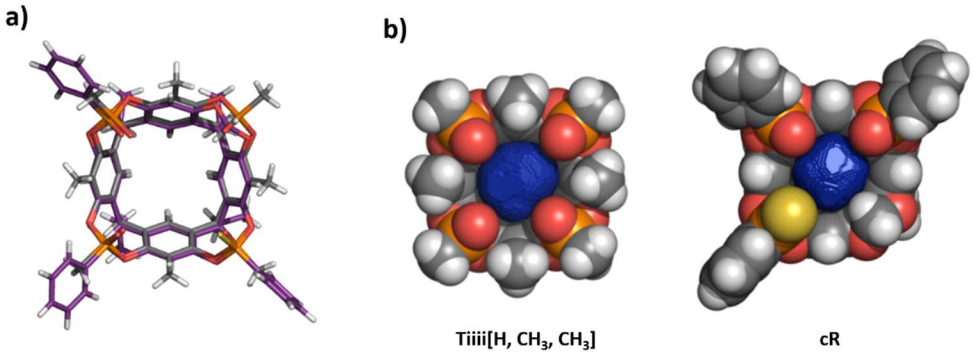

***Figure 2.6** – a) Superimposition of the achiral **Tiiii[H, CH_3, CH_3]** (carbon atoms depicted in grey) and chiral **cR** (carbon atoms depicted in violet) cavitands. b) Surfaces of the void volume available inside the cavity of the achiral **Tiiii[H, CH_3, CH_3]** and chiral **cR** cavitands.*

Furthermore a water molecule, placed on a crystallographic two-fold symmetry axis, contributes to the stabilization of the complex, as shown in figure 5, by acting as a

bridge between the OH group of the guest and an adjacent P=O unit of the host ($OH_{R\text{-}2\text{-}BuOH}\cdots O_{water}$ 2.163(8) Å, $OH_{water}\cdots O{=}P$ 2.135(7) Å). At the upper rim of the **cR** cavitand the presence of a P=S unit, with the bulky sulfur atom pointing towards the inner cavity, is partially compensated by the small methylene bridge (replacing a P=O unit). In fact, the comparison between the chiral thio-derivative and the symmetric **Tiiii[H, CH_3, CH_3]** cavitand shows that these substitutions do not significantly affect the cavity space available for the guest inclusion. This is evidenced in figure 2.6a where the overlapping of the crystallographic models of **Tiiii[H, CH_3, CH_3]** and **cR** are shown. Indeed, calculations[25] revealed a void volume of 49.1 $Å^3$ for the asymmetric **cR** (figure 2.6b) cavitand only slightly smaller than the volume of 53.0 $Å^3$ calculated for the symmetrical **Tiiii[H, CH_3, CH_3]** cavitand (figure 2.6a).

The complexation ability of **cR** and **cS** toward 2-butanol in solution could not be assessed, since no shift of the host P=O signal or the guest proton signals could be observed in solution, even in low dielectric solvents like benzene and hexane.

The discrimination of the two enantiomers of 2-butanol in the solid state is particularly relevant because of their low degree of chirality as evaluated by the "Continous Chirality Measure" developed by Avnir *et al*.[26] This method computes the distance between the actual object and its corresponding nearest achiral object. The computed degree of chirality can assume a value ranging from 0 for an achiral molecule to 100. For example, the amino acid ***N*-methyl-L-Leucine** has a degree of chirality of 8.84 while the **2-butanol** has a calculated value of only 1.9.[27] These numbers suggest that it should be much more problematic to develop a receptor system able to selectively discriminate one of the two enantiomers of **2-butanol** than the corresponding pair of the amino acid ***N*-methyl-L-Leucine**. Considering the low chirality degree of 2-butanol, **cR** demonstrated a remarkable ability to discriminate enantiomers. In this context, another class of chiral guests, e.g. *N*-methyl amino acids, were used to explore the enantioselective behavior of our chiral cavitand.

2.5 RECOGNITION OF N-METHYL AMINO ACIDS

2.5.1 IN THE SOLID STATE

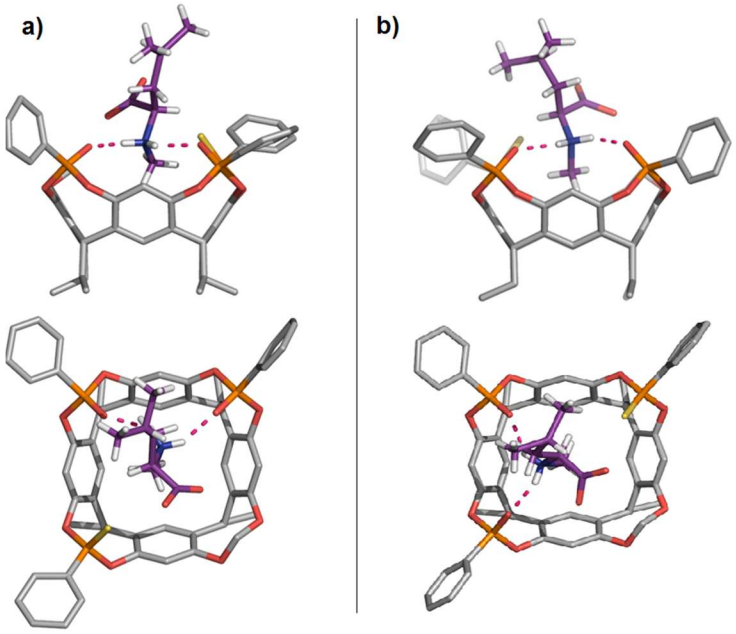

***Figure 2.7** – X-ray molecular structures of the complexes a) **cR@N-methyl-D-Leucine** (top: front view, bottom: top view) and b) **cS@N-methyl-D-Leucine** (top: front view, bottom: top view).*

Co-crystallization of the racemic cavitand with the racemic *N*-methyl-leucine was obtained by sitting drop tehcnnique. In the solid state, two diastereomeric complexes, namely **cR@*N*-methyl-D-Leu** and **cS@*N*-methyl-D-Leu**, were obtained in a unique crystal cell. In the two diastereoisomeric complexes, the non-covalent interactions are the same, namely: i) two hydrogen bonds between the phosphonate moieties of the cavitand and the ammonium protons, ii) cation-dipole interactions between the phosphonate moieties and the positively charged nitrogen of the ammonium, and iii), CH-π interaction between the π-basic cavity of the receptor and the *N*-methyl unit. The lateral chain of the amino acid is pointing outward the cavity. The observed enantioselectivity is due to the shape complementarity between one receptor and its congruent guest. Indeed, the P=S moiety creates a steric hindrance

between the receptor and the incongruent guest, which does not fit correctly in the cavity, leading to its discrimination.

2.5.2 ENANTIOSELECTIVE RECOGNITION IN SOLUTION

The enantioselectivity of the cavitand was investigated in solution through ^{1}H and ^{31}P NMR experiments. The racemic mixture of the cavitand dissolved in deuterated chloroform, was titrated with enantiopure ***N*-Me-L-leucine hydrochloride**, as a solid. The experiments were performed at 253 K in order to observe the system in slow exchange conditions. ***N*-Me-L-leucine** is not soluble in chlorinated solvents. However, upon complexation, the complex resulted fully soluble in $CDCl_3$. Indeed, the cavitand acts a solid-liquid extractant.

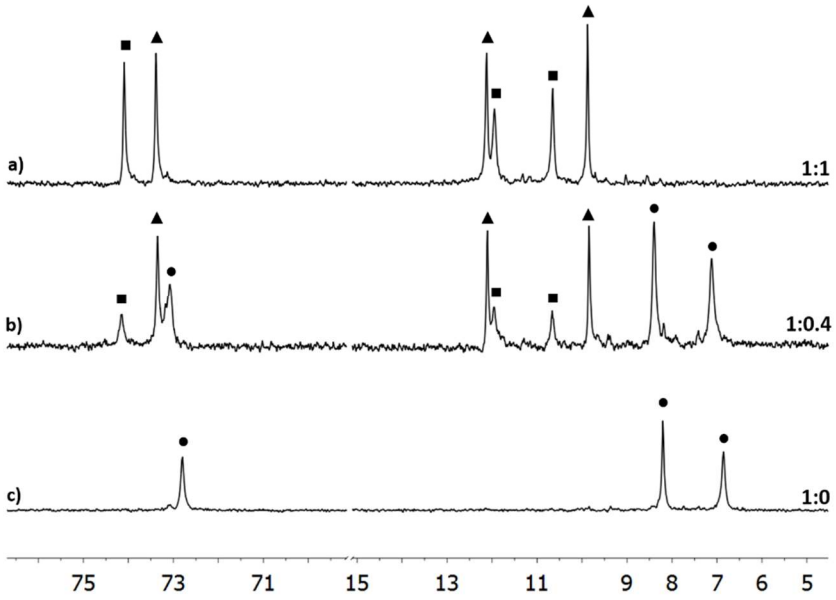

***Figure 2.8** – ^{31}P NMR titration of racemic cavitand with N-Me-L-leucine at 253K (● free cavitand, ▲ favored complex, ■ disfavored complex). a) Racemic cavitand; b) 1:0.4 host guest ratio; c)1:1 host-guest ratio.*

Upon addition of the guest, at 1:0.4 host-guest ratio, the P=O signals of the free host were still visible (8.40, 7.11 ppm), and two new sets of signals appeared, corresponding to the formation of two diastereoisomeric complexes, one favored, as

highlighted by the biggest shift of the P=O signals (12.10, 9.83 ppm) and one disfavoured, being the P=O signals less shifted (11.96, 10.85 ppm). Signals of the P=S group (72.79 ppm) follow the same splitting pattern, with one signal for the favored complex (73.35 ppm) and one for the disfavored complex (74.15 ppm). At 1:0.4 host-guest ratio, the P=O integrals indicate a 2.5:1 diastereoisomeric ratio. When one equivalent of guest is added, signals of the free host disappear, and the diastereoismeric ratio changes to 1:1.

At ^{1}H NMR, the inclusion of the guest in the cavity is monitored by the upfield shift of the N^{+}-**CH_3** at negative ppm, due to the shielding effect of the aromatic cavity.

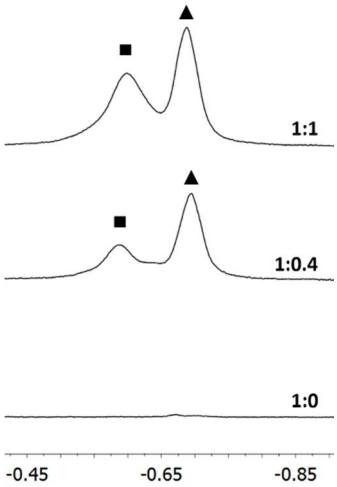

Figure 2.9 *– ^{1}H NMR titration of the racemic cavitand with **N-Me-L-Leu**. Host/guest ratios: a) host only; b) 1:0.4; c) 1:1; ■ disfavoured complex; ▲ favoured complex.*

The formation of two diastereoisomeric complexes is confirmed by the presence of two peaks at –0.69 ppm and –0.60 ppm, respectively for favored and disfavored complex. The higher upfied shift of the favored complex is a clear indication of the enantioselective properties of the cavitand. This position of the guest in the cavity is consistent with the results obtained at the solid state. In solution, the lateral chain of the amino acid is pointing outward, so this partial enantioselectivity can be extended

to all amino acids. In excess of the receptor, the guest accommodates better one enantiomer. The selective complexation of *N*-Me-L-leucine by one enantiomer is due to the steric repulsion between the guest and the mismatched receptor. Considering the results obtained in the solid state, it is expected that the favored cavitand is **cS**, and the mismatched one is **cR**. However, at 1:1 host guest ratio, the P=O···N^+ interaction overwhelms the steric repulsion, so the full complexation of the guest by both enantiomers leads to the saturation of the cavities, causing the disappearance of the free host signals, and the increase of the disfavored complex, up to 1:1 diastereisomeric ratio.

2.6 CONCLUSIONS

In summary, we synthesized a new, inherently chiral phosphonate cavitand, for the enantioselective recognition of *N*-methyl-amino acids and **2-butanol**. The racemic mixture was optically resolved by semi-preparative chiral HPLC, and characterized by circular dichroism. In the solid state, X-ray crystal structures demonstrated full enantioselectivity towards both ***N*-methyl-leucine** and **2-butanol**. Regarding amino-acids, the position of the guest in the receptor, with the lateral chain pointing outwards the cavity, as highlighted by solid state studies, makes the recognition indifferent to the nature of the amino-acid substituent. In solution, partial enantioselectivity was observed for ***N*-methyl leucine** in excess of the cavitand receptor. Upon addition of stoichiometric amount of the guest, the enantioselectivity is lost, due to the high affinity of the receptor for the *N*-methyl-ammonium ions. Overall, **cR** and **cS** cavitands are outstanding chiral receptors for the enantioselective discrimination of chiral alcohols and *N*-methyl amino acids upon crystallization.

2.7 ACKNOWLEDGMENTS.

Special thanks to Dr. Francesca Maffei for her contribution in the project, to Dr. Laure Guy and Prof. Jean-Pierre Dutasta (ENS Lyon, France) for the chiral

separation, to Dr. Giavanna Brancatelli and Prof. Silvano Geremia for the solid state studies.

2.8 REFERENCES

[1] V. Schurig, *J. Chromatogr. A,* **2002**, *965*, 315-356.

[2] W. H. Pirkle; T. C. Pochapsky, *Chem. Rev.* **1989**, *89*, 347-632.

[3] M. Trojanowicz, *Electrochem. Commun.* **2014**, *38*, 47-52

[4] M. P. Tiwari, A. Prasad, *Anal. Chim. Acta,* **2015,** *853*, 1-18.

[5] K.-X. Xu, P.-F. Cheng, J. Zhao; C.-J Wang, *J. Fluoresc.* **2011**, *21*, 991-1000.

[6] S. Kobayashi, Y. Yamashita, *Acc. Chem. Res.* **2011**, *44*, 58-71.

[7] L. Zheng, L.; S. Sonzini, M. Ambarwati, E. Rosta, O. Scherman; A. Herrmann, *Angew. Chem. Int. Ed.,* **2015,** *54***,** 13007-13011.

[8] S. Cherenok, J.-P. Dutasta, V. Kalchenko, *Curr. Org. Chem.,* **2006**, *10*, 2307-2331.

[9] A. D'Urso, A, C. Tudisco, F. P. Ballistreri, G. G. Condorelli, R. Randazzo, G. Tomaselli, R. M. Toscano, G. Trusso Sfrazzetto; A. Pappalardo, *Chem. Commun.* **2014**, *50*, 4993-4996.

[10] S. Liu, Y. He, G. Qing, K. Xu, H. Qin, *Tetrahedron Asymmetry,* **2005**, *16*, 1527-1534.

[11] X. X. Zhang, J. S. Bradshaw, R. M. Izatt, *Chem. Rev.* **1997**, *97*, 3312-3362.

[12] A. Szumna. *Chem. Soc. Rev.* **2010**, *39*, 4274-4285.

[13] A Dalla Cort, L. Mandolini, C. Pasquini, L. Schiaffino, *New J. Chem.* **2004**, *28*, 1198-1199.

[14] S. Y. Li, Y. W. Xu, J. M. Liu, C. Y. Su, *Int. J. Mol. Sci.* **2011**, *12*, 429-455.

[15] A. Asadi, D. Ajami, J. Rebek, *Chem. Sci.* **2013**, *4*, 1212-1215.

[16] J. Vachon, S. Harthong, B. Dubessy, J. P. Dutasta, N. Vanthuyne, C. Roussel, J.-V. Naubron, *Tetrahedron: Asymmetry,* **2010**, *21*, 1534-1541.

[17] J. Vachon, S. Harthong, E. Jeanneau, C. Aronica, N. Vanthuyne, C. Roussel, J.-P. Dutasta, *Org. Biomol. Chem.,* **2011**, *9*, 5086-5091.

[18] R. Pinalli, E. Dalcanale, *Acc. Chem. Res.* **2013**, *46*, 399-411.

[19] E. Biavardi, C. Tudisco, F. Maffei, A. Motta, C. Massera; G. G. Condorelli, E. Dalcanale, *Proc. Natl. Acad. Sci.* **2012**, *109*, 2263-2268.

[20] D. Menozzi, R. Pinalli, C. Massera, F. Maffei, E. Dalcanale, *Molecules,* **2015**, *20*, 4460-4472.

[21] a) L. Aurelio, R. T. C. Brownlee and A. B. Hughes, *Chem. Rev.* **2004**, *104*, 5823–5846; b) J. D. Bain, D. A. Wacker, E. E. Kuo and A. R. Chamberlin, *Tetrahedron*, **1991**, *47*, 2389–2400. c) J. Ellman, D. Mendel and P. Schultz, *Science*, **1992**, *255*, 197–200. d) C. Merryman and R. Green, *Chem. Biol.* **2004**, *11*, 575–582.

[22] L. M. Tunstad, J. A. Tucker, E. Dalcanale, J. Weiser, J. A. Bryant, J. C. Sherman, R. C. Helgeson, C. B. Knobler and D. J. Cram, *J. Org. Chem.* **1989**, *54*, 1305–1312.

[23] B. Cantadori, P. Betti, F. Boccini, C. Massera and E. Dalcanale, *Supramol. Chem.* **2008**, *20*, 29–34.

[24] R. De Zorzi, G. Brancatelli, M. Melegari, R. Pinalli, E. Dalcanale and S. Geremia, *CrystEngComm,* **2014**, *16*, 10987-10996.

[25] G. J. Kleywegt and T. A. Jones, *Acta Crystallogr.* **1994**, *D50*, 178−185.

[26] C. Dryzun, A. Zait, and D. Avnir, *J. Computation. Chem.* **2011**, *32*, 2526-2538; b) A. Zayit, M. Pinsky, H. Elgavi, C. Dryzun and D. Avnir, *Chirality*, **2011**, *23*, 17-23.

Chapter 3

MOLECULAR RECOGNITION OF L-LACTIC ACID WITH PHOSPHONATE CAVITANDS[1]

*A tetraphosphonate cavitand (**Tiiii**), and two diphosphonate cavitands (**ABii** and **ACii**), were probed for the molecular recognition of L-Lactic acid. In solution, ^{1}H and ^{31}P NMR studies showed that the three receptors form inclusion complexes with L-Lactic acid. The interactions involved in the recognition event are hydrogen bonding and CH-π interactions. The number and position of the phosphonate units at the upper rim of the cavitands regulates the affinity towards the guest. In the solid state, crystals obtained from inclusion complexes with **ABii** and **ACii** confirmed the results obtained in solution. **ABii** exhibited the stronger affinity for L-Lactic acid.*

[1] The content of this work has been submitted in : T. Barboza, R. Pinalli, C. Massera and E. Dalcanale*, *CrystEngComm,* submitted*: Di-phosphonate cavitands as molecular cups for L-lactic acid.*

3.1 INTRODUCTION

2-Hydroxypropanoic acid, better known as lactic acid, is a chemical commodity currently employed in several industrial processes, produced via bacterial fermentation. It is an additive (E270) used in food industry as preservative, flavouring agent and decontaminant in meat processing;[1] it also appears in formulations for detergents, soap, cosmetics and pharmaceutical products.[2] Moreover, once condensed into the cyclic diester lactide, it is the monomer of the biodegradable polymer poly lactic acid (PLA).[3] Its biologically relevant enantiomer, namely the dextrorotatory (S)-(+)-lactic acid (L-Lactic acid), is formed in blood and muscle tissues following the anaerobic metabolism of glucose. Its detection in biological fluids such as sweat and blood is presently based on electrochemical biosensors, using lactate oxidase to provide chemical selectivity.[4] The alternative approach of a synthetic receptor for lactic acid detection is still unexplored. In this paper, we report the binding properties of three isomeric di-phosphonate cavitands, namely **Tiiii[C_3H_7, CH_3, Ph], ABii[C_3H_7, CH_3, Ph]** and **ACii[C_3H_7, CH_3, Ph]** (Scheme 1), toward L-lactic acid in solution and in the solid state.

Phosphonate cavitands are a well-known class of synthetic receptors,[5] whose molecular recognition properties have been widely exploited for supramolecular sensing.[6] They are characterized by a pre-organized π-basic cavity, suitable for CH-π interactions, and a variable number of P=O groups at the upper rim, acting as H-bond acceptors. Their selectivity toward C_1-C_4 linear alcohols[7] stems from the simultaneous presence of both interaction modes. We reasoned that lactic acid, comprising a methyl group and two hydroxyl moieties, is a perfect analyte for this family of organic hosts since it has two H-bond donors flanked by a methyl group. So far, none of the studies that have been reported on the detection of lactic acid in recent years,[8] is based on host-guest supramolecular interactions.

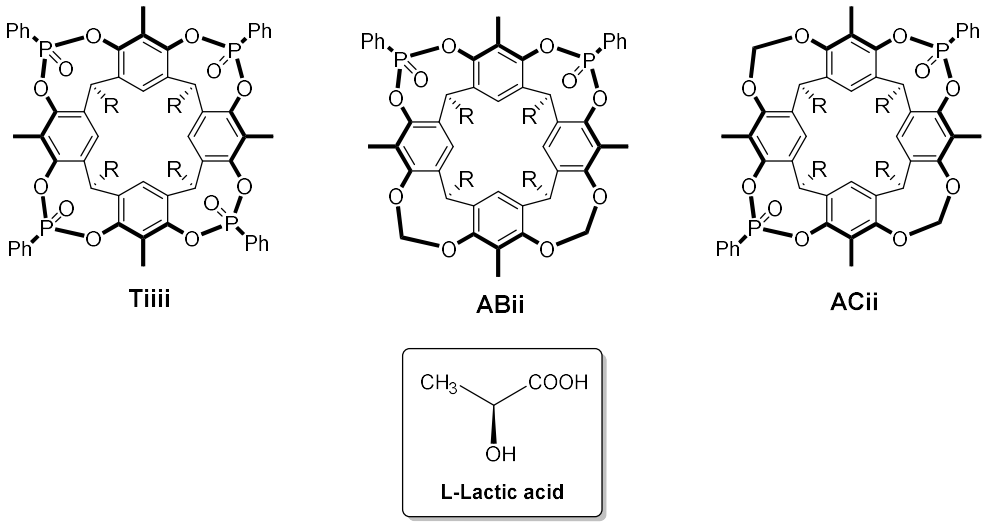

Scheme 3.1 *- Chemical structures of a) L-lactic acid, and b) Phosphonate cavitands* ***Tiiii[C_3H_7, CH_3, Ph], ABii[C_3H_7, CH_3, Ph]*** *and* ***ACii[C_3H_7, CH_3, Ph]*** *cavitands.*

3.2 SYNTHESIS

Tiiii[C_3H_7, CH_3, Ph] was prepared from the corresponding resorcinarene **Res[C_3H_7, CH_3]** by bridging it with $PPhCl_2$, followed by oxidation *in situ* with H_2O_2, (Scheme 3.2). The reaction is totally stereoselective, both in the bridging and oxidation steps.[5]

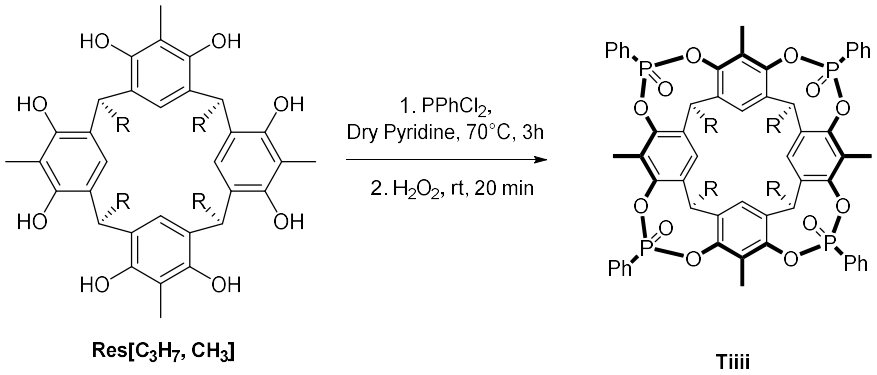

Scheme 3.2 *– synthesis of* ***Tiiii[C_3H_7, CH_3, Ph]***

The synthesis of **ABii[C_3H_7, CH_3, Ph]**[7a] starts from the same resorcinarene, which is reacted with CH_2BrCl under basic conditions. The reactions yields a mixture of partially bridged resorcinarenes, namely 3MeRes, **(AB)2MeRes**, and 1MeRes. **(AB)2MeRes** is reacted with $PPhCl_2$ and H_2O_2, under the same conditions described above (Scheme 3.3). **ABii** was obtained in 27% yield, after column chromatography purification.

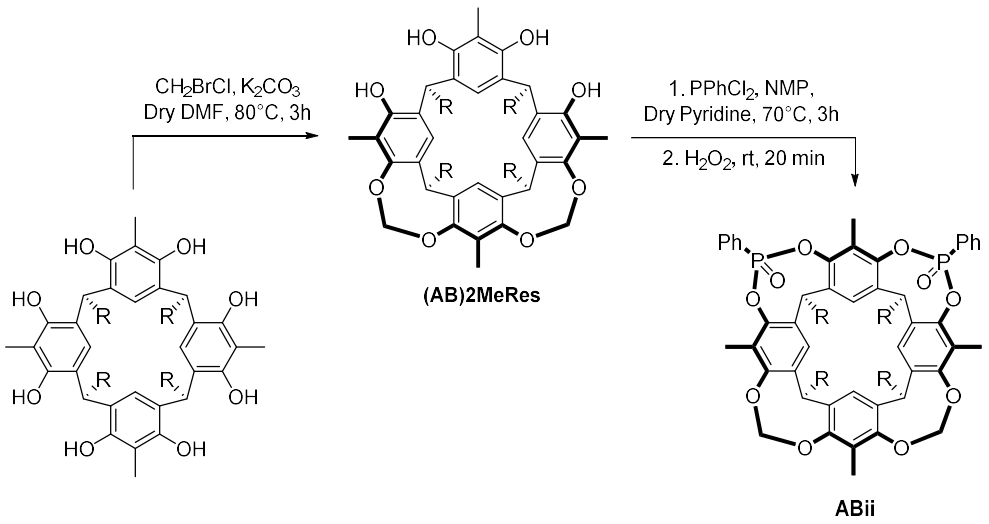

Scheme 3.3** – Synthesis of **ABii[C_3H_7, CH_3, Ph]

The synthesis of **ACii[C_3H_7, CH_3, Ph]** follows a different approach, because **AC2Me** could not be isolated in the synthetic scheme shown above. The synthesis of **ACii** starts from the corresponding **Tiiii** cavitand. Two P=O units are excised by addition of 2.5 eq of catechol under basic conditions.[7a] The reaction with catechol leads exclusively to the formation of the **(AC)iiRes** isomer, because the presence of the free OH enriches the aromatic cavity, and lessens the reactivity of the vicinal position. The free OH are then reacted with CH_2BrCl to obtain **ACii** in a quantitative yield.

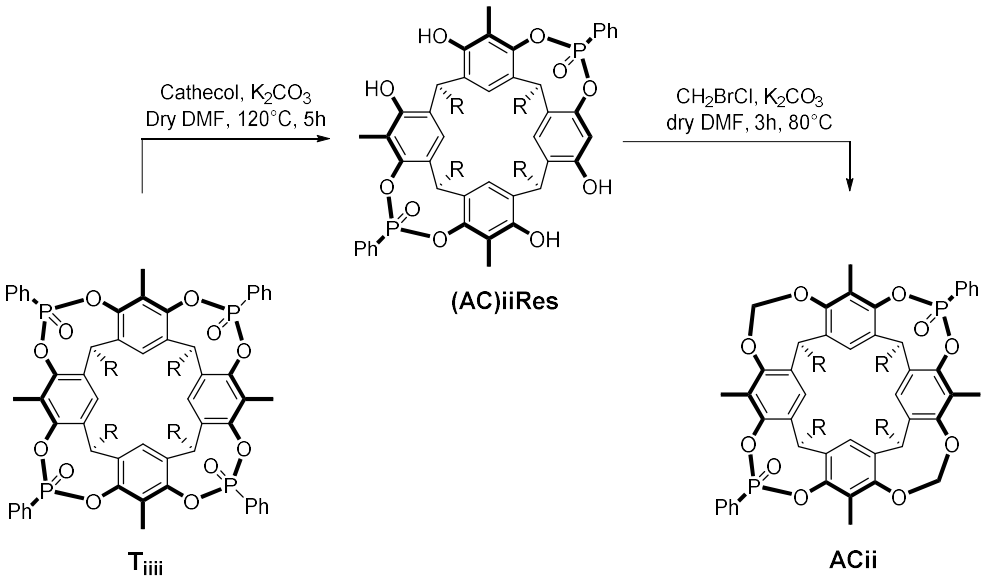

Scheme 3.4** – Two steps synthesis of **ACii[C_3H_7, CH_3, Ph]

3.3 COMPLEXATION OF L-LACTIC ACID IN SOLUTION

The complexation of L-Lactic acid by **Tiiii**, **ABii** and **ACii** was investigated in solution by means of ^{1}H and ^{31}P NMR. Due to its poor solubility in chlorinated solvents, L-lactic acid (**LLA**) was first dissolved in deuterated acetone prior to the addition to the cavitand solution. In the ^{31}P NMR spectra, the affinity of the guest for the cavitands is reflected by the shift of the phosphorous signal, since the complex is in fast exchange with respect to the NMR time scale. At 1:1 host-guest ratio, the phosphorous signal is shifted of 1.08, 1.69 ppm and 1.67 ppm respectively for **ACii**, **ABii** and **Tiiii**. These results clearly indicate that L-lactic acid is complexed by all three cavitands, with a preference for **ABii** and **Tiiii**, which display a larger chemical shift. In the case of **ABii**, the initial phosphorous singlet is split into two signals (Figure 3.1). This splitting is maintained in the NMR tube heated to 328 K, a clear indication that the splitting is not due to slow exchange in the ^{31}P NMR.

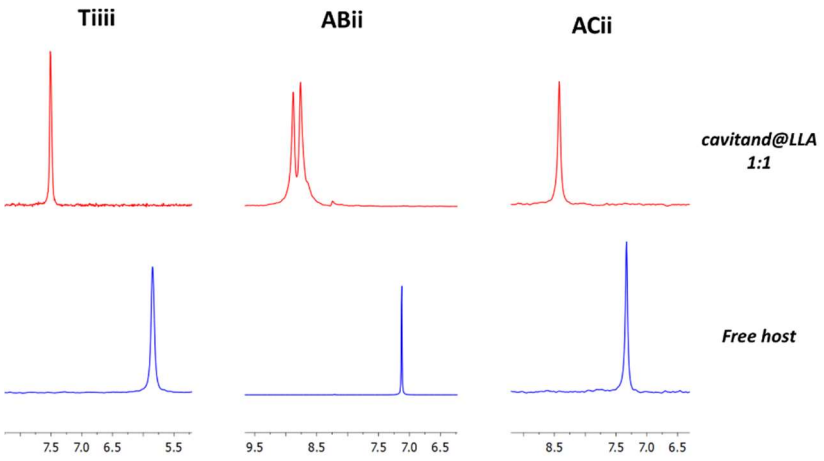

Figure 3.1 *- ^{31}P NMR spectra (162 MHz, $CDCl_3$, room temperature) of* ***Tiiii****,* ***ABii*** *and* ***ACii*** *1:1 complexes. Below: the free cavitands. Above: the cavitand@LLA complexes.*

Therefore, the formation of two signals is attributed to the desymmetrization of the **ABii@LLA** complex. In both **ABii** and **ACii** cavitands, the guest can assume two possible orientations in the cavity, with one P=O engaged in H-bonding either with the OH or with the COOH. Being **ABii** a concave prochiral receptor, it forms two diastereomeric complexes upon complexation of chiral **LLA**, while **ACii** does not, due to the presence of a residual symmetry plane in the **ACii@LLA** complex.

^{31}P NMR competition experiments were run to define a complexation affinity ranking among the three receptors. Equimolar pairs of cavitands, namely **Tiiii** *vs* **ABii**, **Tiiii** *vs* **ACii**, and **ABii** *vs* **ACii**, were titrated with L-lactic acid in deuterated acetone solution. At the 1:1:1 ratio, where half of the cavities are empty the chemical shift trend is the following (Figure 3.2):

- In the **ABii** *vs* **ACii** experiment, the signals of **ABii** displayed a larger shift (1.54 ppm) compared to **ACii** (1.11 ppm).
- In the **Tiiii** *vs* **ABii** experiment, the signal of **ABii** displayed a larger shift (1.81 ppm) compared to **Tiiii**. (1.40 ppm).

- In the **Tiiii** *vs* **ACii** experiment, the signal of **Tiiii** displayed a larger shift (1.24 ppm) compared to **ACii** (0.92 ppm).

These results allow to establish the following order of relative affinity for L-lactic acid: **ABii > Tiiii > ACii**. The relative order of affinity can be rationalized by considering the combination of two factors: (i) steric hindrance which affects mainly the strength of C-H•••π interactions (see crystal structures) and (ii) number of P=O units available for H-bonding. Disphosphonate **ABii** and **ACii** cavitands are sterically less hindered than **Tiiii**. On the other hand, the presence of four P=O groups in **Tiiii** offers an increasing number of binding options available. In the case of alcohols, this has been shown to be an effective way to entropically stabilize the complex.[7] The combination of reduced steric hindrance and the favorable position of the vicinal P=O makes **ABii** the best receptor for **LLA**. In **ACii**, the reason of its reduced affinity with respect to **ABii** cannot be inferred by ^{31}P NMR only. In **Tiiii**, both AB and AC complexation modes are possible, but the steric hindrance weakens the C-H•••π contribution. The overall balance leads to the relative affinity indicated above.

The same trend is shown by ^{1}H NMR spectra, where the inclusion of the guest can be monitored by the shift of the CH_3 signal (Figure 3.3): the shielding effect exerted by the aromatic cavity on the methyl group results in a high-field shift at -2.15 ppm for **ABii**, -2.03 ppm for **ACii**, and -0.43 ppm for **Tiiii**, at a host:guest ratio of 1:0.25. The shift of the methyl signal upon complexation is correlated to the deepth of the inclusion. The observed trend in upfield shift of the methyl residue is corroborated by the solid state data (Figures 3.4 and 3.5) for the **ABii** *vs* **ACii** case.

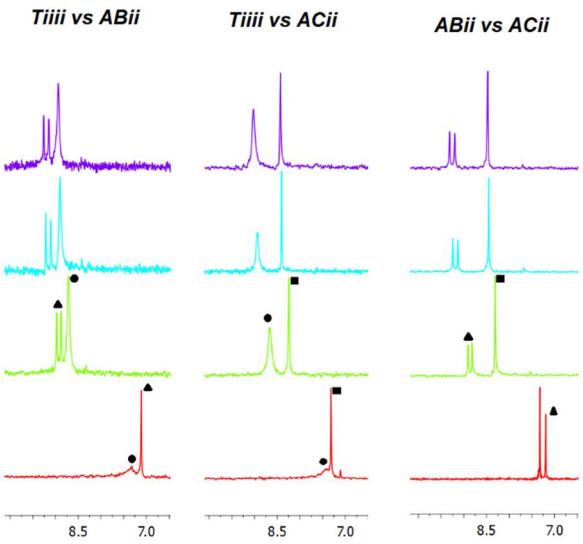

Figure 3.2 *– ^{31}P NMR titrations (162 MHz, $CDCl_3/d_6$-acetone) of Tiiii vs ABii, Tiiii vs ACii and ABii vs ACii, for the following cavitand$_1$:cavitand$_2$:guest ratio: 1:1:0 (red), 1:1:1 (green), 1:1:2 (cyan), 1:1:3 (violet). Shapes code: (●) Tiiii, (▲) ABii, (■) ACii.*

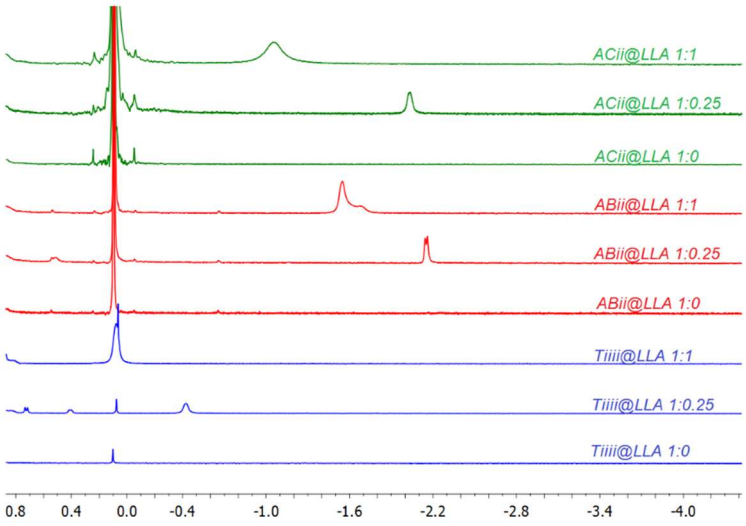

Figure 3.3 *- ^{1}H NMR titrations (400 MHz, $CDCl_3/d_6$-acetone) of* ***Tiiii*** *(blue),* ***ABii*** *(red) and* ***ACii*** *(green), for respectively 1:0, 1:0.25 and 1:1 host guest ratio (zoom at high field region).*

3.4 RECOGNITION OF L-LACTIC ACID IN THE SOLID STATE

In the solid state, lactic acid forms inclusion complexes with the **ACii** and **ABii** cavitands, through the formation of C-H···π interactions and hydrogen bonds, as evidenced by the molecular structure obtained through single-crystal X-ray diffraction analysis (Figures 3.4 and 3.5). In the case of the **ACii** isomer, two independent complexes are present in the asymmetric unit, which show analogous coordination modes and differ only in the orientation of the phenyl rings on the P=O groups. In the case of the **ABii** analogue, a further molecule of lactic acid is present in the crystal lattice, its hydroxyl group forming a hydrogen bond with the carboxylic oxygen of the guest.

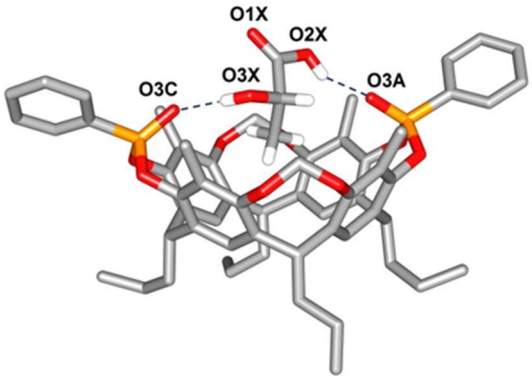

***Figure 3.4** - Molecular structure of one of the two independent complexes **ACii[C_3H_7, CH_3, Ph]@$C_3H_6O_6$** with partial labelling scheme. Only the hydrogen atoms of the lactic acid are shown. Color code: phosphorus, orange; oxygen, red; carbon, grey; hydrogen, white; hydrogen bond, blue dotted lines.*

In both cases the methyl group of the acid enters the cavity and experiences C-H···π interactions with the benzene rings forming the cavitand walls. At the same time, both the hydroxyl and carboxyl OH groups are involved in hydrogen bonds with the P=O moieties at the upper rim. The geometrical parameters for these sets of interactions are comparable for the two isomers (see Appendix C). However, the

distance of the methyl group of the lactic acid from the least-squares plane passing through the lower rim of the cavitand is of 2.985(4) Å in the **ABii** complex, shorter than the value of 3.197(1) and 3.239(1) Å found for the two independent **ACii** complexes, respectively. The fact that the methyl group enters inside the **ABii** cavity more deeply, is attributed to the different steric hindrance generated at the upper rim in the two isomers, in good agreement with the NMR data in solution.

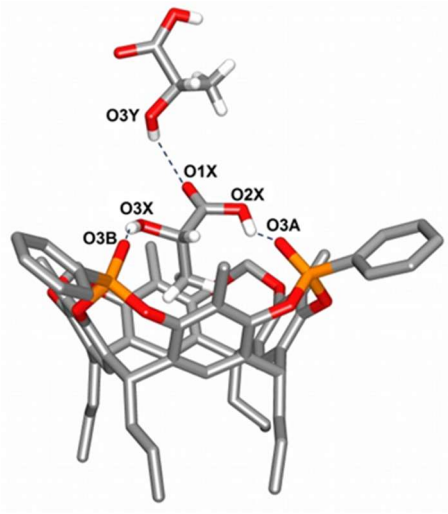

***Figure 3.5** - Molecular structure of the complex **ABii[C_3H_7, CH_3, Ph]@$C_3H_6O_6$•$C_3H_6O_6$•C_6H_{14}** with partial labelling scheme. Only the hydrogen atoms of the lactic acid are shown. Color code: phosphorus, orange; oxygen, red; carbon, grey; hydrogen, white; hydrogen bond, blue dotted lines.*

3.5 CONCLUSIONS

Three phosphonate cavitands, **Tiiii**, **ABii** and **ACii**, were probed for the recognition of L-lactic acid in solution and in the solid state. By the combined use of NMR spectroscopy and X-ray diffraction analysis, it was possible to investigate and elucidate the complexation at the molecular level. In particular, it was evidenced that the presence of a pre-organized, π-basic cavity, decorated with phosphonate groups at the upper rim, allows the formation of a one-to-one complex stabilized by multiple weak supramolecular interactions. A reduced steric hindrance confers to **ABii** a

greater affinity for L-lactic acid. Despite of their sterically hindered upper rims, **Tiiii** and **ACii** can form stable complexes with L-lactic acid.

3.6 ACKNOWLEDGEMENTS

Special Thanks to Dr Chiara Massera for solid state studies.

3.7 REFERENCES

[1] a) European Parliament and Council Directive No 95/2/EC of 20 February 1995 on food additives other than colours and sweeteners (OJ No L 61, 18. 3. 1995, p. 1);

b) R. Datta, S.-P. Tsai, P. Bonsignore, S.-H. Moon and J. R. Frank, *FEMS Microbiol. Rev.* **1995**, *16*, 221;

c) J. Vijayakumar, R. Aravindan, and T. Viruthagiri, *Chemical Engineering World*, **2007**, *42*, 101.

[2] a) R. L. Yates, and D. C. Havery, *J. Cosmet. Sci.* **1999**, *50*, 315. b) *Guidance for Industry: Labeling for Cosmetics Containing Alpha Hydroxy Acids*, Office of Cosmetics and Colors in the Center for Food Safety and Applied Nutrition (CFSAN) at the U.S. Food and Drug Administration, **2005**; c) R. Datta and M. Henry, *J. Chem. Technol. Biotechnol*., **2006**, *81*, 1119.

[3] a) D. Garlotta*, J. Polymers and the Environment*, **2001**, *9*, 63; b) R. A. Gross and B. Kalra, *Science*, **2002**, *297*, 803; c) R. A. Auras, L.-T. Lim, S. E. M. Selke, H. Tsuji, *Poly(lactic acid): Synthesis, Structures, Properties, Processing, and Applications*, John Wiley&Sons, Inc., Hoboken, N. J, **2010**; d) A. J .R. Lasprilla, G. A. R. Martinez, B. H. Lunelli, A. L. Jardini, R. M. Filho, *Biotechnol. Adv.* **2012**, *30*, 321.

4 a) M. L. Goodwin, J. E. Harris, A. Hernández and L. B. Gladden, *J. diabetes Sci. Technol.* **2007**, *1*, 558; b) W. Jia, A. J. Bandodkar, G. Valdés-Ramírez, J. R. Windmiller, Z. Yang, J. Ramírez, G. Chan and J. Wang, *Anal. Chem*. **2013**, *85*, 6553.

[5] R. Pinalli, M. Suman and E. Dalcanale, *Eur. J. Org. Chem.* **2004**, 451.

[6] R. Pinalli and E. Dalcanale, *Acc. Chem. Res.* **2013**, *46*, 399.

[7] a) M. Suman, M. Freddi, C. Massera, F. Ugozzoli and E. Dalcanale, *J. Am. Chem. Soc.* **2003**, *125*, 12068; b) E. Biavardi, S. Federici, C. Tudisco, D. Menozzi, C. Massera, A. Sottini, G. G. Condorelli, P. Bergese and E. Dalcanale, *Angew. Chem. Int. Ed.* **2014**, *53*, 9183.

[8] a) W. Jia, A. J. Bandodkar, G. Valdés-Ramírez, J. R. Windmiller, Z. Yang, J. Ramírez, G. Chan, J. Wang, *Anal. Chem.* **2013**, *85*, 6553; b) B. H. Chu, B. S. Kang, F. Ren, C. Y. Chang, Y. L. Wang, S. J. Pearton, A. V. Glushakov, D. M. Dennis, J. W. Johnson, P. Rajagopal, J. C. Roberts, E. L. Piner, K. J. Linthicum, *Appl. Phys. Lett.* **2008**, *93*, 042114; c) S. Ma, Q. Liao, H. Liu, Y. Song, P. Li, Y. Huang and Y. Zhang, *Nanoscale,* **2012**, *4*, 6415; d) Y. Lei, N. Luo, X. Yan, Y. Zhao, G. Zhanga and Y. Zhang, *Nanoscale,* **2012**, *4*, 3438; e) Y. Zhao, X. Yan, Z. Kang, X. Fang, X. Zheng, L. Zhao, H. Du, Y. Zhang, *J. Nanopart. Res.* **2014**, *16*, 1; f) S. Ma, X. Zhang, Q. Liao, H. Liu, Y. Huang, Y. Song, Y. Zhao, Z. Yanguang, Y. Zhang, *Sens. Actuators B: Chemical* **2015**, *212*, 41; g) F. Wu, Y. Huang and C. Huang, *Biosensors & Bioelectronics*, **2005**, *21*, 518.

Chapter 4

RECOGNITION OF A HUMAN SWEAT MARKER WITH PHOSPHONATE CAVITANDS

*A tetraphosphonate cavitand (**Tiiii**), and two diphosphonate cavitands (**ABii** and **ACii**), were probed for the molecular recognition of 3H3MHA (3-methyl-3-hexanoic acid), a specific human sweat marker, for the sensing of hidden persons. The complexation of 3H3MHA was investigated in solution and in the solid state. The ability of **Tiiii** to complex potential interferents (short alkyl chain carboxylic acids) was also explored. ^{1}H and ^{31}P NMR experiments showed that 3H3MHA is preferentially complexed. Solid-phase microextraction (SPME) analyses were carried out on fibres coated with **Tiiii** and **ABii**, to test the receptor capabilities towards artificial sweat. Vapors of 3H3MHA, among other volatile fatty acids and possible interferents, were preconcetrated on the fibers, thermally desorbed and identified by GC-MS. Preconcentration tests with MEMs cartridge and IMS/GC were performed with **ABii**.*

4.1 INTRODUCTION

To face the growing threat of terrorism, human and drugs trafficking, Police and custom services exploit the exceptional dogs' olfactory properties to detect illicit substances and hidden persons[1,2,3]. However, the use of dogs requires intensive training, and their limited operability time reduces the effectiveness of controls. In this context, the development of sniffing systems mimicking canine skills but overcoming their drawbacks appears an appealing alternative.

The design of a device able to detect human traffic requires to identify the volatile organic compounds (VOCs) specifically released by human presence.[4] In this context, selectivity and sensitivity are key features in the development of the sensor. Indeed, the instrument must selectively recognize one or a set of compounds corresponding to the chemical signature of human emanations, and be insensitive to potential interferents.[5] Furthermore, the target human markers are released at trace level in air (ppb), among other volatile compounds which are not specific to human presence. Therefore, it is necessary to selectively pre-concentrate the target analytes, thanks to a sorbent material which can selectively uptake the relevant VOCs. Then, under thermal desorption, the analytes are released and delivered to a detection unit for further identification and quantification. In this context, the selectivity of the sorbent material is an important parameter. To satisfy the requirements of selectivity and sensitivity, one innovative strategy consists in taking advantage of miniaturized preconcentrators units, equipped with selective supramolecular receptors, which interact with the target analytes by non-covalent interactions.[6]

In the case of human detection, literature survey reports high abundance of volatile fatty acids. Some of them results from metabolism of long chain fatty acids or amino acids, and therefore are present in mammalian excretions, such as acetic acid, propionic acid, lactic acid[7]. However, some other compounds are specific to human metabolism. One of them is 3-hydroxy-3 methylhexanoic acid (**3H3MHA**, Scheme 4.1), a volatile β-hydroxy acid identified as a specific human sweat marker.[8] This

molecule contains two hydrogen bond donors, namely OH and COOH functions. As H-bond acceptor, phosphonate cavitands are ideal candidates for the selective recognition of 3H3MHA. Furthermore, the acidity of the COOH moiety enforces the hydrogen bonding. The presence of two potential interaction points, combined with the C_6 skeleton of the guest, raises the question of the steric hindrance at the upper rim of the cavitand. Indeed, the number and position of the P=O moieties offer several possibilities of complexation. We selected a set of three cavitands, namely i) **Tiiii**, a tetraphosphonate cavitands, which maximizes the number of interaction points and the steric hindrance, ii) **ABii**, a disphosphonate cavitand having two P=O moieties in vicinal position, and iii) **ACii**, a disphosphonate cavitand having two P=O moieties in distal position. The diphosphonate cavitands present a reduced steric hindrance with respect to the tetraphosphonate one.

The ability of the three phosphonate cavitands to complex **3H3MHA** was investigated in solution by ^{1}H and ^{31}P NMR experiments, in the solid state via X-ray diffraction analysis on single crystals, and at the solid-gas interface by SPME fibers experiments.

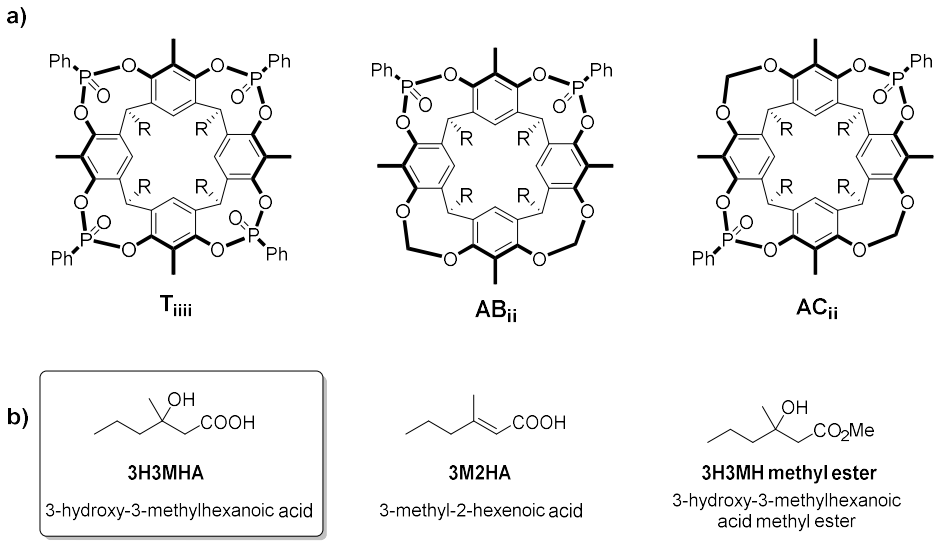

Scheme 4.1 *- a) structures of **Tiiii**, **ABii** and **ACii**. (R = C_3H_7) and - b) structure of **3H3MHA** and related guests used in this work.*

4.2 RECOGNITION OF 3H3MHA IN SOLUTION

The complexation of **3H3MHA** by **Tiiii**, **ABii** and **ACii** was investigated in solution, by means of ^{31}P and ^{1}H NMR experiments (figure 1). In presence of one equivalent of the guest, **Tiiii** displayed a significant shift of the phosphorous signal ($\Delta\delta$ = 0.84 ppm), diagnostic of the molecular recognition event, while **ABii** and **ACii** showed a much lower affinity for this guest considering their low shift ($\Delta\delta$ = 0.09 and 0.15 ppm respectively for **ABii** and **ACii**). The presence of only one peak indicates that the system is in fast exchange with respect to the NMR time scale. These results are consistent with the complexation mode of short alkyl chain alcohols by phosphonate cavitands: the reduced number of P=O groups minimizes the probability of hydrogen bonding with the guest, therefore the overall interaction is lessened.

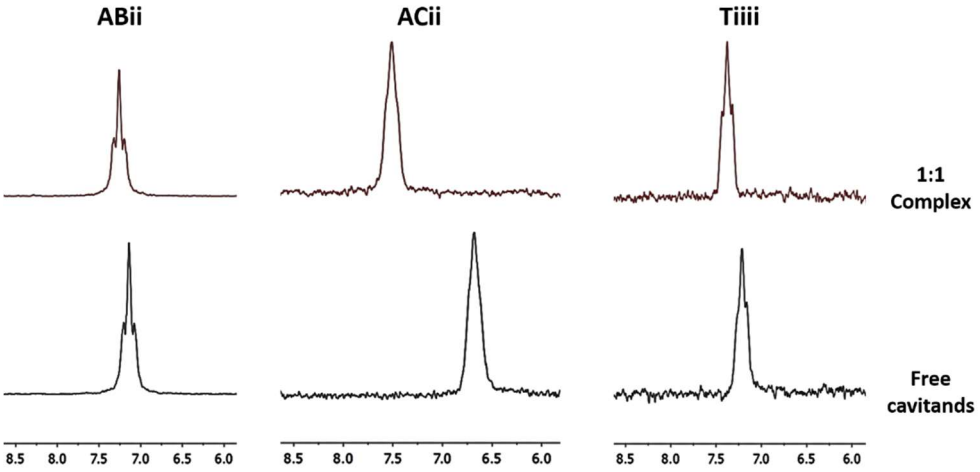

***Figure 4.1** – ^{31}P NMR titrations of **ABii**, **ACii**, **Tiiii** with 3H3MHA*

In the ^{1}H NMR spectra, the inclusion of the guest in the cavity is monitored by the shift of the terminal CH_3: the shielding effect exerted by the aromatic cavity on the terminal methyl induces an upfield shift of the signal. These results shows that the guest is included with the aliphatic part inside the aromatic cavity. The maximum shift is observed at a very low host-guest ratio. Indeed, the signal corresponding to the terminal CH_3 is an average value of the complexed and non-complexed species

of the guest of the guest in solution. The value of the chemical shift reflects the complexed/non complexed ratio. When the concentration of the guest is very low, the complexed/non complexed ratio is high, so the chemical shift tends to its maximum value. While adding progressively the guest, the complexed/non complexed ratio decreases, pushing the chemical shift towards the non-complexed value.

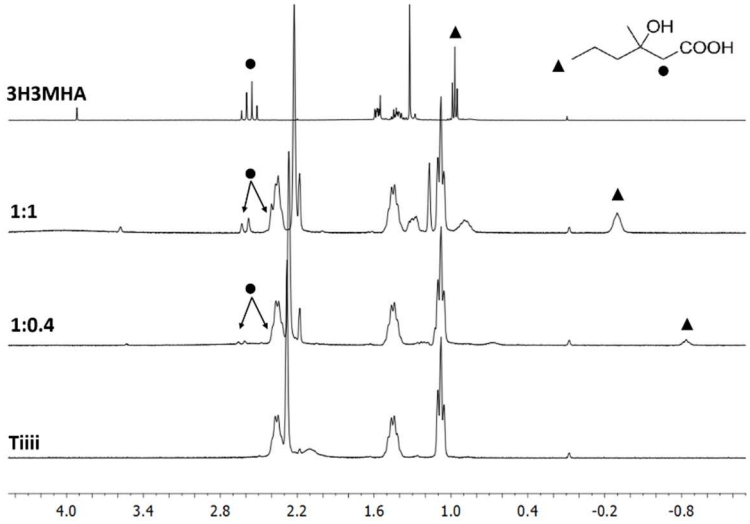

Figure 4.2 *– ^{1}H NMR spectra of the titration of* ***Tiiii*** *with 3H3MHA (300 MHz, $CDCl_3$, zoom in highfield region).*

Since two H-bond donors of the guest may interact either with the cavitand or with another guest molecule, the possibility of a stoichiometric ratio different from the expected 1:1 for the **Tiiii@3H3MHA** was considered. A Job's plot experiment reported in figure 3 was performed and confirmed the 1:1 stoichiometry of the complex.

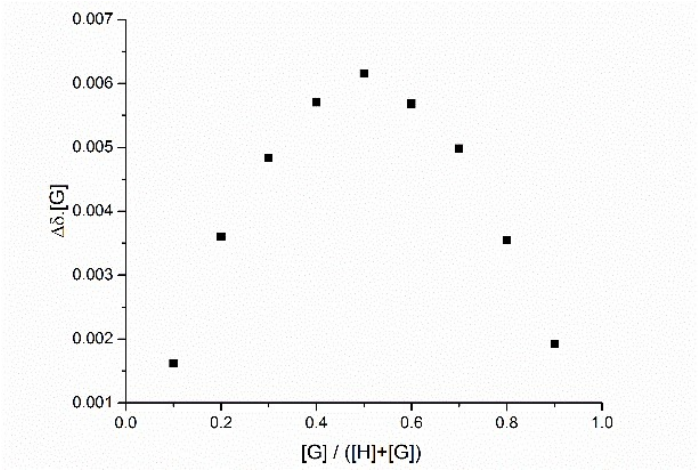

Figure 4.3 *– Job's plot of the complex* ***Tiiii@3H3MHA*** *(^{31}P). [H] is the concentration of* ***Tiiii****. [G] is the concentration of* ***3H3MHA****. Δδ is difference between the 31P chemical shift of the free guest and the 31P chemical shift of the complex at [H]:[G] ratio.*

The role of the OH and COOH functions was investigated by exploiting derivatives of **3H3MHA**, namely **3H3MHA methyl ester** (3-hydroxy-3-methyl hexanoic acid methyl ester), and **3M2HA** (3-methyl-2-hexenoic acid), represented in figure 4.4, removing respectively the COOH and OH groups. The complexation is completely suppressed when either one of the OH or COOH functions is missing. These results enlighten the synergistic interactions of both the OH and COOH functions and this synergy gives to the cavitand receptor its remarkable selectivity.

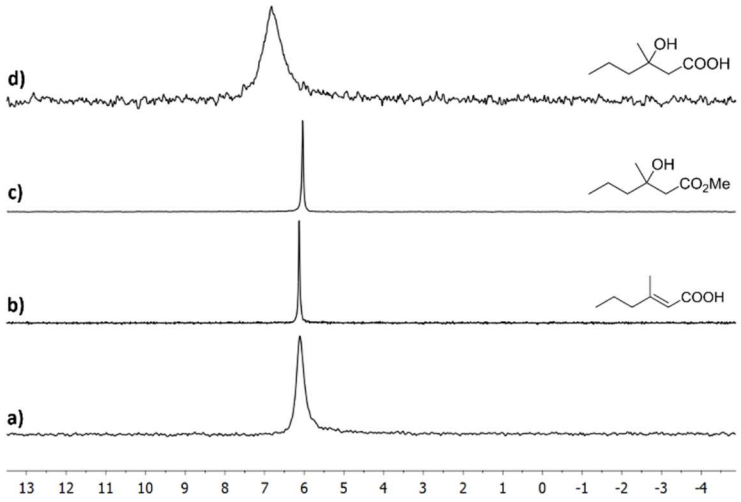

Figure 4.4 *– ^{31}P NMR spectra of **Tiiii** complexed with 3H3MHA derivatives. a) Free **Tiiii**; b) **Tiiii@3M2HA** 1:1; c) **Tiiii@3M3MHA** methyl ester 1:1 methyl ester; d) **Tiiii@3M3MHA** 1:1*

4.3 COMPLEXATION OF 3H3MHA IN THE SOLID STATE

Crystals of the complex **Tiiii@3H3MHA** were obtained from slow evaporation of a CH_2Cl_2/Hexane mixture. They were analyzed via X-ray diffraction analysis, but the poor quality of the data allowed only a partial resolution of the crystal structure of the complex (figure 4.5). The OH group of the guest forms a hydrogen bond with the P=O group of the cavitand, and it is also involved in an intramolecular hydrogen bond with the COOH moiety. The terminal methyl group, included in the cavity, interacts with the aromatic walls by CH-π interactions. Contrary to the expectations, the COOH group is not directly H-bonding to any P=O bridge. The complexation is reminiscent of those of alcohols by the same cavitand, where the two synergistic interactions with the guest are with the alcoholic OH and the terminal methyl group of the chain.

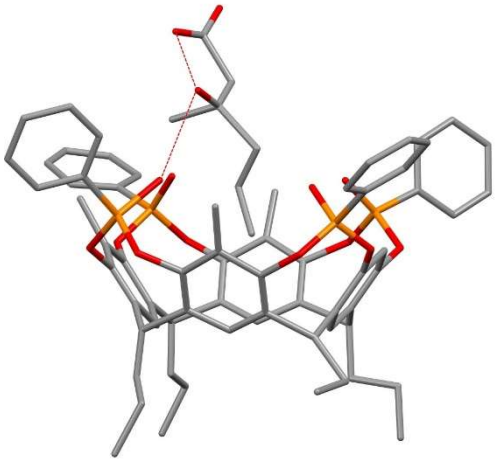

Figure 4.5 *– Molecular structure of the complex* ***Tiiii@3H3MHA****.*

4.4 COMPLEXATION OF VOLATILE CARBOXYLIC ACIDS IN SOLUTION

Although short chain carboxylic acids were found to be present in human sweat, they are not specific to human emanations. Therefore, they can be considered as potential interferents. Their carboxylic function can bind the P=O moieties by hydrogen bonding, stronger than alcohols, due to their higher acidity. Based on the short alkyl chain alcohols model[9], it is expected that these acids follow the same affinity pattern, depending on the alkyl chain length. In order to evaluate the affinity of **Tiiii** for short chain carboxylic acids, titration experiments were performed at ^{31}P and ^{1}H NMR, adding to a solution of **Tiiii** different short alkyl chain carboxylic acids as guests, from acetic to caproic acid. The results are shown in figure 6 for the case of butyric acid.

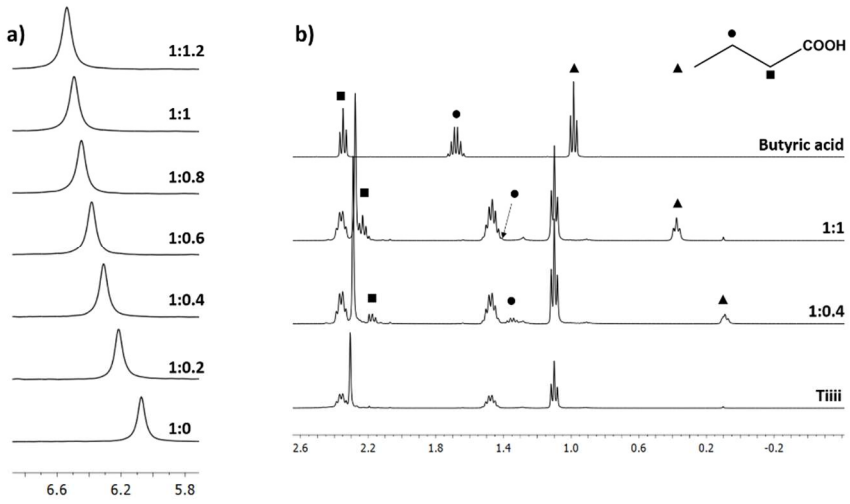

Figure 4.6 *– Typical ^{31}P and ^{1}H NMR titration of* ***Tiiii*** *with short alkyl chain alcohols, example of the butyric acid. a) ^{31}P titration, host-guest ration from 1:0 to 1:1.2. b) ^{1}H titration, zoom in the high field region.*

At ^{31}P NMR, the shifts of the phosphorous signals indicates that **Tiiii** recognizes acetic, propionic and butyric acids (Chart 4.1). No shift of the phosphorous signal was detected for valeric and caproic acids. At ^{1}H NMR, the upfield shift of the terminal methyl is the result of the inclusion of the aliphatic chain inside the cavity. As shown by caproic and valeric acids, if the alkyl chain length is too long, the methyl of the guest cannot occupy the cavity with a concomitant H-bond of the COOH with one P=O, so no complexation occurs. With shorter alkyl chains, the maximum affinity is observed for acetic, propionic and butyric acid.

^{1}H and ^{31}P NMR experiments revealed that **3H3MHA** is preferentially complexed by **Tiiii** among other short alkyl volatile acids. Since VFA are also present in human sweat, **Tiiii** cavitand turned out to be suitable to be used as selective preconcentrator for **3H3MHA**.

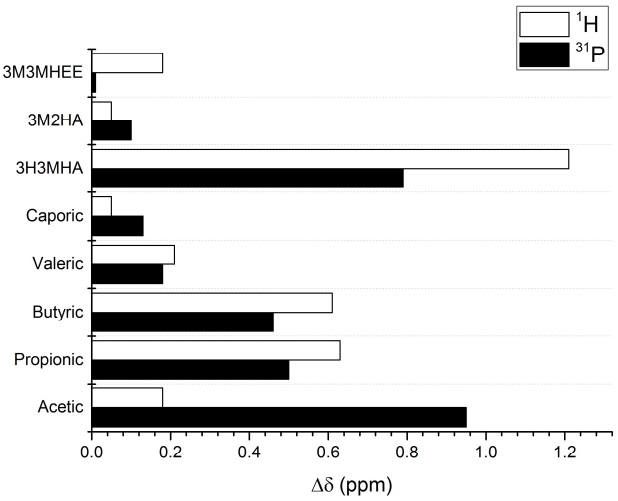

Chart 4.1 *– Overall complexation preferences of* ***Tiiii****, comparing the phosphorous shifts (black bars) and the terminal methyl shifts (white bars)*

4.5 SOLID-GAS INTERFACE

4.5.1 THERMAL STABILITY OF PHOSPHONATE CAVITANDS

Equipped with the data collected above, we moved on to test the **Tiiii** and **ABii** cavitand ability as real preconcentrator. The preconcentration process requires high temperatures for thermal desorption, therefore the selected receptors must be stable at high temperatures over a long period. Thermal stability of **Tiiii** and **ABii** was evaluated by thermogravimetric analysis (TGA) under nitrogen.

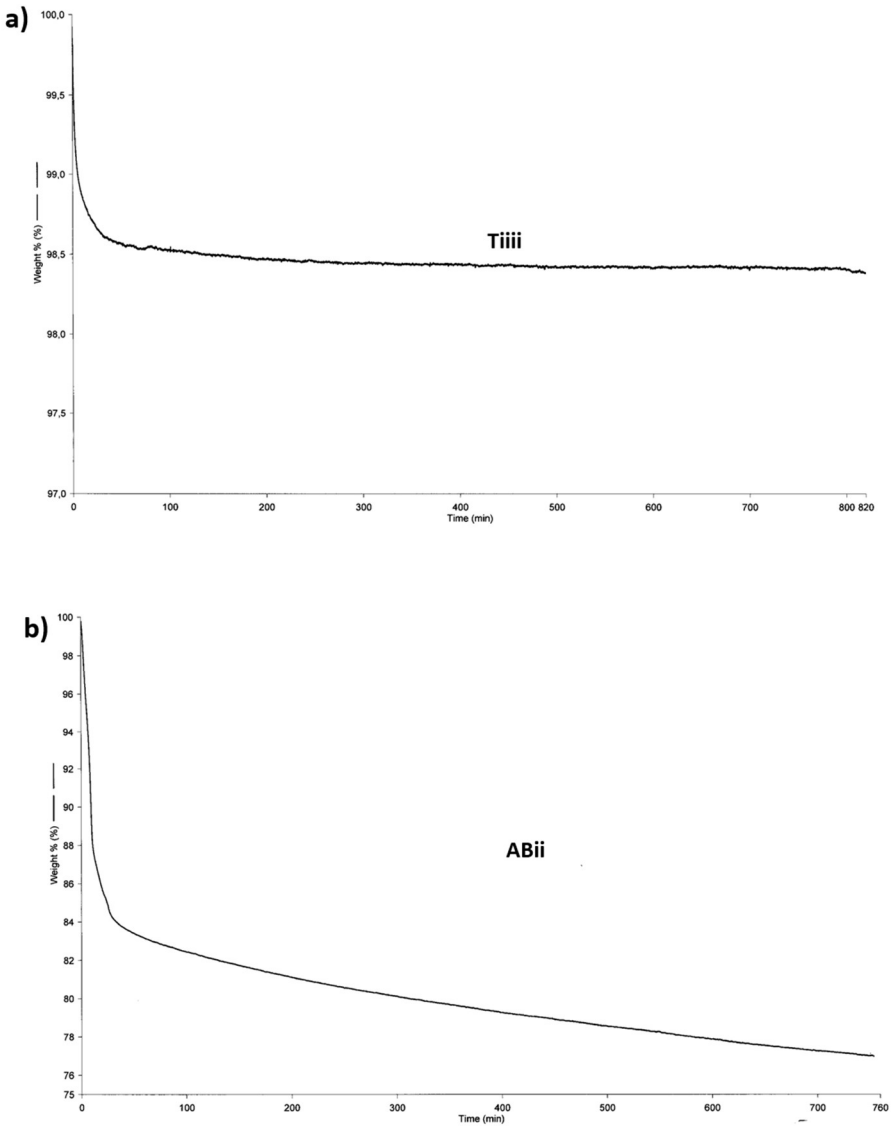

Figure 4.7 *– TGA traces of a)* ***Tiiii*** *at 200°C and b)* ***ABii at*** *250°C, under nitrogen.*

Figure 4.7 reports the TGA traces of **Tiiii** and **ABii**, heated for several hours at respectively 200°C and 250°C, under nitrogen, to test their thermal stability over time. In the first 50 minutes of the experiments, **Tiiii** showed a 1.5% loss weight, corresponding to the evaporation of residual solvents. No further loss of weight was

observed over 13 hours, demonstrating that **Tiiii** is indefinitely stable at 200°C under nitrogen. The TGA curve of **ABii** is characterized by two slopes. The first one, corresponding to the first 30 minutes of the experiment, shows a rapid weight loss of 16%, is attributed to the evaporation of residual solvents. The second slope indicates a constant weight loss of 7% over 12 hours, highlighting the slow degradation of the compound upon long exposure to this temperature. Considering the moderate thermal stability of **ABii**, its use as a preconcentrator lowers the performances of the sensing device. However, it is suitable for preliminary tests. Furthermore, desorption experiments were performed below 250°C, limiting the slow decomposition of the receptor.

4.5.2 SPME EXPERIMENTS

Cavitands properties at the solid-gas interface were investigated by SPME-GC experiments, testing the real detection conditions. SPME fibers were functionalized with **Tiiii** and **ABii** cavitands, previously meshed and then attached to the SPME fibers via epoxy resin glue. The cavitands were compared to commercial polymeric fibers, namely polyacrylate fiber (PA), and divinylbenzene/carboxen polydimethysiloxane fiber (DVB/CAR/PDMS). All the fibers were tested with an artificial sweat, of which the quantitative and qualitative composition, reported in Chart 4.2, is close to the natural sweat. This mixture is made of a large part of fatty acids, ketones, aldehydes and alcohols. The volatile fatty acids fraction is composed of lactic acid, butyric acid, valeric acid and isovaleric acid, heptanoic acid, **3H3MHA**, **3M2HA**, and 3-Hydroxyoctanoic acid. Among these substances, only butyric acid and **3H3MHA** are expected to be recognized by **Tiiii**, according to NMR studies. In solution, lactic acid is recognized by both **Tiiii** and **ABii** (cf. chapter 3), but due its low volatility (boiling point: 122°C, vapor pressure: 0.0813 mm Hg at 25°C)[10], it is not expected to be extracted.

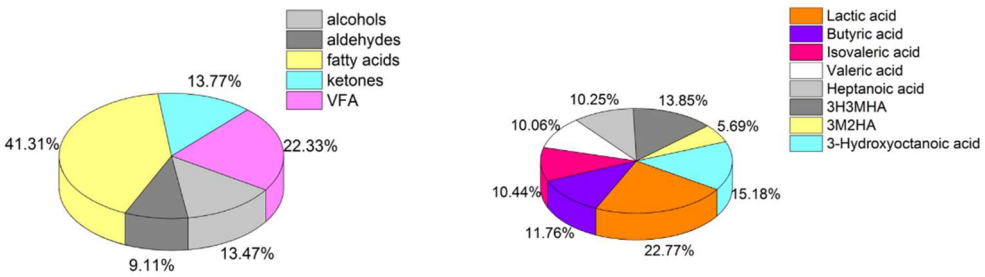

Chart 4.2 *– chart of the artificial sweat composition. Left: global sweat composition. Right: details composition of the VFA fraction.*

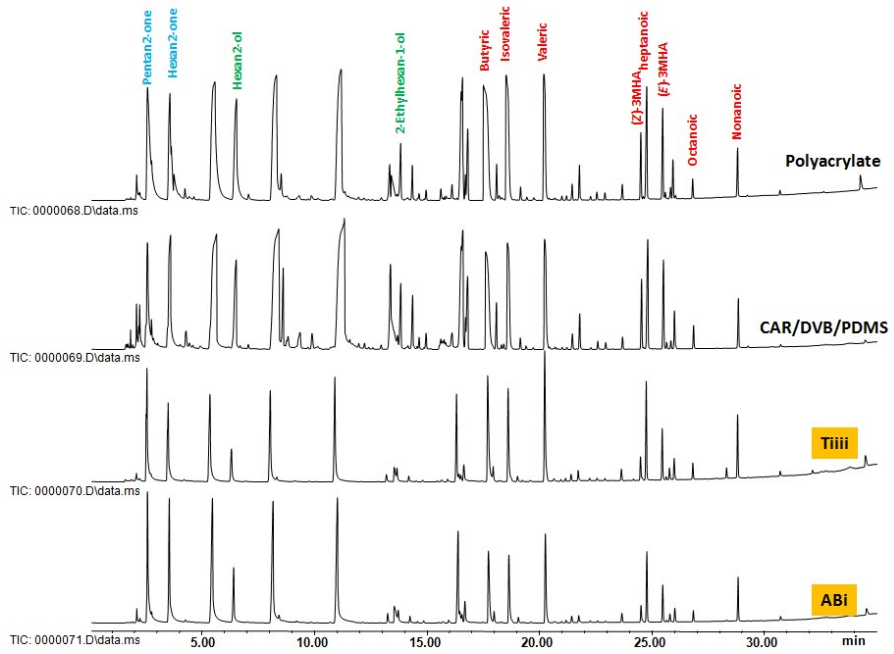

Figure 4.8 *– SPME-GC chromatograms of a) Polyacrylate b) CAR/DVB/PDMS c)* ***Tiiii*** *and d)* ***ABii****.*

Three runs of SPME-GC cycles were performed. Typical chromatograms of SPME-GC experiments are reported in figure 4.8, for each fiber. The desorption was performed at 230°C. The cleaner aspect of **Tiiii** and **ABii** chromatograms is due to the thinner fiber coatings. Indeed, commercial SPME fibers presented higher extraction capacities with respect to **Tiiii** and **ABii**, due to their thicker coating. In **ABii** and **Tiiii** chromatograms, the numerous peaks corresponding to compounds

which are not supposed to be recognized by the cavitands on **Tiiii** and **ABii** chromatograms, are the result of non-specific interactions.

Extraction ratios of volatile fatty acids over all substances were calculated for each fiber. **Tiiii** present a slightly increased selectivity for the volatile fatty acids, with an extraction ratio of 0.41 (table 4.1).

	DVB/CAR/PDMS	Polyacrylate	ABii	Tiiii
1st run	0.21	0.29	0.26	0.39
2nd run	0.23	0.33	0.27	0.39
3rd run	0.24	0.34	0.28	0.41
Mean ratio	**0.27**	**0.32**	**0.27**	**0.41**

***Table 4.1** – Extraction ratios of volatile fatty acids over all substances.*

4.5.3 PRECONCENTRATOR

Tiiii and **ABii** were both used in the MEMs preconcentrator cartridge. However, the following results were obtained only with **ABii**. Indeed, tests performed with **Tiiii** were not successful. This is attributed the fact that the complexation of **3H3MHA** by **Tiiii** is stronger than with **ABii**. With **Tiiii**, the complete desorption process requires very high temperature, causing the decomposition of both the analytes and the cavitand. All these high boiling point analytes experience multiple complexations upon moving along the cartridge (like gas-solid partition in a gas chromatograph stationary phase), making the desorption problematic. In SPME instead the complexation event is mostly single.

Preliminary preconcentration tests were performed with the setup described in figure 4.9 (top).

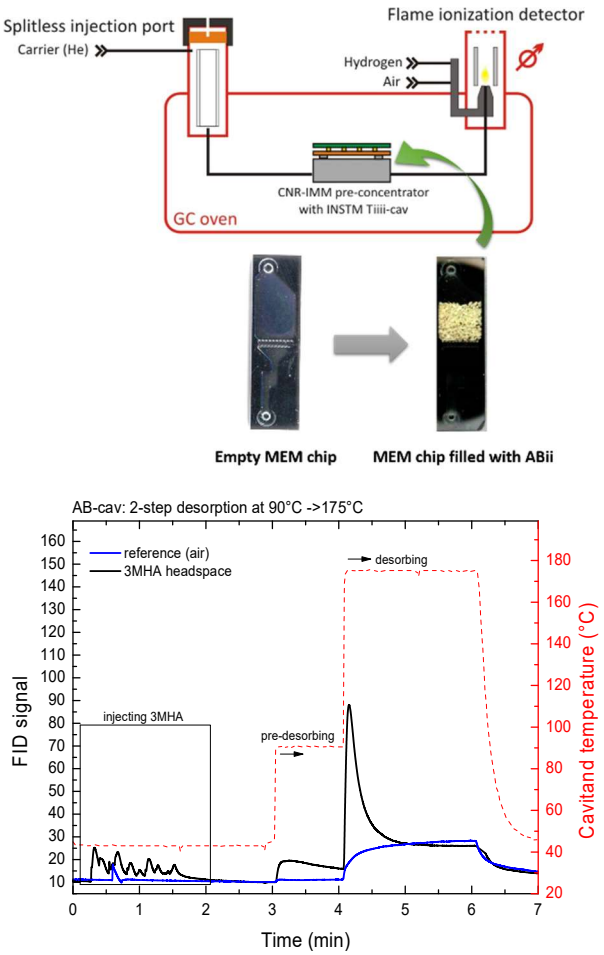

Figure 4.9 *– left: preconcentration setup experiment, and details of MEM chip. Right: FID chromatogram for the desorption of 3H3MHA with ABii preconcentration cartridge.*

The setup is placed in a GC oven, and is constituted by a splitless injection port (SLIP), the preconcentration cartridge, and a flame ionization detector (FID). The SLIP performs the uptake of **3H3MHA** headspace, and carries the vapors to the preconcentration cartridge. Upon heating, the preconcentrated vapors are desorbed and delivered to the FID. The desorption is performed in two step: firstly, during the pre-desorption step, the temperature is increased and maintained at 90°C during one minute. Secondly, the temperature is increased up to 175°C. Figure 4.9 (bottom) reports a preconcentration experiment performed with **ABii**. The detection of

3H3MHA is reported by the black line. In the first two minutes, the **3H3MHA** headspace vapors are sucked into the cartridge. When the pre-desorption is started at 3 min, the FID response indicates that a low quantity of analyte is desorbed. The desorption starts at 4 min., and the peak appearing a few seconds later highlights the release of the analyte. This experiment confirmed the preconcentration capability of **ABii**.

In order to test the preconcentration in the real device, the preconcetrator was coupled with the IMS (Ion Mobility Spectrometer)/GC system. The experiments were performed by the Doggies project partner ISAS (Dr. Wolfgang Vautz, Leibniz Institute, Dortmund). Figure 4.10 shows IMS/GC spectra, by injecting diluted **3H3MHA** either from sample loop, or preconcentrated. In the spectra corresponding to the sample loop injection, no analyte were detected by the IMS/GC system. When using the **ABii** preconcentrator, several compounds were detected. In particular, a spot corresponding to **3H3MHA** is evidenced. Other spots decrease after several humid blanks, therefore they were attributed to contaminations.

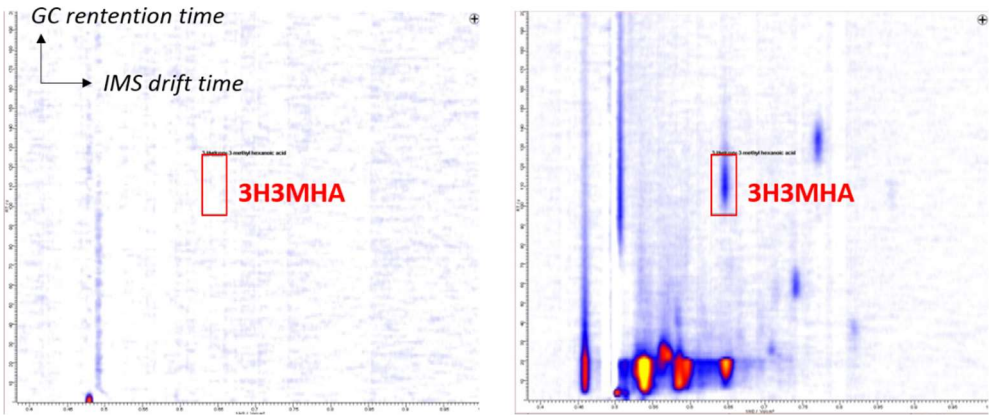

Figure 4.10 *– IMS/GC chromatograms. Left: diluted 3H3MHA injected in the sample loop. Right: sample from the preconcentrator.*

4.6 CONCLUSIONS

Tetraphosphonate cavitand **Tiiii**, and disphosphonate cavitands **ABii** and **ACii**, were probed for the recognition of the human sweat marker **3H3MHA**. In solution, **3H3MHA** was recognized by **Tiiii**, but not with **ABii** and **ACii**. The sweat marker interacts with the cavitand by H-bonding and CH-π interactions. The recognition is driven by hydrogen bonding between the P=O of the cavitand and the OH of the guest, combined with a synergistic intramolecular H-bond between the OH and the COOH of the guest. **Tiiii** was also able to bind short alkyl chain carboxylic acids, from acetic acid to butyric acid, which are also sweat markers. NMR experiments confirmed that **3H3MHA** was preferentially complexed by **Tiiii**. At the solid-gas interface, SPME experiments show that the selectivity **of Tiiii** for **3H3MHA** is significantly reduced due to the presence of non-specific interactions. However, **Tiiii** displayed a slightly increased selectivity for volatile fatty acids, with respect to commercial fibers and **ABii**. **ABii** was successfully used for preconcentration tests. IMS/GC experiments confirmed the preconcentration capabilities of **ABii** in a real sensing system.

4.7 ACKNOWLEDMENTS

Special thanks to Dr. Jean-Jacques Filippi (University of Nice, France) for providing the pure sweat marker and performing SPME-GC fiber experiments, Prof. Federica Bianchi (University of Parma) for SPME experiments, Dr. Chiara Massera (University of Parma) for X-ray structures, Dr. Stefano Zampolli (CNR Bologna) for preconcentration tests, and Dr. Wolfgang Vautz (ISAS, Leibniz Institute, Dortmund). This work was supported by DOGGIES (FP7-SEC-2011-1-DOGGIES-285446)

4.8 EXPERIMENTAL SECTION

4.8.1 SYNTHESIS

The synthesis of **Tiiii**, **ABii** and **ACii** is reported in Appendix C.

Prior to the introduction of **Tiiii** and **ABii** in the MEMs preconcentration cartridge, the cavitands were precipitated from a CH_2Cl_2/Hexane mixture then filtered. The resulting raw powder was meshed. The fraction used in the cartridge correspond to the 60-80 mesh fractions (177-210 μm).

4.8.2 General Procedure for NMR titrations

Cavitands (8.32 μmol) were dissolved in 600 μL of $CDCl_3$. A stock solution of the guest (10 eq) was prepared in $CDCl_3$. ^1H and ^{31}P NMR spectra were recorded after each addition, at room temperature.

4.9 References

[1] H. Kalmus, *Anim. Behav,* **1953**, *3*, 25-31.

[2] P. G. Hepper, *Perception,* **1988**, *17*, 549-554.

[3] G. A. A. Schoon, J. C. De Bruin, *Forensic Sci. Int.* **1994**, *69*, 111-118.

[4] H. Kataoka, K. Saito, H. Kato and K. Masuda, *Bioanalysis*, **2013**, *5*, 1443–1459.

[5] A. Rayms-Keller, Patent US H2256 H, **2011.**

[6] S. Zampolli, P. Betti, I. Elmi and E. Dalcanale, *Chem. Commun.* **2007**, 2790–2792.

[7] A. Natsch, S. Derrer, F. Flachsmann, J. Schmid, *Chem. Biodiversity,* **2006**, *3*, 1-20.

[8] A. Natsch, H. Gfeller, P. Gygax, J. Schmid, G. Acuna, *J. Biol. Chem.* **2003**, *278*, 5718-5727.

[9] M. Melegari, M. Suman, L. Pirondini, D. Moiani, C. Massera, F. Ugozzoli, E. Kalenius, P. Vainiotalo, J.-C. Mulatier, J.-P. Dutasta, E. Dalcanale, *Chem. Eur. J.* **2008**, *14*, 5772–9.

[10] Daubert, T.E., R.P. Danner. Physical and Thermodynamic *Properties of Pure Chemicals Data Compilation*. Washington, D.C.: Taylor and Francis, **1989.**

Chapter 5

DETECTION OF AMPHETAMINE PRECURSORS WITH QUINOXALINE-BRIDGED CAVITANDS[1]

Selective uptake of the methamphetamine and amphetamine precursors safrole and benzyl methyl ketone (BMK) in air was obtained exploiting the molecular recognition properties of the quinoxaline-bridged cavitand (QxCav). The interactions responsible for the observed complexation were studied elucidating the molecular structures of the inclusion compounds with the analytes. Then, solid-phase microextraction (SPME) analyses were carried out on fibres coated with QxCav to test the receptor prowess towards the drug precursors uptake from air. Both safrole and BMK, concentration of which in the vapour phase is in the low microgram per cubic metre regime, are collected and pre-concentrated by the QxCav–SPME fibre, then thermally desorbed and identified via GC–MS.

[1] This chapter has been published in: R. Pinalli, T. Barboza, F. Bianchi, C. Massera, F. Ugozzoli, E. Dalcanale, *Supramol. Chem.*, **2013**, *25*, 682-687.

5.1 INTRODUCTION

Amphetamines and methamphetamines belong to one of the fastest growing class of synthetic drugs, which are rapidly replacing heroin and, to a minor extent, cocaine among drug addicted and occasional consumers alike.[1] Their widespread diffusion constitute a major challenge for our societies, with significant impact on human health and social security. These drugs are manufactured in clandestine laboratories from a small number of key precursors, whose trading is strictly regulated. The most important ones are safrole (**2**) for ecstasy (MDMA),[2] and benzyl methyl ketone (**3**) (BMK) for amphetamine, while 1,3-benzodioxole (**1**) can be considered a model compound for all MDMA precursors (Scheme 5.1). Both **2** and **3** are liquids with high boiling points and low, but not negligible, vapor pressure. Usually these precursors are hidden in trucks used for the transport of chemicals, canned in drums mixed up with those of other chemicals. The challenge is the realization of instruments for their rapid and reliable detection by custom officers at borders by simply sniffing the air around the drums. Despite of the large number of analytical techniques developed for drug precursors identification in the lab, the development of a dedicated, reliable and easy to use field-sensor is still an open issue[3,4]. An innovative solution is the implementation of a supramolecular pre-concentration unit in the device, capable of selectively trapping the target analytes in reasonable quantity and deliver them to a suitable detector through a heating pulse.

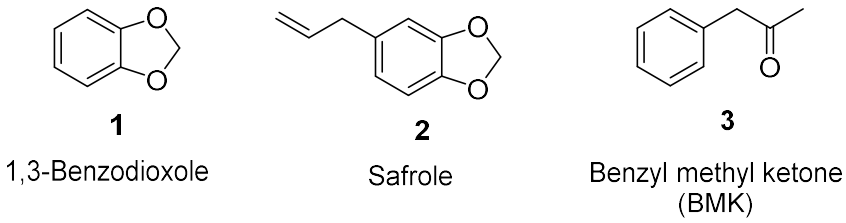

Scheme 5.1 *- Chemical structure of the target analytes.*

The design of an appropriate pre-concentration unit for these drug precursors has been based on our experience in selective detection of volatile aromatic compounds (BTEX) with quinoxaline-bridged cavitands (**QxCav**, Scheme 5.2).[5,6] The molecular recognition properties of **QxCav** toward aromatic hydrocarbons like benzene and toluene are well documented both in the gas phase[7,8] and in the solid state.[9] π-π[10] and CH-π interactions[11] are responsible for the observed complexation, both with the quinoxaline cavity walls and with the resorcinarene scaffold.[12] These multiple weak interactions, made possible by the complete confinement of the guest within the cavity, render **QxCav** the receptor of choice for selecting aromatic over aliphatic hydrocarbons. Moreover, **QxCav** is totally insensitive to water, the major interferent in environmental sensing.[5] The transfer of these complexation properties at the gas-solid interface has been already proven with **QxCav** in gas sensing using both mass[13] and surface plasmon resonance transducers.[14] SPME gel-coating based on **QxCav** as receptor has also been developed and proposed as a valid alternative to commercial fibers for selective determination of benzene and chlorobenzene at ultra-trace levels in environmental air and water samples.[15]

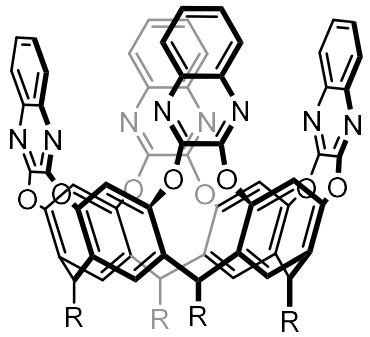

Scheme 5.2 *– General structure of QxCav.*

This chapter describes the use of a **QxCav** as suitable receptor for the detection of BMK and safrole directly in the vapor phase. The type and number of interactions responsible for the observed complexation properties of **QxCav** toward the proposed analytes have been determined through the molecular structures of the corresponding

complexes. Then, solid-phase microextraction (SPME) analyses were performed on fibers coated with **QxCav** to test the receptor prowess toward the drugs precursors BMK and safrole in the vapor phase. As stated above, 1,3-benzodioxole was also tested as model compound for the entire class of ecstasy precursors (safrole, isosafrole, etc.).

5.2 CRYSTAL STRUCTURES OF THE COMPLEXES

The interactions between **QxCav** and guests **1** and **2** were studied in the solid state *via* X-ray diffraction analysis on single crystals obtained by slow evaporation of acetone solutions. Surprisingly, in the case of **QxCav@1**, the dioxolane ring of the guest is not pointing inside the π-basic cavity of the host, as could be expected on the basis of preferential C-H···π interactions with the resorcinarene scaffold. Instead, as shown in Figure 5.1, the benzodioxole enters the cavity with the aromatic ring perfectly fitting the space created by the four quinoxaline walls. The guest is slightly tilted to facilitate the formation of a weak C-H···π interaction with the cavitand (see blue dotted line in Figure X. C-H···centroid: 2.445(3) Å and 160.34(2)°).

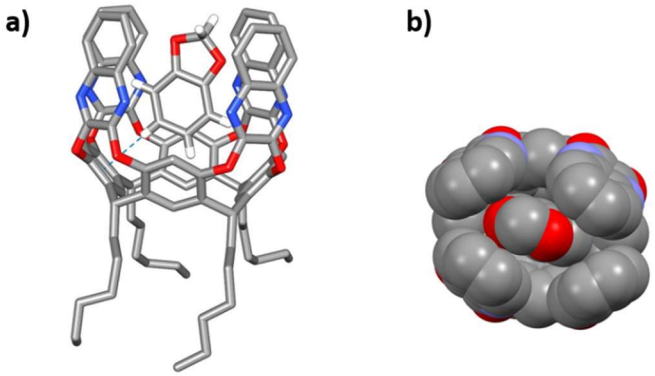

Figure 5.1 *- a) Molecular structure of **QxCav@1**. The lattice acetone molecules and the H atoms of the cavitand have been omitted for clarity. b) Top view of the complex in space filling mode (the H atoms and aliphatic chains have been omitted for clarity).*

On the contrary, in the case of the complex with safrole, the guest is oriented according to our expectations with the dioxolane ring pointing inside the cavity, forming two C-H···π interactions with the aromatic rings of the resorcinarene scaffold (see blue dotted lines in Figure 5.2; C-H···centroid: 2.705(4) Å, 2.793(2) Å, 165.26(6)° and 156.01(4)°, respectively). The different orientations displayed by the two guests is probably due to the steric hindrance generated by the aliphatic chain attached to the benzene ring, which cannot be accommodated in the **QxCav** cavity. Therefore, the presence of substituents on the aromatic ring of benzodioxole does not interfere with the recognition process of **QxCav**.

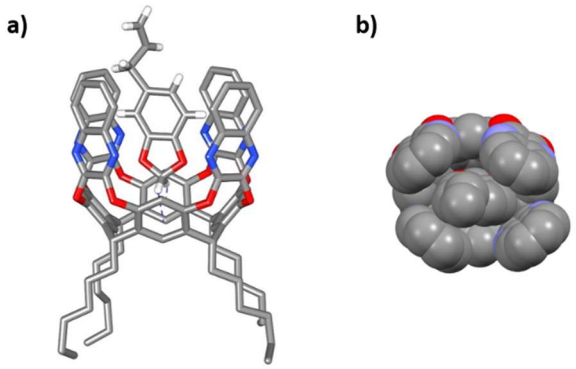

***Figure 5.2** - Left: Molecular structure of **QxCav@2**. The H atoms of the cavitand have been omitted for clarity. Right: Top view of the complex in space filling mode (the H atoms and aliphatic chains have been omitted for clarity).*

5.3 QXCAV SPME PREPARATION AND DRUG PRECURSOR ANALYSES

The effectiveness of **QxCav** in detecting amphetamines and methamphetamines precursors was tested using the three analytes, namely benzodioxole (**1**), safrole (**2**) and BMK, (**3**). A SPME fiber coated with **QxCav** was used for the environmental sampling of the drug precursors. The coating was prepared according to a procedure

already developed in our lab using sol-gel technology to anchor the supramolecular receptor on the silica support of the fiber (Figure 5.3a).[15]

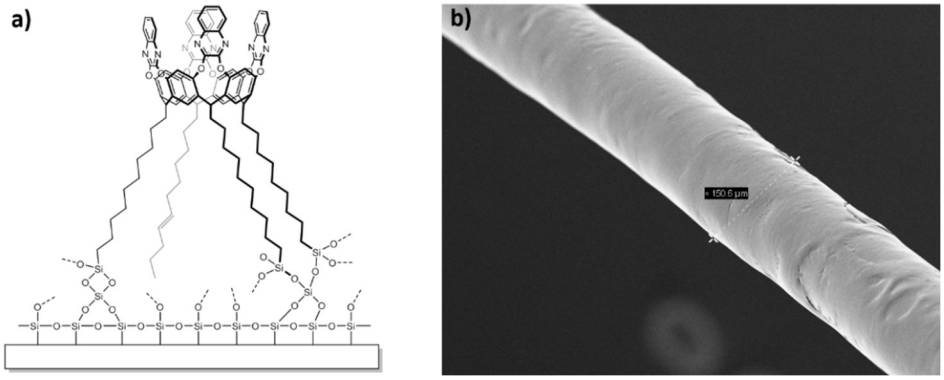

Figure 5.3 *– a) QxCav gel. b) SEM image of the SPME fiber coated with the QxCav gel.*

More precisely, the hydrosilylation step used to functionalize the lower rim of the cavitand allowed the insertion of 3 hydroxysilyl groups on the terminal double bond of the alkyl chains of the cavitand, thus enabling its participation as cross-linking agent in the sol-gel process with an adequate gelation time. The chemical anchoring of **QxCav** on the fiber support produced a coating thickness of 65 ± 13 µm (n=2) with an homogeneous and uniform distribution of the cavitand all along the fiber (Figure 5.3b). The SPME sampling of amphetamine precursors was performed by introducing few microliters of a solution containing the analytes (using hexane as solvent) into an empty vial. After evaporation of the solution, the **QxCav** SPME fiber was exposed to the headspace of the vial at room temperature for 20 min. The capability of **QxCav** in sampling BMK, safrole and benzodioxole from the gas phase was assessed by achieving LOD (Limit of Detection) and LOQ (Limit of Quantification) values in the low µg/m^3 range (Table 5.1).

Analytes	LOD (µg/m^3)	LOQ (µg/m^3)
Benzodioxole (1)	2	6,5
Safrole (2)	3,3	9,9
BMK (3)	4,4	14,8

Table 5.1 *- LOD and LOQ values in air.*

In addition, the high selectivity of the coating was proved by the low amount of hexane extracted, being this hydrocarbon only scarcely retained by the coating as a consequence of non-specific interactions with the gel. The thermal desorption of hexane and other aliphatic hydrocarbons commonly present in air is obtained by operating at low temperatures (<100°C), whereas higher values (250°C) are required to desorb the amphetamine precursors.

The SPME uptake of **1** and **2** are comparable, confirming that the presence of the aliphatic chain in **2** does not interfere with the complexation, as inferred by the molecular structure shown in Figure 4.

The RSD (Relative Standard Deviation) values lower than 17% confirm the good performance reached in terms of intra-day repeatability and intermediate precision. As for intermediate precision, ANOVA performed on the data acquired over three days showed that the mean values were not significantly different, thus proving the reliability of the QxCav-based fiber for the determination of the drug precursors at trace levels (Figure 5.4).

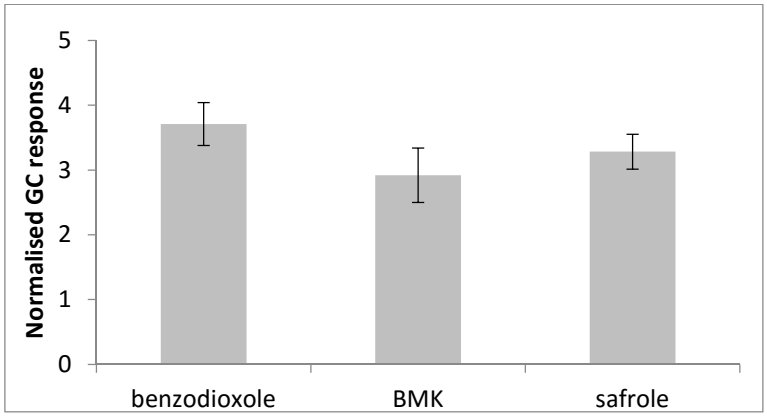

***Figure 5.4** - SPME-GC-MS analysis of an air sample containing a mixture of benzodioxole (99,7 µg/m^3), safrole (132 µg/m^3) and BMK (109,5 µg/m^3). Normalization performed using the response factors.*

5.4 CONCLUSIONS

The remarkable molecular recognition properties of **QxCav** towards aromatic compounds have been exploited in the analytical detection of amphetamine and methamphetamine drug precursors. The X-ray analysis of the inclusion complexes showing that both guests **1** and **2** are engulfed in spite of their structural differences, matches nicely the SPME results. The interplay between the solid state and SPME analyses allows to identify **QxCav** as a suitable receptor to be used in sensing devices for the target analyte detection. In this specific case, the **QxCav** SPME fiber can be used for drug precursor sampling on the field, followed by GC-MS analysis. To be embedded in a real sensing device, it will be necessary to translate the molecular recognition event into a readable signal with high fidelity. Work is in progress to obtain a fluorescence readout of the selective inclusion.

5.5 ACKNOWLEDGMENTS

The work described here was supported by the EC through the FP7 project “DIRAC” (FP7-SEC-2009-242309).

5.6 REFERENCES

[1] World Drug Report – Global Illicit Drug Trends, Undoc.org (retrieved 26.11.11).

[2] Safrole and BMK are listed in Tables I and II respectively of the Convention against Illicit Traffic in Narcotic Drugs and Psychotropic Substances of 1988.

[3]A. Secchi, A. M. Fiorello, M. Dispenza, S. D'Auria, A. Varriale A. Ulrici, R. Seeber, J. Uotila, V. Venditto; P. Ciambelli, J. C. Antolin, F. Colao, T. Kuusela, I. Tittonen, I. Sievila, G. Maisons, *Proc. SPIE,* **2012**, *8545*, 85450G/1-85450G/6.

[4]S Mengali, N. Liberatore, D. Luciani, R. Viola, G. C. Cardinali, I. Elmi, A. Poggi, S. Zampolli, E. Biavardi, E. Dalcanale, F. Bonadio, O. Delemont, P. Esseiva, F. S. Romolo, *Proc. SPIE,* **2013,** *8631*, 86312F/1-86312F/10.

[5]S. Zampolli, P. Betti, I. Elmi, E. Dalcanale, *Chem. Commun.* **2007**, 2790–2792.

[6]S. Zampolli, I. Elmi, F. Mancarella, P. Betti, E. Dalcanale, G. C. Cardinali, M. Severi, *Sens. Actuators B,* **2009**, *141*, 322-328.

[7]M. Vincenti, E. Dalcanale, P. Soncini, G. Guglielmetti, *J. Am. Chem. Soc.* **1990**, *112*, 445-446.

[8] M. Vincenti, E. Dalcanale, *J. Chem. Soc., Perkin Trans. 2,* **1995**, 1069-1076.

[9] P. Soncini, S. Bonsignore, E. Dalcanale, F. Ugozzoli, *J. Org. Chem.* **1992**, *57*, 4608-4612.

[10] C. A. Hunter, K. R. Lawson, J. Perkins, C. J. Urch, *Chem. Soc., Perkin Trans. 2,* **2001**, 651-669.

[11]E. A. Meyer, R. K. Castellano, F. Diederich, *Angew. Chem. Int. Ed.,* **2003**, *42*, 1210-1250

[12]F. Bianchi, R. Pinalli, F. Ugozzoli, S. Spera, M. Careri, E. Dalcanale, *New J. Chem.,* **2003**, *27*, 502-509

[13] J. Hartmann, P. Hauptmann, S. Levi, E. Dalcanale, *Sens. Actuators B,* **1996**, *35*, 154-157.

[14] E. B. Feresenbet, E. Dalcanale, C. Dulcey, D. K. Shenoy, *Sens. Actuators B,* **2004**, *97*, 211-220.

[15]F. Bianchi, M. Mattarozzi, P. Betti, F. Bisceglie, M. Careri, A. Mangia, L. Sidisky, S. Ongarato, E. Dalcanale, *Anal. Chem.,* **2008**, *80*, 6423-6430.

Chapter 6

FUNCTIONALIZATION OF POROUS SILICA WITH ETQXBOX

*This chapter reports the synthesis of a new conformationally blocked quinoxaline cavitand (**EtQxBox**), functionalized with four terminal double bonds at the lower rim. The synthetic strategy is based on a new procedure for the deprotection of the methoxy groups in the octamethoxy quinoxaline cavitand, necessary for the preservation of the double bonds at the lower rim. A porous silicon wafer was successfully functionalized with **EtQxBox**. The characterization of the layer and the complexation properties at the solid-gas interface were investigated with nitrobenzene, and monitored by FT-IR.*

6.1 INTRODUCTION

As described in Chapter 1, quinoxaline cavitands display outstanding recognition properties towards volatile aromatic hydrocarbons at the solid gas interface. Our group successfully exploited QxCav as molecular receptors for BTEX. Indeed, a stand-alone mini-GC system for BTEX monitoring was developed, using quinoxaline cavitands in a preconcentration units.[1] In this system, the BTEX are selectively preconcentrated through the preconcentrator unit, then separated by a mini-GC column. Rigidified quinoxaline cavitands, **EtQxBox** and **MeQxBox**, showed a substantial improvement in selectivity towards BTEX, with respect to QxCav.[2]

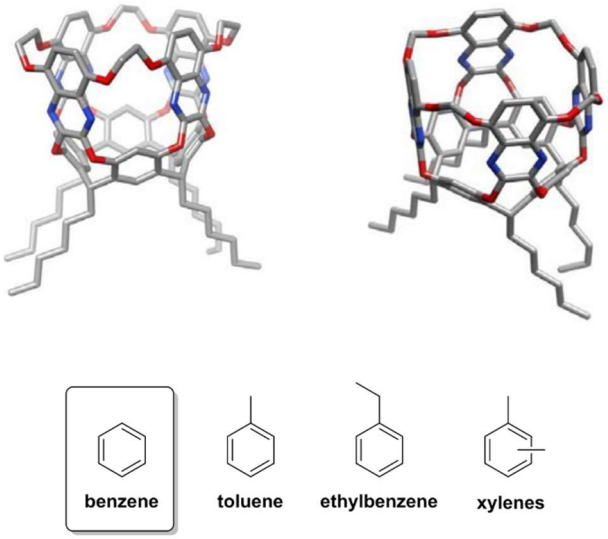

Figure 6.1 *– Molecular structures of* ***EtQxBox*** *(left) and* ***MeQxBox*** *(right) and the BTEX family (bottom).*

Thanks to its high performances, **EtQxBox** was incorporated in the above mentioned sensing device, where the preconcentration cartridge is filled with raw powder of the receptor. This method presents several drawbacks. First of all, the compound needs to be precipitated and sifted to afford a powder with suitable mesh. It is important to crystallize the cavitand powder before sifting it, in order to avoid aggregation of the

crystals. Crystal aggregation, in fact, could create a non-homogenous powder. The sift procedure is necessary in order to have a powder of selected and homogeneous mesh. The optimized mesh has been identified in the range of 60-80 mesh. This mesh guarantees the correct gas flow inside the preconcentrator cartridge. A lot of material is wasted in the process. Secondly, most of the cavities are trapped into the powder particles, therefore only a small proportion of the cavities are actually exposed to the sample. Under these conditions, the full potential of **EtQxBox** cavitand is not exploited. To overcome these drawbacks, the covalent grafting of the cavitands onto a silicon surface seems to be the best solution. This strategy allows to obtain a self-assembled, well organized layer of the receptor, with all the cavities exposed to the analytes. Moreover, this strategy avoids cavitand wasting by eliminating the precipitation and meshing steps. Finally, the porous silicon based preconcentrator, with parallel capillaries producing a *column-like* effect, is expected to facilitate the separation of the BTEX. A further advantage of this strategy is that organic monolayers deposited on inorganic surfaces[3] allow to minimize non-specific interactions, which adversely affect molecular recognition at interfaces.[4] Furthermore, coated silicon surfaces are amenable of integration in silicon-based devices.

Taking advantage of our experience in cavitand-decorated surfaces,[5] we designed and synthesized a new **EtQxBox**, functionalized with four double bonds at the lower rim, for covalent grafting onto porous silicon surface by thermal hydrosilylation reaction.

6.2 SYNTHESIS

The convergent synthesis of **EtQxBox** bearing four terminal double bonds at the lower rim starts from the preparation of two synthons: the first one is the quinoxaline **5** (scheme 6.1), while the second one is the double bond footed resorcinarene **6** (Scheme 6.2).[6]

6.2.1 SYNTHESIS OF THE QUINOXALINE

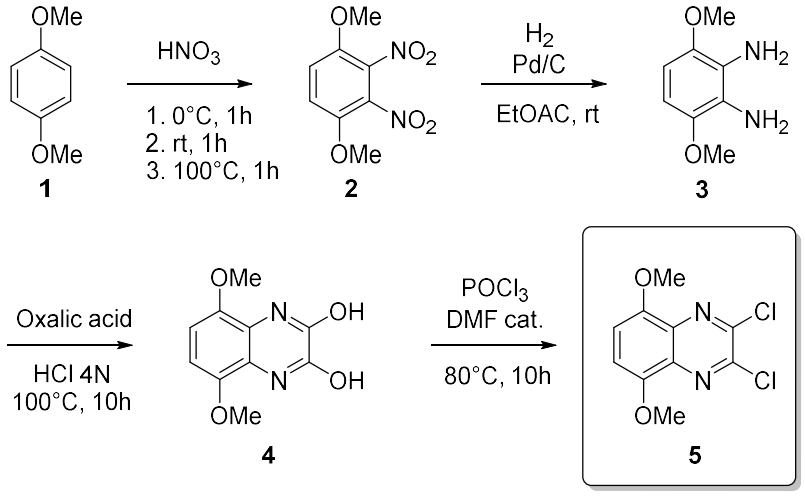

*Scheme 6.1 – synthesis of the quinoxaline **5**.*

Quinoxaline **5** is obtained in four steps starting from commercial dimethoxy hydroquinone **1**. Electrophilic substitution performed in nitric acid provided **2** and its 2,4-dinitro isomer, separated by chromatography. **2** was reduced to the diamino compound **3**, under hydrogen atmosphere in presence of a catalytic amount of Pd/C. The two amino groups of **3** were reacted with oxalic acid to form the 2,3-dihydroxy quinoxaline **4**. Finally, the reaction of **4** with $POCl_3$ leads to the 2,3-dichloro-5,8-dimethoxyquinoxaline **5**, in presence of catalytic quantity of DMF.

6.2.2 BRIDGING OF THE RESORCINARENE

Formation of the quinoxaline cavitand

Resorcinarene **6** is obtained from the standard condensation of resorcinol and undecylenic aldehyde in acidic conditions, and bears four double bond at its lower rim. **6** was reacted with four equivalents of the quinoxaline **5**, in a microwave reactor,

in presence of K_2CO_3 in anhydrous conditions, affording the octamethoxy cavitand **7**.

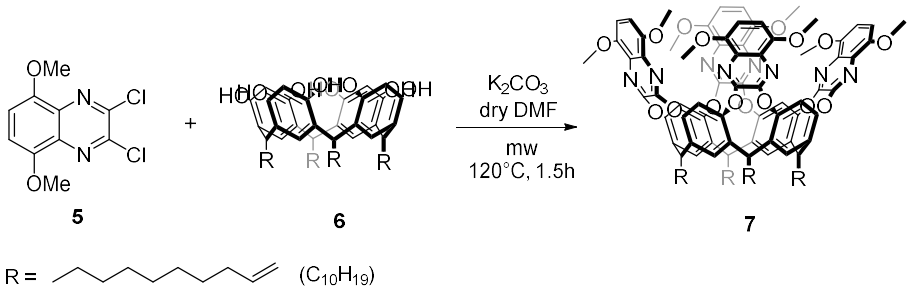

Scheme 6.2 *– formation of the quinoxaline cavitand 7.*

Deprotection of the methoxy groups

In the standard procedure used in the synthesis of the **EtQxBox**, the deprotection of the methoxy groups of the quinoxaline is performed by aluminium trichloride in anhydrous toluene. The presence of the double bonds at the lower rim of the resorcinarene is not compatible with $AlCl_3$. Therefore, new deprotection conditions were elaborated. The deprotection of **7** was performed in two steps.

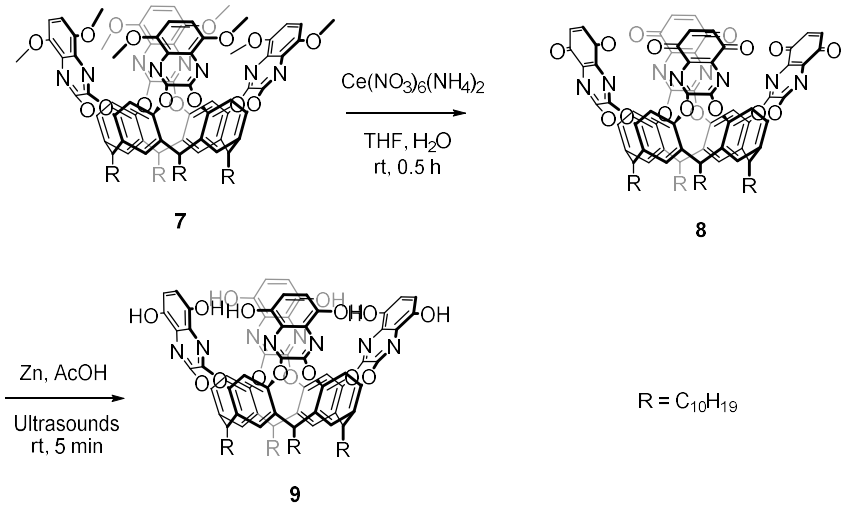

Scheme 6.3 *– two-step deprotection of the methoxy groups.*

The first one consists in the oxidative elimination of the eight methoxy residues by Cerium Ammonium Nitrate (CAN),[7] leading to the tetraquinone cavitand **8**. The crude is washed by extraction and a further column chromatography is necessary to obtain the tetraquinone cavitand as a pure compound. In the ^{1}H NMR spectrum, the deprotection was confirmed by the disappearance of the methoxy signal. Furthermore, the diagnostic methine triplet (3.63 ppm) indicates that the cavitand is mainly in the *kite* conformation. Due to its low stability, the tetraquinone **8** was immediately used in the next step. **8** is reduced by sonication in presence of metallic zinc (reducing agent), and acetic acid (proton donor), during 5 minutes.[8] The compound is purified by filtration to remove the zinc, followed by extraction in EtOAc/H_2O, to remove the excess of acetic acid and $Zn(OAc)_2$ formed during the reaction. ^{1}H NMR analysis confirmed the presence of the eight OH groups in d_6-acetone or d_6-DMSO (singlet around 8.3 ppm). The diagnostic methine triplet is present at 4.08 ppm, indicating that the cavitand is still in the *kite* conformation.

Rigidification of the cavity

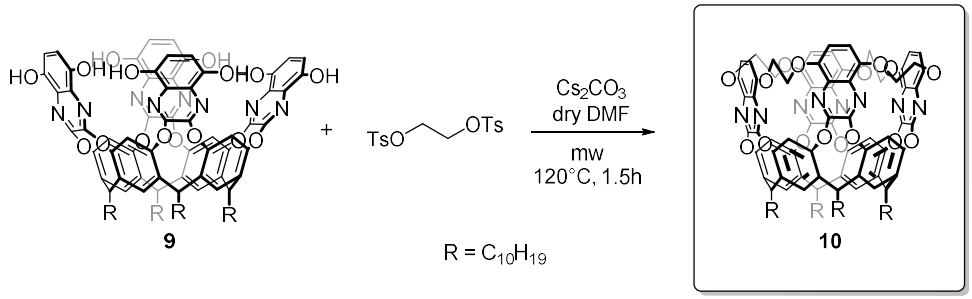

***Scheme 6.4** – Formation of the final compound EtQxBox 10.*

Following the previously established procedure, **8** was reacted under microwave irradiation with ethylene glycol ditosylate, in presence of anhydrous Cs_2CO_3, affording the final compound **EtQxBox (10)** in 50% yield. The characterization was performed by ^{1}H NMR (figure 6.2):

- The signals at 4.69 and 4.50 ppm correspond to the CH_2 of the ethylenoxy bridges, respectively CH_{in} and CH_{out}, which are magnetically different.
- The signals at 5.88 and 5.08-4.99 ppm, are relative to the presence of the terminal double bond
- The signal of the diagnostic methane (5.81 ppm), superimposed to the one of the double bond (5.88 ppm), indicates the *vase* conformation of the cavitand.

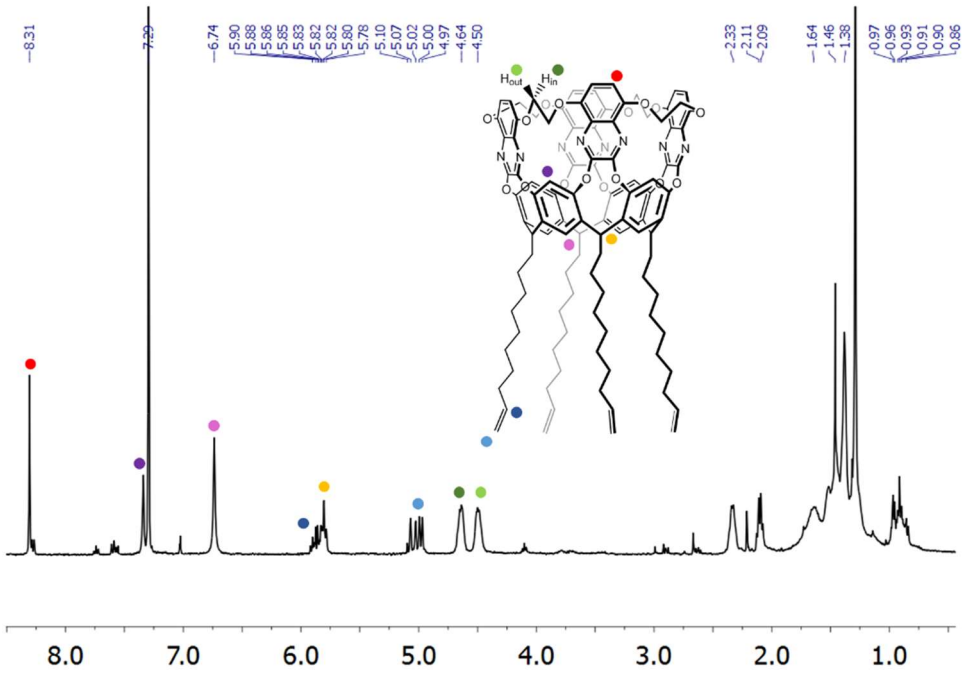

***Figure 6.2** – ^{1}H NMR spectrum of **EtQxBox[$C_{10}H_{19}$, H]** ($CDCl_3$, 400 MHz)*

6.3 FUNCTIONALIZATION OF POROUS SILICA WITH ETQXBOX

6.3.1 PROCEDURE

The preparation of the cavitand-decorated silicon wafer is described in figure 3. **EtQxBox 10** was covalently attached on porous silica (**PSi**), following a well-established procedure, in collaboration with the group of Prof. Condorelli, Messina University.[9] The silicon wafer, previously activated, was soaked in a mesitylene solution of cavitand and reacted for 4 hours at 180°C (figure 6.3). The functionalized silica was washed three times with $CHCl_3$ in order to remove all the physisorbed material.

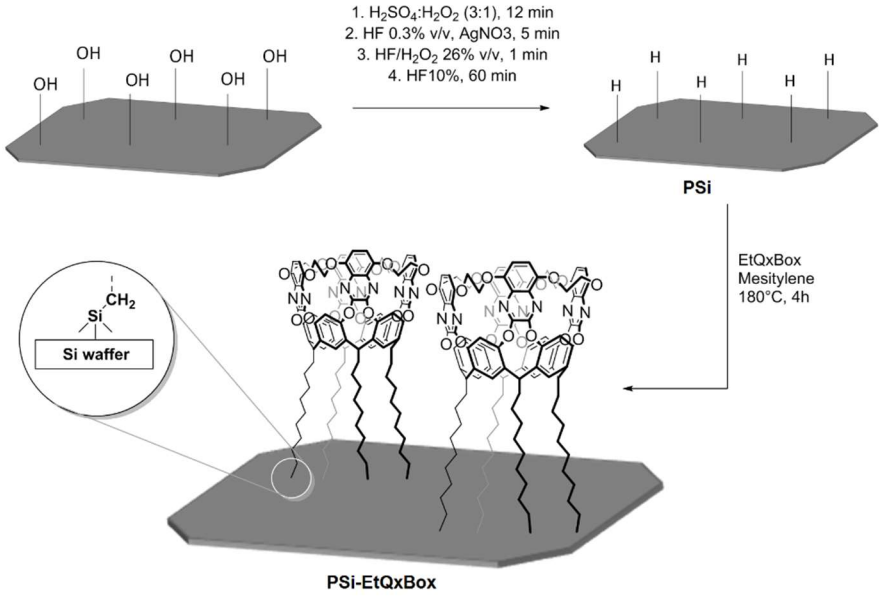

Figure 6.3 *– Functionalization of silicon wafer with* ***EtQxBox 10.***

6.3.2 CHARACTERIZATION OF THE LAYER

FT-IR spectra of **PSi** and **PSi-EtQxBox** wafers are compared in figure 6.4. In particular, three specific regions are reported: from 900 to 1600 cm^{-1}, containing aromatic C-O and CH bending region, from 2000 to 2300 cm^{-1} corresponding to the

Si-H and O-Si-H stretching region, and from 2700 to 3200 cm^{-1}, corresponding to aromatic and aliphatic C-H stretching.

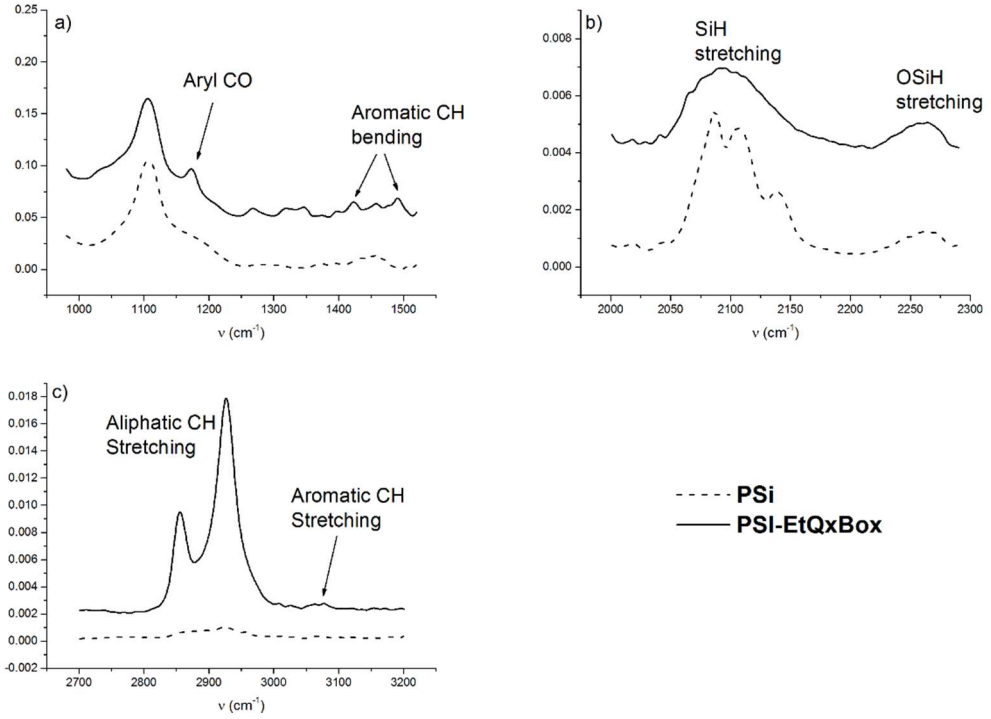

***Figure 6.4** – FT-IR spectra of **PSi** and **PSi-EtQxBox**.*

In the **PSi-EtQxBox** spectra, signals at 2852 and 2928 cm^{-1} are attributed to the aliphatic C-H stretching (respectively symmetric and asymmetric). Another signal corresponding to the aromatic C-H stretching is present at 3077 cm^{-1}. The absence of these signals in the HF-etched **PSi** wafer demonstrates the effective anchoring of the cavitand on the surface. in the HF-etched **PSi** spectrum, distinct signals at 2085, 2107 and 2267 cm^{-1}, are due to respectively to SiH, SiH_2 and SiH_3. In the **PSi-EtQxBox** spectrum, the SiH_x signal is broadened and centered at 2094 cm^{-1}, confirming that SiH_x bonds were partially replaced by Si-C bonds by hydrosilylation reaction. In the **PSi-EtQxBox** spectrum, bands at 1172 and 1272 cm^{-1}, are attributed to the aromatic C-O bond of the ethylenoxy bridges. Finally, signals at 1347 and

1493 cm^{-1} are characteristic of aromatic CH-bending due to the presence of the receptor on the surface.

6.3.3 SOLID-GAS INTERFACE COMPLEXATION STUDIES

Solid-gas complexation tests were performed, exposing **PSi-EtQxBox** to vapors of nitrobenzene. Nitrobenzene is an aromatic compound expected to be complexed by **EtQxBox**, and presents IR absorption bands at 1345 and 1523 cm^{-1}, which enables to monitor the complexation at the solid-gas interface by FT-IR.

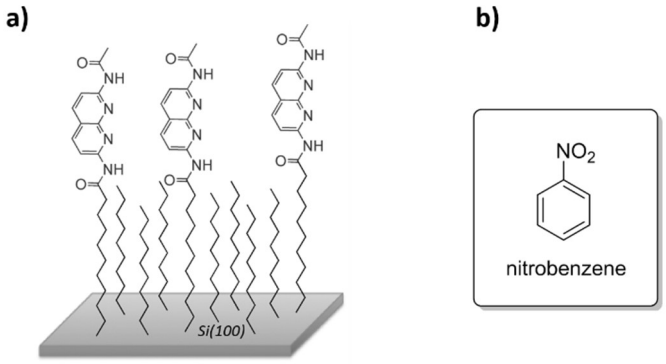

Figure 6.5 *– a) Porous silicon decorated with NaPy (**PSi-NaPy**) and b) molecular structure of nitrobenzene.*

PSi-EtQxBox was exposed to nitrobenzene vapors for 30 minutes at room temperature, under a sealed bell. FT-IR spectrum of **PSi-EtQxBox** was immediately recorded. After the desorption, performed by flowing nitrogen at 150°C for 30 minutes, the FT-IR spectrum of the desorption was recorded. In order to evaluate non-specific interactions, the same treatments were applied to **PSi-NaPy** (figure 6.5a). This organic-coated wafer was chosen for control experiment because of its availability in the lab.

Figure 6 reports the adsorption and desorption FT-IR spectrum **PSi-EtQxBox**. In the adsorption spectrum, the bands at 1345 and 1523 cm^{-1} indicate the presence of the nitro group, respectively for asymmetric and symmetric N-O stretching, diagnostic of the presence of the nitrobenzene on the surface. Considering the very low

contribution of non-specific interactions (figure 6.6, **PSi-NaPy after adorption**), the presence of the bands at 1345 and 1523 cm^{-1} in the adsorption spectrum confirms the complexation of the nitrobenzene by the cavitand. In the desorption spectra, N-O stretching bands disappeared, demonstrating the effective desorption of nitrobenzene upon exposure of the wafer to air. These preliminary results monitored by FT-IR confirm the complexation properties of **EtQxBox** at the solid gas interface.

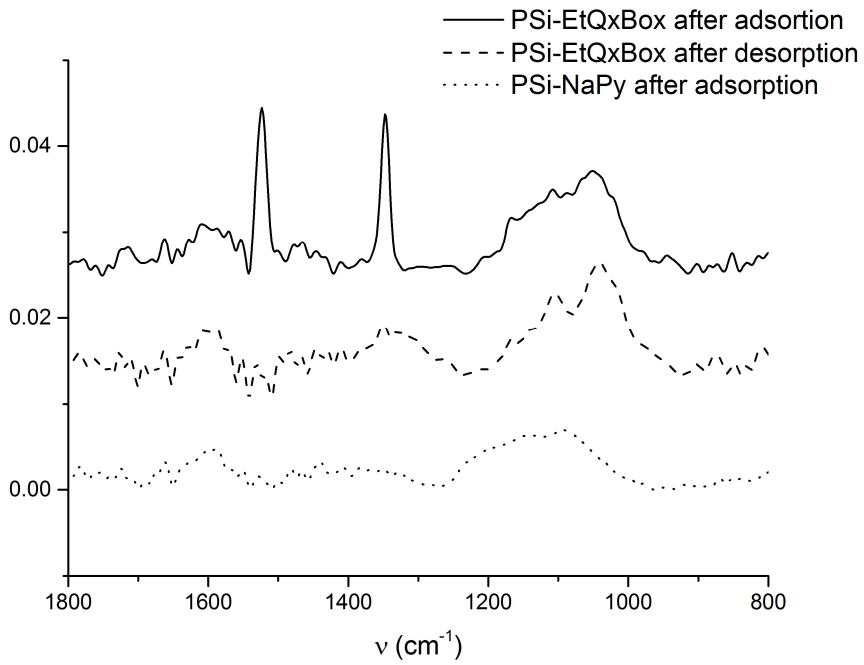

***Figure 6.6** – Overlaid FT-IR spectra of **PSi-EtQxBox** (after adsorption and desorption) and **PSi-NaPy** (after adsorption).*

6.4 CONCLUSION

The synthesis of a new **EtQxBox**, functionalized with four double bonds at the lower rim, was achieved. In particular, a new procedure for the deprotection of the methoxy groups in the octamethoxy cavitand was developed for the preservation of the double bonds at the lower rim. The first step consists in the oxidative elimination of the methoxy groups, leading to the tetraquinone cavitand. The second step consists in

reducing the tetraquinone cavitand with Zinc and acetic acid, affording the octahydroxy cavitand bearing eight free OH, available for further bridging. These mild condition reactions can be applied to other octamethoxy-Qx cavitands bearing at the lower rim sensitive functional groups. Porous silicon (**PSi**) was successfully functionalized with this **EtQxBox**. The characterization, performed by FT-IR, confirmed the effective functionalization of the surface. Adsorption tests at the solid-gas interface were performed with nitrobenzene vapors. Adsorption/desorption experiments, monitored by FT-IR, demonstrated the reversible complexation of nitrobenzene by **EtQxBox** at the solid-gas interface.

6.5 ACKNOWLEDGMENTS

Special thanks to Dr. Jakub W. Trzcinsky for his contribution in this project, and Prof. G. G. Condorelli and his group for the functionalization of Si wafer and solid-gas complexation studies.

6.6 EXPERIMENTAL SECTION

2,3-dinitro-1,4-dimetoxybenzene (2)

Dimethoxyhydroquinone (5.0 g, 0.036 mmol) was slowly added to 100 mL of nitric acid 65 % at 0°C. The mixture was stirred at 0°C for 1 h, then at room temperature for 1h and finally heated at 100°C for 1h. After cooling at room temperature, the crude was poured into iced water. The yellow precipitate was filtrated and washed with water. The crude was purified by column chromatography (SiO_2, Hexane/EtOAC 8:2 to 6:4). The product is obtained as a bright yellow solid in 56% yield.

^{1}H NMR ($CDCl_3$, 300 MHz)**:** 7.15 (s, 2H, H_{Ar}), 3.95 (s, 6H, -OCH_3).

^{13}C NMR ($CDCl_3$, 300 MHz): 29.70 (-OCH_3), 57.38 (-CH), 116,56 (-CNO_2), 145.18 (-COC).

ESI-MS: *m/z*= 251.1 $[M + Na]^+$

2,3-diamino-1,4-dimetoxybenzene (3)

Compound 2 was dissolved in 200 mL of EtOAc in a PARR apparatus, and Pd/C was added in catalytic quantity. The reaction is driven under hydrogen atmosphere for 48 hours, then filtered over celite under nitrogen atmosphere, and finally evaporated. The reddish oil was immediately used in the next step**.**

^{1}H NMR (*d_6*-DMSO, 400 MHz): 6,16 (s, 2H, H_{ar}), 4,13 (s, 4H, -NH_2), 3,70 (s, 6H, -CH_3).

^{13}C NMR (*d_6*-Acetone, 300 MHz): 142,69 (-CO), 124,37 (-C_{NH_2}), 99,65 (-CH), 55,11 (-CH_3).

5,8-dimetossi-2,3-dihydroxyquinoxaline (4)

6.17 g (0.0367 mol) of compound 3 were dissolved in HCl 4N, then oxalic acid (4.29 g, 0.0478 mol) was added. The mixture is stirred at 100°C for 24 hours. After cooling down at 0°C, the crude is filtered, carefully washed with water and dried under vacuum. The product is obtained as off white powder in 81% yield.

^{1}H NMR (d_6-DMSO, 300 MHz): 11.20 (s, 2H, -NH), 6.69 (s, 2H, H_{ar}), 3.79 (s, 6H, -CH_3).

^{13}C NMR (d_6-DMSO, 300 MHz): 155.18 (-COH), 140.7 (-CO), 116.03 (-CN), 105.13 (-CH), 56.64 (-CH_3).

GC-MS: *m/z* = 222 $[M]^+$

2,3-dichloro-5,8-dimetoxy-quinoxaline (5)

Compound **4** (6.60 g, 0.0297 mol) is dissolved in 100 mL of anhydrous 1,2-dichoroethane. $POCl_3$ (55.3 mL, 0.594 mol) is added dropwise to the solution, and 10 drops of anhydrous DMF were added. The mixture was stirred at 80°C for 10 hours. The solvent was removed under vacuum, and the crude was dissolved in dichloromethane. The organic phase was washed with water until the aqueous phase

is colorless. The organic phase is dried over sodium sulfate, then evaporated. After purification by column chromatography (SiO_2, dichloromethane 100%), the pure compound is obtained in 80% yield as a bright yellow solid.

^{1}H NMR ($CDCl_3$, 300 MHz): 7.01 (s, 2H, H_{ar}), 3.99 (s, 6H, -OCH_3)

^{13}C NMR ($CDCl_3$, 300 MHz): 147.64 (-CCl), 144.66 (-$COCH_3$), 132.68 (-CN), 109.28 (-CH_{ar}), 56.26 (-OCH_3)

GC-MS: m/z = 259 $[M]^+$, 243 $[M\text{-}OCH_3]^+$

Resorcinarene Res[$C_{10}H_{19}$, H] (6)

6.32 g (0.0574 mol) of resorcinol were dissolved in 20 mL di MeOH. Undecylenic aldehyde (11.5 ml, 0.0574 dissolved in 20 mL of MeOH is slowly added at 0°C. Then HCl 12N (9.6 mL in 20 mL of MeOH) was added dropwise. After warming up to room temperature, the mixture was stirred for 5 days at 60°C. The reaction was quenched by pouring the crude into ice. The resulting orange precipitate was filtered. The compound was recrystallized three times from acetonitrile, affording the resorcinarene in 9% yield.

^{1}H NMR (d_6-Acetone, 300 MHz): 8.53 (s, 8H, -OH), 7.56 (s, 4H, H_{up}), 6.25 (s, 4H, H_{down}), 5.83 (q, 4H, -CH), 4.96 (m, 8H, -CHCH_2), 4.32 (t, 4H, -CH_{ar}), 2.31 (m, 8H, -CH_{ar}CH_2-), 1.33 (s, 56H, -CH_2).

ESI-MS: m/z= 1042.52 $[M+H]^+$, 1064.49 $[M+Na]^+$, 1080.47 $[M+K]^+$

Octamethoxy quinoxaline cavitand (7)

In a 100 mL flask, 1 g (9.601 10^{-4} mol) of resorcinarene **6** is dissolved in 50 mL of dry DMF, and then K_2CO_3 (2.12 g, 0.154 mol) and quinoxaline **5** (0.995 g, 3.84 10^{-3} mol) were added. The reaction was conducted in a microwave reactor, in *open-vessel* modality, at 120°C for 1.5h. The crude is diluted in a large excess of ethyl acetate or dichloromethane, and washed with water. The organic phase is dried over sodium sulfate and evaporated. The compound is purified by flash column

chromatography (SiO_2, CH_2Cl_2/Acetone 95:5 to 90:10), affording a yellow solid, and active in fluorescence, in 69 % yield.

^{1}H NMR ($CDCl_3$, 300 MHz): 7.43 (s, 4H, H_{up}), 6.93 (s, 8H, $H_{Ar,Quin}$), 6.84 (s, 4H, H_{down}), 5.79 (m, 4H, -CH=), 4.96 (m, 8H, -CH=C*H*$_2$), 4,02 (s, 24H, -OCH_3), 3.95 (t, 4H, ArC*H*-R), 2.30 (m, 8H, -ArCH-C*H*$_2$), 1.33 (s, 56H, -CH_2).

MALDI: *m/z* = 1787.89 $[M+H]^+$

Tetraquinone quinoxaline cavitand (8)

Compound **7** (1.0216 g, 5.719 10^{-4} mol) is dissolved in 100 mL of THF, and Cerium Ammonium Nitrate (3.76 g, 6.86 10^{-3} mol, previously diluted in the minimum amount of water) is added. The mixture is stirred at room temperature for thirty minutes, and then quenched by the addition of water. After extraction from ethyl acetate, the compound is purified by flash column chromatography (SiO_2, CH_2Cl_2/Acetone 85:15), affording an orange solid in 80% yield. Due to its poor stability, the compound was immediately used for the next reaction.

^{1}H NMR ($CDCl_3$, 300 MHz): 7.38 (s, 4H, H_{up}), 7.18 (s, 8H, $H_{Ar,Quin}$), 6.80 (s, 4H, H_{down}), 5.80 (m, 4H, -CH=), 4,97 (m, 8H, -CH=C*H*$_2$), 3,63 (t, 4H, ArC*H*-R), 2.30 (m, 8H, ArCH-C*H*$_2$), 1,33 (s, 56H, -CH_2).

Octamethoxy quinoxaline cavitand (9)

Tetraquinone cavitand **8** (0.2052 g, 1.23 10^{-4} mol) is dissolved in 6 mL of acetone. Zinc (0.92 g, 0.014 mol) and 0.5 mL of acetic acid are added in this order. The suspension is sonicated for 5 minutes. The crude is filtered over celite, dissolved in EtOAc and washed with water, until complete removal of acetic acid. After evaporation, the pure compound is obtained as a bright yellow solid in 90% yield.

^{1}H NMR (d_6-DMSO, 400 MHz): 8.32 (s, 8H, -OHar), 8,10 (s, 4H, H_{up}), 7.90 (s, 4H, H_{down}), 6.94 (s, 8H, $H_{Ar,Quin}$), 5.83 (m, 4H, -CH=), 4.95 (m, 8H, -CH=CH_2), 4.08 (t, 4H, ArCH-R), 2,30 (m, 8H, -ArCH-CH_2), 1,22 (s, 56H, -CH_2-).
MALDI-MS: m/z =1673.71 $[M+H]^+$

EtQxBox[$C_{10}H_{19}$] (10)

In a microwave vessel, cavitand 9 (80 mg, $4.78 \cdot 10^{-5}$ mol) is dissolved in 5 mL di dry DMF. Cs_2CO_3 (202 mg, $5.73 \cdot 10^{-4}$ mol). Diethylene glycol ditosylate (106 mg, 2,86·10-4 mol) is added under nitrogen. The mixture is reacted in a microwave reactor at 120°C for 1.5 hour. The crude was extracted with CH_2Cl_2/H_2O, dried over sodium sulfate and evaporated. The compound is purified by preparative TLC (SiO_2, Acetone 100%), affording the desired compound as a bright yellow solid, in 50% yield.
^{1}H NMR ($CDCl_3$, 400 MHz): 8.31 (s, 4H, H_{up}), 7.55 (s, 4H, H_{down}), 6.74 (s, 8H, $H_{Ar,Quin}$), 5.88 (t, 4H, -CH=), 5.81 (t, 8H, ArC*H*-R), 5,04 (m, 4H, -CH=CH_2), 4.64 – 4.50 (m, 8H, ArOCH_2CH_2O), 2,11 (m, 8H, -ArCH-CH_2), 1.32 (s, 56H, -CH_2-).
MALDI-MS: *m/z* = 1777.8230 $[M + H]^+$, 1799.8094 $[M+Na]^+$

6.7 REFERENCES

[1] S. Zampolli, P. Betti, I. Elmi, E. Dalcanale, *Chem. Commun*., **2007**, 2790-2792.

[2] J. W. Trzcinski, F. Bianchi, R. Pinalli, C. Massera, E. Dalcanale, EP 2,924,041.

[3] A. B. Descalzo, R. Martínez-Máñez, F. Sancenón, K. Hoffmann and K. Rurack, *Angew. Chem. Int. Ed.,* 2006, **45**, 5924–5948.

[4] M. Tonezzer, M. Melegari, G. Maggioni, R. Milan, G. DellaMea, E. Dalcanale, *Chem. Mater.,* **2008**, *20*, 6535–6542.

[5] a) E. Biavardi, M. Favazza, A. Motta, I. L. Fragalà, C. Massera, L. Prodi, M. Montalti, M. Melegari, G. G. Condorelli, E. Dalcanale, *J. Am. Chem. Soc.,* **2009**, *131*, 7447–7455. b) E.

Biavardi, C. Tudisco, F. Maffei, A. Motta, C. Massera, G. G. Condorelli, E. Dalcanale, *Proc. Natl. Acad. Sci.,* **2012**, *109*, 2263–2268.

[6] V. A. Azov, P. J. Skinner, Y. Yamakoshi, P. Seiler, V. Gramlich, F. Diederich, *Helv. Chim. Acta*, **2003**, *86*, 3648–3670.

[7] B. Venugopalan, C.P. Bapat, P. J. Karnik, N. J. De Souza, *Indian J. Chem*., **1990**, *29B*, 364-365.

[8] G. P. Marchand, G. Madhusudhan Reddy, *Synthesis,* **1991**, 198-200.

[9] C. Tudisco, P. Betti, A. Motta, R. Pinalli, L. Bombaci, E. Dalcanale, G. G. Condorelli, *Langmuir* **2012**, *28*, 1782–1789.

Appendix A

MATERIALS AND METHODS

Materials. All reagents and chemicals were obtained from commercial sources and used without further purification. Dry pyridine (supplied from Aldrich) was distilled over KOH and stored over 3 Å or 4 Å molecular sieves under Ar or N_2. Anhydrous toluene (supplied from Aldrich) was distilled over CaH_2 and stored over 4 Å molecular sieves under Ar or N_2. Dry DMF (DMF purissim. ≥ 99.5%(GC)) was provided by Aldrich and stored over 4 Å molecular sieves under Ar. Dry diethyl ether (diethyl ether purum ≥ 99.8%(GC), over molecular sieves) was purchased from Fluka and used as received. Silica column chromatography was performed using silica gel 60 (Fluka 230-400 mesh ASTM), or silica gel 60 (MERCK 70-230 mesh).

NMR Measurements: ^{1}H NMR spectra were obtained using a Bruker AVANCE 300 (300 MHz) or a Bruker AVANCE 400 (400 MHz) spectrometer. All chemical shifts (δ) were reported in ppm relative to the proton resonances resulting from incomplete deuteration of the NMR solvents. ^{31}P NMR spectra were obtained using a Bruker AVANCE-400 (161.9 MHz) spectrometer or a Varian INOVA 600 (MHz). All chemical shifts (δ) were recorded in ppm relative to external 85% H_3PO_4 at 0.00 ppm.

MS Measurements: Electrospray ionization ESI-MS experiments were performed on a Waters ZMD spectrometer equipped with an electrospray interface. MALDI was performed on a AB SCIEX MALDI TOF-TOF 4800 Plus (matrix, α–cyano-4-hydroxycinnamic acid).

Appendix B

SUPPLEMENTARY INFORMATION FOR CHAPTER 2

B.1 SYNTHESIS

Tetrathiophosphonate cavitand TSiiii[C_2H_5, H, Ph] (2)

Resorcinarene **1** (R=C_2H_5, 1.50 g, 2.50 mmol), already reported in literature, was dissolved in 50 mL dry pyridine. dichlorophenylphosphine (1.32 mL, 10.20 mmol) was added dropwise under nitrogen atmosphere, and the mixture was stirred at 70°C for 3 hours. After cooling down to 50°C, sulfur (0.51 g, 2.00 mmol) was added, and the mixture was stirred at 50°C for 3 hours. After cooling down to room temperature, the crude was precipitated from water, and then filtered. The product was purified by column chromatography (Hexane/CH_2Cl_2 3:7) affording **2** as white solid (1.85 g, 64%).

^{1}H NMR (400 MHz, $CDCl_3$): δ= 8.17 (m, 8H, P(S)ArH_o), 7.56 (m, 4H, P(S)ArH_p), 7.51 (m, 8H, P(S)ArH_m), 7.30 (s, 4H, ArH_{down}), 6.67 (s, 4H, ArH_{up}), 4.64 (t, 4H, ArCH, J=7.1 Hz), 2.39 (m, 8H, $CH_2$$CH_3$), 1.06 (t, 12H, $CH_2$$CH_3$, J=6.8 Hz);

^{31}P NMR (162 MHz, $CDCl_3$): δ = 77.77 (s, 4P, P=S).

ESI-MS m/z: 1175.3 $[M+Na]^+$

Trithiophosphonate cavitand 3PSiii[C_2H_5, H, Ph] (3)

Cavitand **2** (1.00 g, 0.86 mmol) was dissolved in 30 mL dry DMF 100 mL. Cathecol (0.10 g, 0.91 mmol) and K_2CO_3 (1.20 g, 8.67 mmol) were added and the mixture was stirred at 80°C for 5 hours. The crude was precipitated from HCl 1N then filtered. Purification by column chromatography (SiO_2, 95:5, CH_2Cl_2/EtOAc) affords cavitand **2** as white solid (0.46 g, 52%).

^{1}H NMR (300 MHz, $CDCl_3$): δ= 8.17 (m, 6H, P(S)ArH_o), 7.57-7.53 (m, 9H, P(S)ArH_p+ P(S)ArH_m), 7.32 (s, 2H, ArH_{down}), 7.20 (s, 2H, ArH_{down}), 6.68 (s, 2H, ArH_{up}), 6.49 (s, 2H, ArH_{up}), 4.64 (m, 4H, ArCH), 2.39-2.26 (m, 8H, $CH_2$$CH_3$), 1.07-1.00 (m, 12H, $CH_2$$CH_3$);

^{31}P NMR (162 MHz, $CDCl_3$): δ = 77.42 (s, 1P, P=S), 76.27 (s, 2P, P=S);

ESI-MS m/z: 1015.6 $[M+H]^+$, 1037.3 $[M+Na]^+$, 1054.7 $[M+K]^+$

3PSiiiMe[C_2H_5, H, Ph] (4)

Cavitand 3 (0.20 g, 0.19 mmol) was dissolved in dry DMF (30 mL), then K_2CO_3 (0.16 g, 1.18 mmol) and CH_2BrCl (128 μL, 0.62 mmol) were added under nitrogen. The mixture was stirred at 80°C for 3 hours. The crude was precipitated from water, and then dried under vacuum. The product was obtained pure as a white solid, without any further purification.

^{1}H NMR (300 MHz, $CDCl_3$): δ = 8.17 (m, 6H, P(S)ArHo); 7.60 (m, 3H, P(S)ArHp); 7.54 (m, 6H, P(S)ArHm); 7.26 (s, 4H, ArH_{down}); 6.66 (s, 2H, ArH_{up}); 6.59 (s, 2H, ArH_{up}); 5.75 (d, 1H, $CH_{2(out)}$, J=7.4 Hz); 4.64 (m, 4H, ArCH); 4.51 (d, 1H, $CH_{2(in)}$, J=7.4 Hz); 2.35 (m, 8H, CH_2CH_3); 1.06 (m, 12H, CH_2CH_3);

^{31}P NMR (162 MHz, $CDCl_3$): δ = 7.38 (s, 1P, P=S); 6.50 (s, 2P, P=S);

ESI-MS m/z (%): 1044.3 $[M+NH_4]^+$, 1049.3 $[M+Na]^+$, 1065.3 $[M+K]^+$

2POii1PSiMe[C_2H_5, H, Ph] (cS + cR; 5)

Cavitand **4** (420 mg, 0,408 mmol) was dissolved in 40 mL of $CHCl_3$ (40 ml) then m-CPBA (229 mg, 1,0 mmol) was added. The mixture was stirred at room temperature for one hour. The reaction is quenched by the addition of water. Phases were separated, and the organic phase was washed with water and aqueous solution of $NaHCO_3$ (pH 8). After drying over sodium sulfate, the crude was evaporated and purified by column chromatography (SiO_2, 85:15, CH_2Cl_2/EtOAc v/v), affording **4** (62 mg, 15%) pure as white solids.

(AB)2POii1PSiMe[C_2H_5, H, Ph] (cS + cR)

^{1}H NMR (400 MHz, $CDCl_3$): δ = 8.16 (m, 2H, P(S)ArH_o); 8.00 (m, 4H, P(O)ArH_o); 7.63-7.49 (m, 9H, P(X)ArH_p, P(X)ArH_m, X=O,S); 7.22 (m, 4H, ArH_{down}); 6.96 (s, 1H, ArH_{up}); 6.81 (s, 1H, ArH_{up}); 6.76 (s, 1H, ArH_{up}); 6.65 (s, 1H, ArH_{up}); 5.67 (d,

1H, $CH_{2(out)}$, J=7.4 Hz); 5.16 (d, 1H, $CH_{2(in)}$, J=7.4 Hz); 4.71 (m, 4H, ArCH); 2.35 (m, 8H, CH_2CH_3); 1.07 (m, 12H, CH_2CH_3);

^{31}P NMR (162 MHz, $CDCl_3$): δ = 75.64 (s, 1P, P=S); 8.69 (s, 1P, P=O), 8.60 (s, 1P, P=O);

ESI-MS (m/z): 995.4 $[M+H]^+$, 1017.4 $[M+Na]^+$, 1074.4 $[M+K]^+$.

(AC)2POii1PSiMe[C_2H_5, H, Ph] (5)

Cavitand 5 : **^{1}H NMR (300 MHz, $CDCl_3$)**: δ = 8.17 (m, 2H, $P(S)ArH_{ortho}$); 8.08 (m, 4H, $P(O)ArH_{ortho}$); 7.69-7.50 (m, 9H, $P(X)ArH_{para}$, $P(X)ArH_{meta}$, X=O,S); 7.28 (m, 4H, ArH_{down}); 6.83 (s, 2H, ArH_{up}); 6.81 (s, 2H, ArH_{up}); 5.70 (d, 1H, $CH_{2(out)}$, J=7.4 Hz); 4.92 (d, 1H, $CH_{2(in)}$, J=7.4 Hz); 4.68 (m, 4H, ArCH); 2.37 (m, 8H, CH_2CH_3); 1.07 (m, 12H, CH_2CH_3);

^{31}P NMR (162 MHz, $CDCl_3$): δ = 78.70 (s, 1P, P=S); 8.82 (s, 2P, P=O)

B.2 X-RAY CRYSTALLOGRAPHIC DATA

CRYSTALS OF THE COMPLEX CR@2-(R)-BUTANOL

Empirical formula	$C_{55}H_{49}O_{10}P_3S_1$*$C_4H_{10}O$, H_2O, $C_4H_{10}O$, 0.5 NaBr, $C_{63}H_{69}O_{13}P_3S$
Formula weight	1210.60
T (K)	100(2)
λ (Å)	0.700
Crystal system	Monoclinic
Space group	C 2
Unit cell dimensions (Å, °)	a = 22.736(1), α = 90 b = 21.619(2), β = 121.769(2) c = 14.974(1), γ = 90
V (Å^3)	6257.4(8)
Z	4
ρ_{calc} (g/mm^3)	1.285
F(000)	2540
Reflections collected	33160
Independent reflections	14541 [R(int) = 0.1057]
Resolution limit (Å)	14.41 − 0.64
Completeness to theta = 24.835°	99.5 %
Data / restraints / parameters	14541 / 6 / 726
GooF	1.028
R_1, wR_2 [I > 2 σ (I)]	0.0682, 0.1762
R_1, wR_2 (all data)	0.0997, 0.2024
CCDC number	1432477

Table A.1 *- Crystallographic data and refinement details for crystals of the complex cR@2-(R)-Butanol.*

CRYSTALS OF THE COMPLEX CR/CS@N-METHYL-(±)-LEUCINE

Co-crystallization experiments

Crystals of the host-guest complex were grown through the vapor diffusion method, through the sitting drop technique. Routinely, sample solution was prepared by adding to the **cR/cS** racemate TFE (trifluoroethanol) solution (final concentration 11 mM), a ten-fold excess of **(±)-*N*-Methyl-Leucine hydrochloride** (0.5 mM in TFE) and well solutions (reservoir solutions) were prepared by mixing the precipitating agent, polyethylene glycol (PEG) 300, with TFE in the 5–55% range (v/v). A 4 μL aliquot of the sample solution was deposited on a micro-bridge inserted in a well of the Linbro box and mixed with an equal volume of the reservoir solution. The 8 μL drops were set to equilibrate by vapor diffusion with 1 mL reservoir solutions in sealed wells at 4°. Single rod-like crystals suitable for X-ray analysis by synchrotron radiation were obtained after 1 month.

Empirical formula	$C_{55}H_{49}O_{10}P_3S_1$, $C_7H_{15}N_1O_2$, 2.75 ($C_2H_3F_3O_1$)
Formula weight	1415.23
T (K)	100(2)
λ (Å)	0.700
Crystal system	Monoclinic
Space group	$P\ 2_1/n$
Unit cell dimensions (Å, °)	a = 16.272(1), α = 90
	b = 18.162(1), β = 91.033(3)
	c = 23.712(2), γ = 90
V (Å^3)	7006.5(8)
Z	4
ρ_{calc} (g/mm^3)	1.271
F(000)	2800
Reflections collected	38307
Independent reflections	12525 [R(int) = 0.1057]
Resolution limit (Å)	23.71 − 0.70
Completeness to theta = 24.835°	96.9 %
Data / restraints / parameters	12525 / 54 / 951
GooF	1.025
R_1, wR_2 [I > 2 σ (I)]	0.0790, 0.2068
R_1, wR_2 (all data)	0.0899, 0.2143
CCDC number	1432693

Table A.2 *- Crystallographic data and refinement details for crystals of the complex cR/cS@N-Methyl-(±)-Leucine.*

Appendix C

SUPPLEMENTARY INFORMATION FOR CHAPTER 3

C.1 SYNTHETIC PROCEDURES

Tiiii was synthesized according to literature procedure.[1]

(AB)2MeRes[C_3H_7, CH_3]

Resorcinarene [C_3H_7, CH_3] (1.0 g, 1,40 mmol) was dissolved in dry DMF. K_2CO_3 (773 mg, 5.6 mmol) then CH_2Br_2 (203 µL, 2.90 mmol) was added. The mixture was stirred at 80°C for 3 hours. The crude was poured in 300 mL of HCl 1N. The precipitate was filtered, washed with water, and dried under vacuum. The crude was purified by flash chromatography (SiO_2, Hexane/THF 7:3) and afforded the pure compound as a white solid, in a 33% yield.

^{1}H NMR (400 MHz, $CDCl_3$): 7.13 (s, 2H, H_{down}), 7.09 (s, 1H, H_{down}), 6.93 (s, 1H, H_{down}), 5.77 (d, 2H, H_{in}), 4.80 (t, 2H, $H_{methyne}$), 4.36 (t, 2H, $H_{methyne}$), 4.22 (d, 2H, H_{out}), 2.32-2.06 (m, 8H, CH_2-CH_2), 2.13 (s, 3H, $CH_{3,up}$), 1.97 (s, 9H, $CH_{3,up}$), 1.50-1.21 (m, 8H, CH_2CH_3), 1.10-0.92 (m, 12H, CH_2CH_3).

ABii[C_3H_7, CH_3, Ph]

(AB)2MeRes[C_3H_7, CH_3] (150 mg, 0.203 mmol) was dissolved in dry pyridine, then dichlorophenylphosphine (690 µL, 0.507 mmol) and N-methylpyrrolidine (211 µL, 2.03 mmol) were added. The mixture was stirred at 60°C for 2 hours. After cooling at room temperature, 500 µL of H_2O_2 were added and the mixture was stirred at room temperature for 45 minutes. The crude was poured in water, and the white precipitate was filtered and carefully washed with water. The compound was purified by flash chromatography (SiO_2, CH_2Cl_2/MeOH 95:5), and obtained as white solid in 27% yield.

^{1}H NMR (400 MHz, $CDCl_3$): 8.10 (m, 4H, H_{ortho}), 7.66 (m, 2H, H_{para}), 7.58 (m, 4H, H_{meta}), 7.10 (s, 1H, H_{up}), 7.07 (s, 2H, H_{up}), 7.02 (s, 1H, H_{down}), 5.86 (d, 2H, CH_{in}), 4.85 (t, 2H, $H_{methyne}$), 4.77 (t, 2H, $H_{methyne}$), 4.70 (d, 2H, H_{out}), 2.37-2.15 (m, 12H,

CH_2CH_2 + $CH_{3,up}$), 2.11 (s, 6H, $CH_{3,up}$), 2.07 (s, 3H, $CH_{3,up}$), 1.42 (m, 8H, CH_2CH_3), 1.05 (m, 12H, CH_2CH_3).

^{31}P NMR (162 MHz, $CDCl_3$): 7.13 (s, 2P, P=O).

MALDI-MS: 981.2789 $[M+H]^+$; 1003.2531 $[M+Na]^+$: 1003.3716, found; 1019.2304 $[M+K]^+$

ACiiRes[C_3H_7, CH_3, Ph]

Tiiii[C_3H_7, CH_3, Ph] (1.0 g, 0.833 mmol) was dissolved in dry DMF. First catechol (229 mg, 0.208 mmol) then K_2CO_3 (689 mg, 4.99 mmol) were added. The mixture was stirred at 120°C for 5 hours. After cooling at room temperature, the crude was precipitated from HCl 1N. The product was purified by column chromatography (SiO_2, CH_2Cl_2/MeOH 93:7), affording the compound as a white solid in 66% yield.

^{1}H NMR (400 MHz, $CDCl_3$): 8.15 (m, 4H, H_{ortho}), 7.66 (m, 2H, H_{para}), 7.59 (m, 4H, H_{meta}), 7.40 (broad singlet, 4H(OH), 7.14 (s, 4H, H_{down}), 4.75 (t, 2H, H_a), 4.42 (t, 2H, H_a), 2.33 (m, 4H, CH_2CH_2), 2.23-2.08 (m, 4H + 12H, CH_2CH_2 + $CH_{3,up}$, 1.47 (m, 4H, CH_2CH_3), 1.29 (m, 4H, CH_2CH_3), 1.09 (m, 6H, CH_2CH_3), 0.93 (m, 6H, CH_2CH_3). ^{31}P NMR (162 MHz, $CDCl_3$): 7.97 (s, 2P, P=O).

ACii[C_3H_7, CH_3, Ph]

ACii[C_3H_7, CH_3] (631 mg, 0.70 mmol) was dissolved in dry DMF, then K_2CO_3 (580 mg, 4.2 mmol) and CH_2Br_2 (182 µL, 2.80 mmol) were added. The mixture was stirred at 80°C for 3 hours. After cooling at room temperature, the crude was poured in distilled water. The precipitate was filtered and carefully washed with water. Purification by flash chromatography (SiO_2, CH_2Cl_2/MeOH 93:7), afforded the pure compound as a white solid in quantitative yield.

^{1}H NMR (400 MHz, $CDCl_3$) 8.15 (m, 4H, H_{ortho}), 7.68 (m, 2H, H_{para}), 7.59 (m, 4H, H_{meta}), 7.09 (s, 4H, H_{down}), 5.84 (s, 2H, CH_{in}), 4.88 (t, 2H, Ha), 4.77 (t, 2H, $H_{methyne}$),

4.70 (s, 2H, CH_{out}), 2.27 (m, 8H, CH_2CH_2), 2.19 (s, 12H, $CH_{3,up}$), 1.44 (m, 8H, CH_2CH_2), 1.07 (m, 12H, CH_2CH_3).

^{31}P NMR (400 MHz, $CDCl_3$) 7.34 (s, 2P, P=O).

Maldi-MS: m/z = 981.2940 $[M+H]^+$; 1003.2685 $[M+Na]^+$; 1019.2260 $[M+K]^+$.

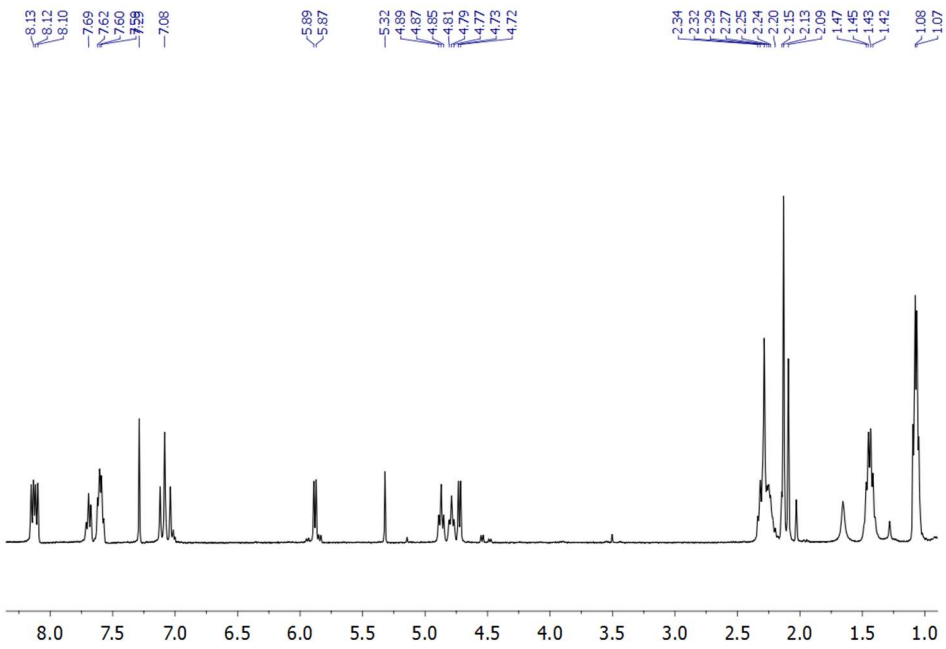

Figure C.1 - *^{1}H NMR spectrum of ABii[C_3H_7, CH_3, Ph] ($CDCl_3$, 400 MHz, 298K).*

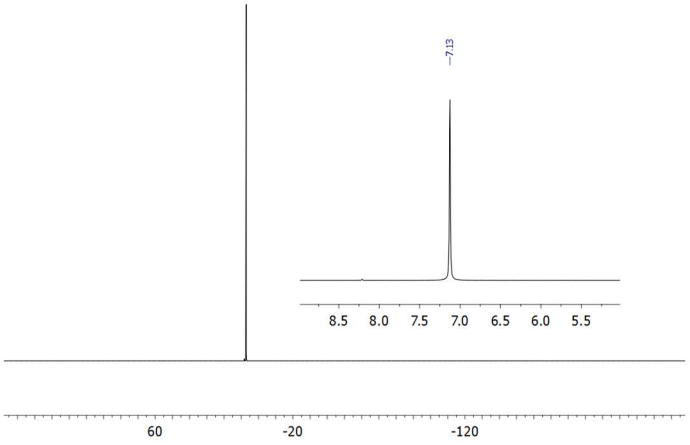

Figure C.2 - *^{31P} NMR spectrum of **ABii[C_3H_7, CH_3, Ph]** ($CDCl_3$, 162 MHz, 298K).*

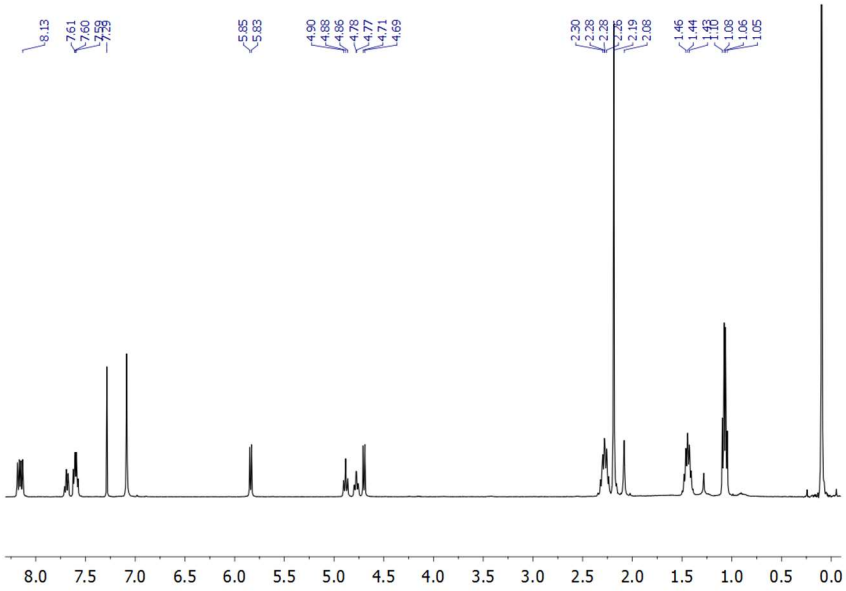

Figure C.3 - *. ^{1}H NMR spectrum of **ACii[C_3H_7, CH_3, Ph]** ($CDCl_3$, 400 MHz, 298K).*

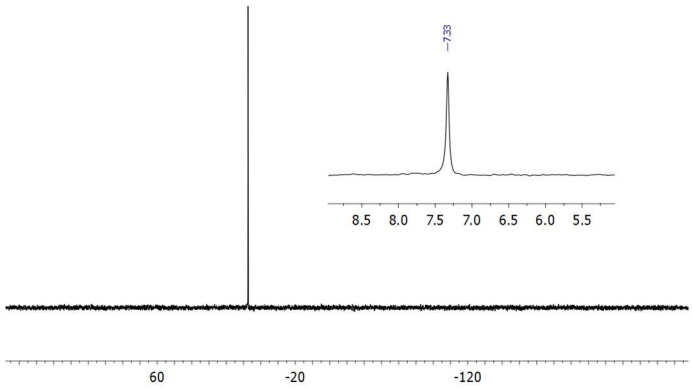

Figure C.4 - *^{31}P NMR spectrum of **ACii[C_3H_7, CH_3, Ph]** ($CDCl_3$, 400 MHz, 298K).*

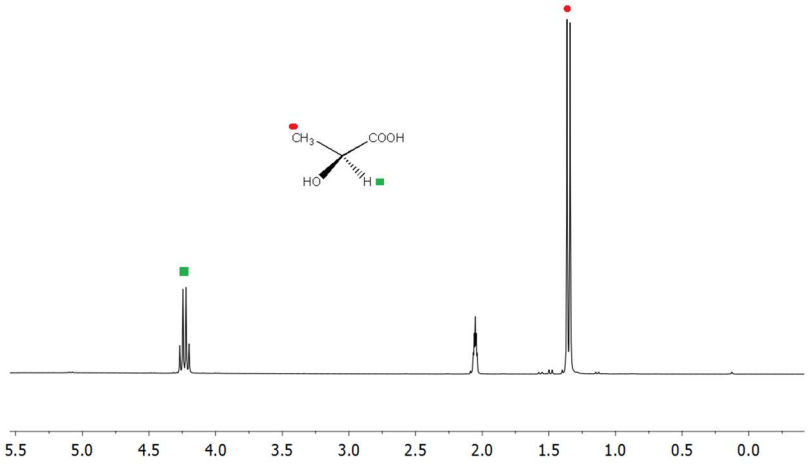

Figure C.5 -. *^{1}H NMR spectrum of commercial L-lactic acid (300 MHz, d_6-acetone, 298K)*

C.2 General method for NMR titrations

Cavitands (10 mg, 10.19 μmol) were dissolved in 500 μL of $CDCl_3$. Being insoluble in chlorinated solvents, L-lactic acid (5 mg, 55.51 μmol) was dissolved in 109 μL of d_6-acetone. The cavitands were titrated at room temperature with the L-Lactic acid solution (5 μL for 0.25 eq). ^{1}H and ^{31}P NMR spectra were recorded at each addition of the guest.

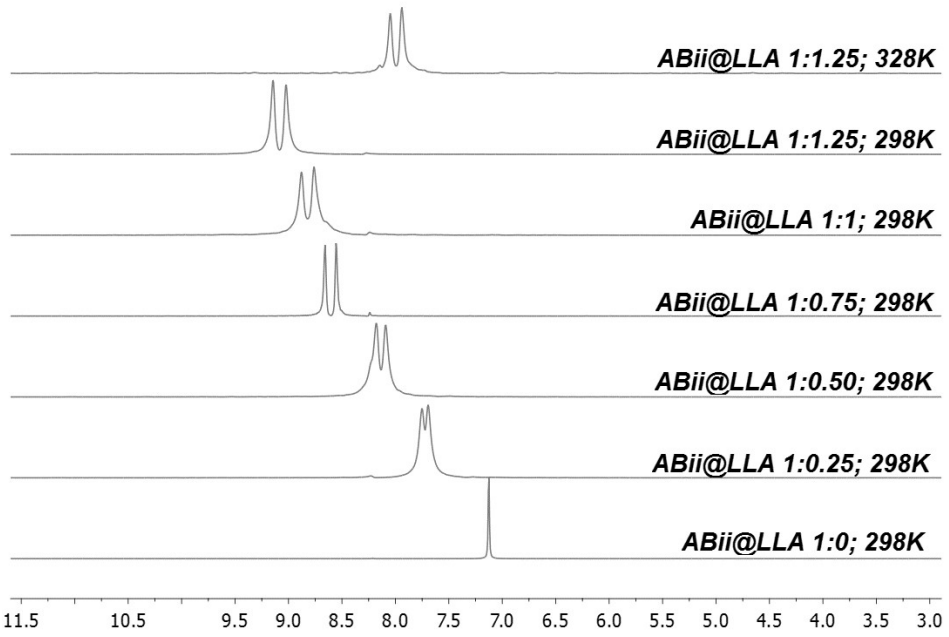

***Figure C.6**.- ^{31}P NMR titration of **ABii[C_3H_7, CH_3, Ph]** ($CDCl_3$, 162 MHz).*

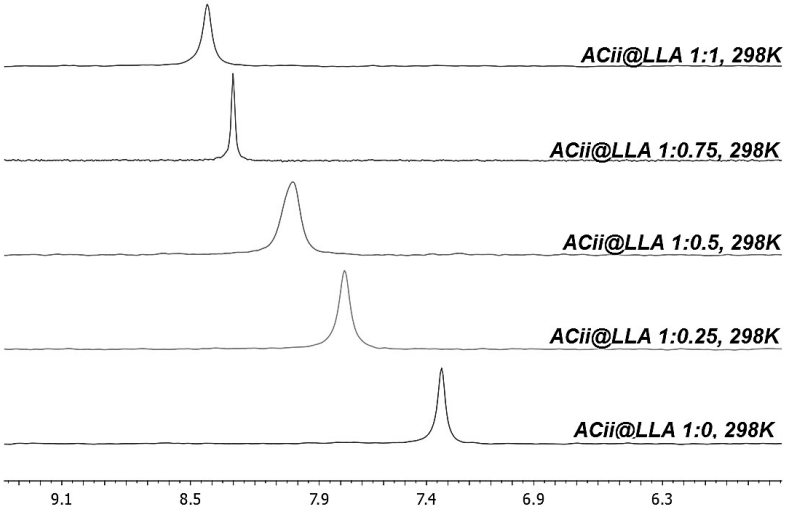

Figure C.7 - *^{31}P NMR titration of **ACii[C_3H_7, CH_3, Ph]** ($CDCl_3$, 162 MHz, 298K).*

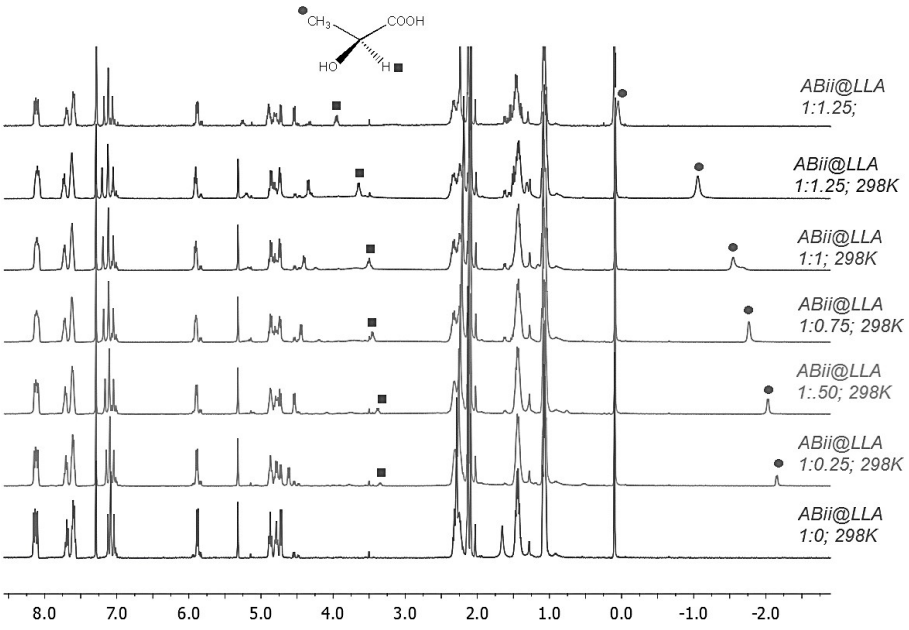

Figure C.8 - *^{1}H NMR titration of **ABii[C_3H_7, CH_3, Ph]** ($CDCl_3$, 400 MHz).*

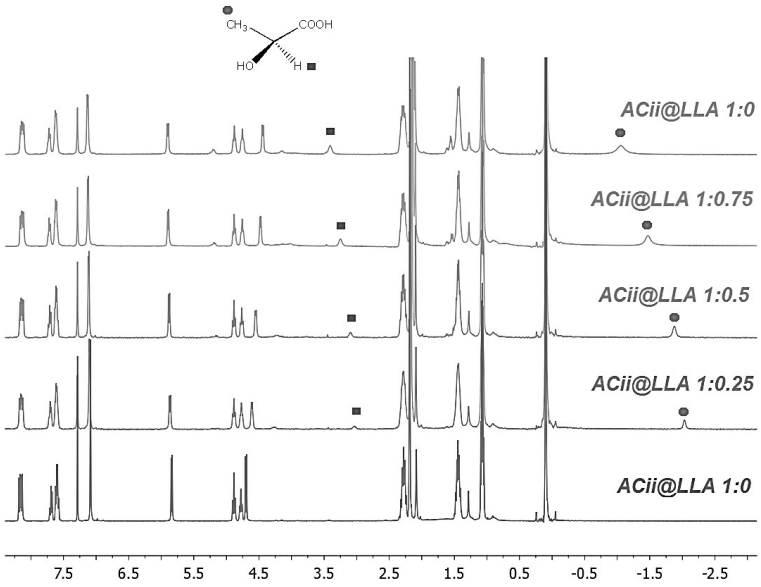

Figure C.9 *- ^{1}H NMR titration of* ***ACii[C_3H_7, CH_3, Ph]*** *($CDCl_3$, 400 MHz, 298K).*

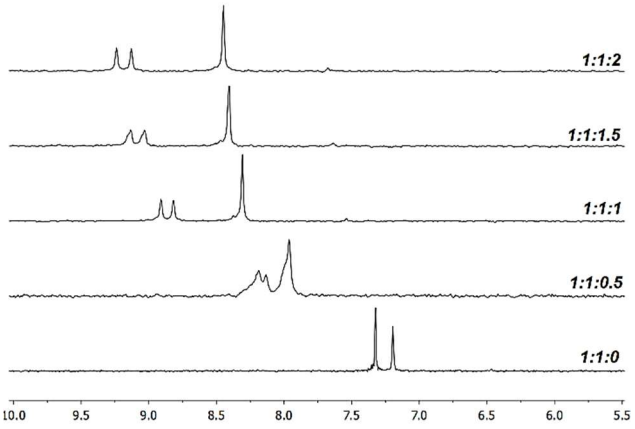

Figure C.10 *- . ^{31}P NMR competitive titration (ABii vs ACii as hosts, L-Lactic acid as guest)*

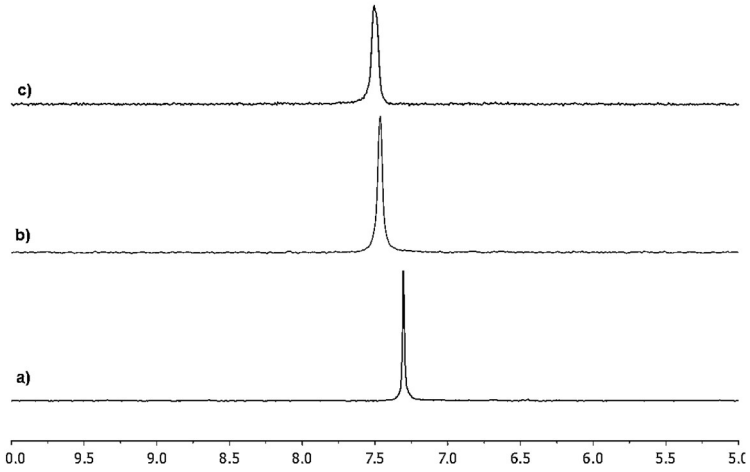

Figure C11 *- . ^{31}P NMR competitive guests titration L-Lactic acid vs EtOH (400 MHz, $CDCl_3$; performed with ACii as host, L-Lactic Acid against EtOH as guests). a) ACii; b) ACii + L-lactic acid (1:0.4). c) ACii + L-lactic acid + EtOH (1:0.4:0.4).*

C.3 X-RAY CRYSTALLOGRAPHY

Crystal data and experimental details for data collection and structure refinement are reported in Table B.1. The crystal structures of compounds **ABii[C_3H_7, CH_3, Ph]@$C_3H_6O_6$•$C_3H_6O_6$•C_6H_{14}** and **ACii[C_3H_7, CH_3, Ph]@$C_3H_6O_6$** were determined by X-ray diffraction methods. Crystals were obtained by slow evaporation of a dichloromethane/hexane solution containing the host and the guest. Intensity data and cell parameters were recorded at 190 K on a Bruker Apex II single crystal diffractometer, employing a MoKα radiation and a CCD area detector. The raw frame data were processed using SAINT and SADABS to yield the reflection data file.[2] The structures were solved by Direct Methods using the SIR97 program[3] and refined on F_o^2 by full-matrix least-squares procedures, using the SHELXL-97 program[4] in the WinGX suite.[5] The PLATON SQUEEZE procedure[6] was used for compound **ABii[C_3H_7, CH_3, Ph]@$C_3H_6O_6$•$C_3H_6O_6$•C_6H_{14}** to treat regions of diffuse solvent which could not be sensibly modeled in terms of atomic sites. Their

contribution to the diffraction pattern was removed and modified F_o^2 written to a new HKL file. The number of electrons (180) per unit cell thus located, are included in the formula, formula weight, calculated density, μ and F(000). This residual electron density was assigned to four molecules of hexane per unit cell. All non-hydrogen atoms were refined with anisotropic atomic displacements with the exception of three carbon atoms in **ABii[C_3H_7, CH_3, Ph]@$C_3H_6O_6$•$C_3H_6O_6$•C_6H_{14}**. The hydrogen atoms were included in the refinement at idealized geometry (C-H 0.95 Å) and refined "riding" on the corresponding parent atoms. The coordinates of some H atoms belonging to hydroxyl groups of the lactic acid were found in the difference Fourier map and then kept fixed through the refinement. The weighting schemes used in the last cycle of refinement were $w = 1/ [\sigma^2 F_o^2 + (0.1870P)^2]$ and $w = 1/ [\sigma^2 F_o^2 + (0.1572P)^2 + 1.3887P]$, where $P = (F_o^2 + 2F_c^2)/3$, **for ABii[C_3H_7, CH_3, Ph]@$C_3H_6O_6$•$C_3H_6O_6$•C_6H_{14}** and **ACii[C_3H_7, CH_3, Ph]@$C_3H_6O_6$** respectively. Molecular geometry calculations were carried out using the PARST97 program.[7] Drawings were obtained using Mercury[8] and UCSF Chimera.[9]

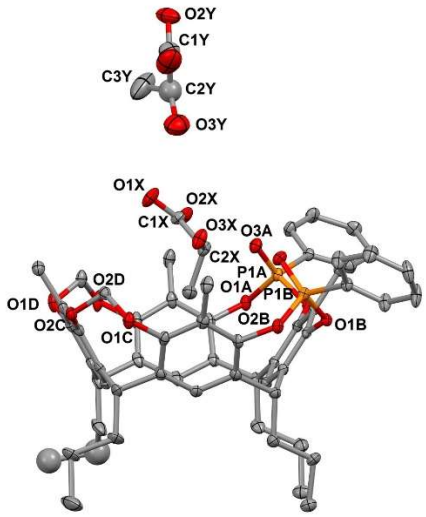

Figure C.12 *- Ortep view (20% probability level) with partial labeling scheme* ***of ABii[C_3H_7, CH_3, Ph]@$C_3H_6O_6$•$C_3H_6O_6$•C_6H_{14}****. Hydrogen atoms have been omitted for clarity.*

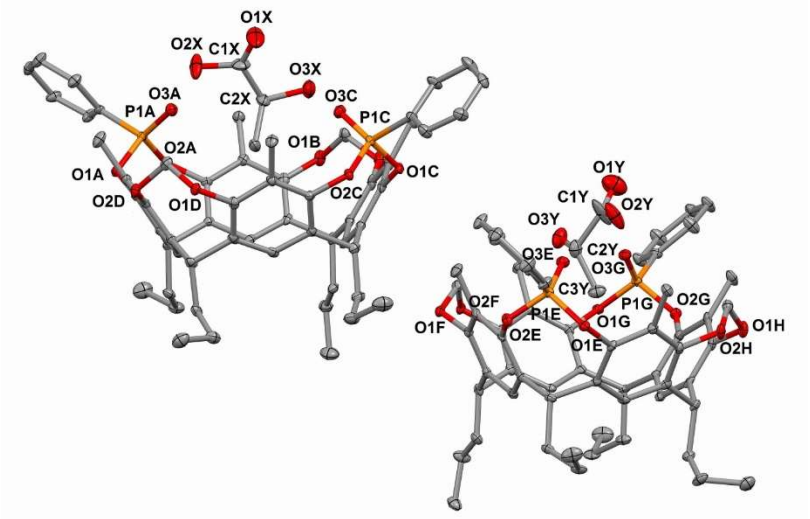

Figure C.13 *- Ortep view (20% probability level) with partial labeling scheme of the two indipendent complexes* ***ACii[C_3H_7, CH_3, Ph]@$C_3H_6O_6$****. Hydrogen atoms have been omitted for clarity.*

ABii		**ACii**[1]	
C-H···π interactions (Å, °)			
3.770(2); 146.71(8)		3.806(4); 132.34(9) 3.793(3); 137.09(9)	
3.782(3); 147.58(9)		3.839(2); 147.31(9) 3.834(3); 143.27(9)	
3.829(2); 149.24(9)		3.934(4); 156.38(9) 3.924(4); 134.34(9)	
H-bonds (Å, °)			
O2X···O3A	2.644(4)	O2X-H2XO···O3A O2Y-H2YO···O3E	2.637(6); 147.68(5) 2.622(4); 145.24(3)
O3X-H3X···O3B	2.757(5); 163.46(9)	O3X···O3C O3Y···O3G	2.819(7) 2.768(6)
O3Y-H3Y···O1X	2.922(8); 147.53(9)	-	-

Table C.1*. Geometrical parameters of the weak interactions involved in the formation of the complexes between LLA and cavitands ABii and ACii. [1]Two sets of values are present, relative to the two independent complexes in the unit cell.*

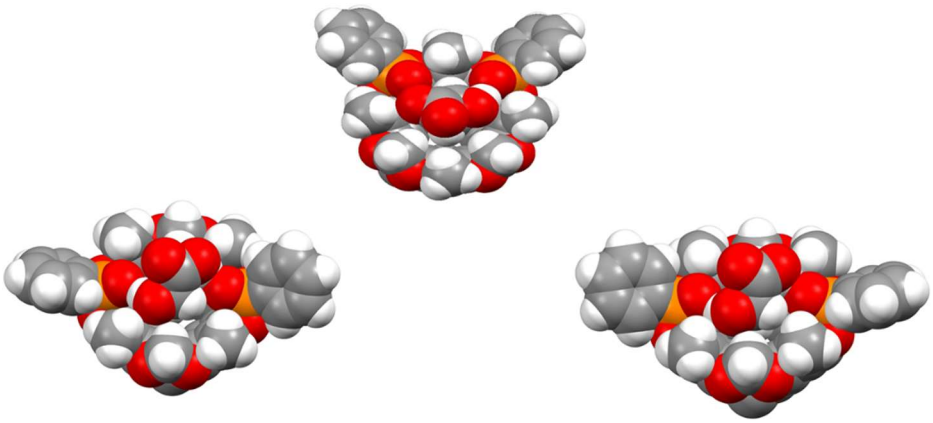

***Figure C.14** - Space and filling view of the two complexes **ABii[C_3H_7, CH_3, Ph]@$C_3H_6O_6$** (above) and **ACii[C_3H_7, CH_3, Ph]@$C_3H_6O_6$** (below, both independent complexes are shown). The alkylic chains at the lower rim have been omitted for clarity. The steric hindrance provided by the frontal methylenic groups is evident for the **ACii** isomer, but it is not present for the **ABii** one.*

Compound	ABii	ACii
Formula	$C_{70}H_{88}O_{16}P_2$	$C_{61}H_{68}O_{13}P_2$
Molecular weight	1247.34	1071.09
Crystal system	Orthorhombic	Orthorhombic
Space group	*P212121*	*P212121*
a / Å	14.600(1)	19.079(1)
b / Å	17.903(1)	21.608(1)
c / Å	23.642(2)	26.346(2)
V / Å^3	6179.6(8)	10861.4(11)
Z	4	8
T / K	190(2)	190(2)
ρ / g cm^{-3}	1.341	1.310
μ / mm^{-1}	0.142	0.146
F(000)	2664	4544
Data / parameters	12686 / 730	25974 / 1386
Total reflections	75468	148915
Unique reflections (R_{int})	12686 (0.0466)	25974 (0.1033)
Observed reflections [$I>2\sigma(I)$]	10176	14544
Goodness–of–fit on F^{2a}	1.034	1.012
R indices [$I>2\sigma(I)$][b] R1, wR2	0.0775, 0.2280	0.0824, 0.2204
Largest diff. peak and hole / eÅ^{-3}	1.070, -0.671	1.081, -0.760

[a]Goodness-of-fit S = $[\Sigma w(F_o^2-F_c^2)^2/ (n-p)]^{1/2}$, where n is the number of reflections and p the number of parameters. [b]R1 = $\Sigma \| F_o | - | F_c \| / \Sigma | F_o |$, wR2 = $[\Sigma[w(F_o^2-F_c^2)^2]/\Sigma[w(F_o^2)^2]]^{1/2}$.

Table C.2 *- Crystal data and structure refinement information for compounds* ***ABii[C$_3$H$_7$, CH$_3$, Ph]****@C$_3$H$_6$O$_6$•C$_3$H$_6$O$_6$•C$_6$H$_{14}$ and* ***ACii[C$_3$H$_7$, CH$_3$, Ph]****@C$_3$H$_6$O$_6$.*

C.4 REFERENCES

[1] E. Biavardi, G. Battistini, M. Montalti, R. M. Yebeutchou, L. Prodi, E. Dalcanale, *Chem. Commun. (Camb).*, **2008**, 1638–40.

[2] SADABS Bruker AXS; Madison, Wisconsin, USA, 2004; SAINT, Software Users Guide, Version 6.0; Bruker Analytical X-ray Systems. In Software Users Guide, Version 6.0; Bruker Analytical X-ray Systems, Madison, WI, 1999. G. M. Sheldrick, SADABS v2.03: Area-Detector Absorption Correction. University of Göttingen, Germany, 1999

[3] A. Altomare, M. C. Burla, M. Camalli, G. L. Cascarano, C. Giacovazzo, A. Guagliardi, A. G. G. Moliterni, G. Polidori and R. Spagna, *J. Appl. Crystallogr.,* **1999**, *32*, 115

[4] G. M. Sheldrick, SHELXL-97. Program for Crystal Structure Refinement. University of Göttingen, Germany, 1997; G. M. Sheldrick, *Acta Cryst*., **2008**, *A64*, 112

[5] L. J. Farrugia*, J. Appl. Crystallogr*., **1999**, *32*, 837

[6] SQUEEZE - P. v.d Sluis and A. L. Spek, *Acta Crystallogr., Sect A,* **1990**, *46*, 194

[7]PARST a) M. Nardelli, *Comput. Chem.,* **1983**, *7*, 95-98; b) M. Nardelli, *J. Appl. Crystallogr.,* **1995**, *28*, 659.

[8] Mercury CSD 3.6 (Build RC6)

[9] UCSF Chimera-A visualization system for exploratory research and analysis. E. F. Pettersen, T. D. Goddard, C. C: Huang, G. S. Couch, D. M. Greenblatt, E. C. Meng, T. E. Ferrin, *J Comput Chem*., **2004**, *25*, 1605

Appendix D

SUPPLEMENTARY INFORMATION FOR CHAPTER 5

D.1 SYNTHESIS

The syntheses of **QxCav**[1] and **QxCav** SPME fiber[2] have been already described.

D.2 CRYSTAL STRUCTURES

The crystal structures of the inclusion compounds **QxCav@1** and **QxCav@2** were determined by single-crystal X-ray diffraction methods. Crystallographic and experimental details are summarized in Table C.1.

Intensity data and cell parameters were recorded on a Bruker Apex II single-crystal diffractometer (employing a MoK_α radiation and a CCD area detector) at 190K for **QxCav@1** and 293 K for **QxCav@2**. The raw frame data were processed using SAINT and SADABS to yield the reflection data files.[3] The structures were solved by Direct Methods using the SIR97 program[4] and refined on F_o^2 by full-matrix least-squares procedures, using the SHELXL-97 program[5] in the WinGX suite.[6]

	QxCav@1	**QxCav@2**
Formula	$C_{91}H_{86}N_8O_{10}\cdot 2(C_3H_6O)$	$C_{94}H_{90}N_8O_{10}\cdot 3/2(C_3H_6O)$
Formula weight	1567.83	1578.86
Crystal system	Monoclinic	Monoclinic
Space group	*P21/a*	*P21/n*
a/Å	21.077(6)	17.5450(10)
b/Å	15.965(4)	19.938(2)
c/Å	26.060(7)	25.726(2)
β/°	109.958(4)	106.3370(10)
V/Å^3	8242(4)	8635.9(12)
Z	4	4
D_c/g cm^{-3}	1.263	1.214
F(000)	3328	3352
μ/mm^{-1}	0.084	0.080
$\theta_{min,max}$/°	1.64, 23.41	1.26, 24.45
Reflections collected	37206	88667
Independent reflections	11879 (*R*int = 0.1305)	14233(*R*int = 0.1005)
Obs. Refl. [$I>2\sigma(I)$]	5654	6233
Data / restr. / param	11879/ 1 / 1019	14233/ 18 / 873
R indeces [$I>2\sigma(I)$][a]	R1 = 0.1019, *w*R2 = 0.2555	R1 = 0.1034, *w*R2 = 0.3174
R indeces (all data)	R1 = 0.1943, *w*R2 = 0.3192	R1 = 0.1881, *w*R2 = 0.3701
$\Delta\rho_{min,max}$/e Å^{-3}	-0.503, 0.784	-0.503, 0.760
S[b]	0.999	0.995

[a] $R_1 = \Sigma \; || Fo|-|Fc||/\Sigma|Fo|$, $wR_2 = [\Sigma \; w(Fo^2-Fc^2)^2/ \; \Sigma wFo^4]^{1/2}$. [b] Goodness-of-fit S = $[\Sigma w(Fo^2-Fc^2)^2/(n-p)]^{1/2}$, where *n* is the number of reflections and *p* the number of parameters.

Table C.1 *- Crystallographic data and refinement details for the inclusion compounds* ***QxCav@1*** *and* ***QxCav@2****.*

The PLATON SQUEEZE procedure[7] was used for compound **QxCav@2** to treat regions of diffuse solvent which could not be sensibly modeled in terms of atomic sites. Their contribution to the diffraction pattern was removed and modified F_o^2 written to a new HKL file. The number of electrons thus located are included in the formula, formula weight, calculated density and F(000) and correspond roughly to six molecules of acetone per unit cell.

All non-hydrogen atoms were refined with anisotropic atomic displacements, with the exception of one acetone molecule in **QxCav@1** and of the guest molecule and some of the terminal carbon atoms of the aliphatic chains in **QxCav@2**. The hydrogen atoms were included in the refinement at idealized geometry (C-H 0.95 Å) and refined "riding" on the corresponding parent atoms.

The weighting schemes used in the last cycle of refinement were $w = 1/ [\sigma^2 F_o^2 + (0.1788P)^2]$ (**QxCav@1**) and $w = 1/ [\sigma^2 F_o^2 + (0.2203P)^2]$ (**QxCav@2**), where $P = (F_o^2 + 2F_c^2)/3$.

Drawings were obtained using the programs Mercury[8] and Chimera[9].

Crystallographic data (excluding structure factors) for the structures reported have been deposited with the Cambridge Crystallographic Data Center as supplementary publication no. CCDC-938684 (**QxCav@1**) and -938685 (**QxCav@2**) and can be obtained free of charge on application to the CCDC, 12 Union Road, Cambridge CB2 1EZ, U.K. [Fax: (internat.) + 44-1223/336-033; E-mail: deposit@ccdc.cam.ac.uk]

D.3 SPME ANALYSIS

The SPME experiments were performed by using a manual device. 0.5 µl of a solution in hexane containing the 3 analytes was added in a 20 mL empty vial and let it evaporate. Benzodioxole, safrole and BMK sampling was then performed by

exposing the **QxCav** fiber to the headspace of the vial for 20 min at room temperature. The fiber was then desorbed in the GC injector for 2 minutes at 250°C.

D.4 GC/MS ANALYSIS

A HP 6890 Series Plus gas chromatograph (Agilent Technologies, Palo Alto, CA) equipped with a MSD 5973 mass spectrometer (Agilent Technologies) was used. Helium was used as the carrier gas at a constant flow rate of 1 ml/min; the gas chromatograph was operated in splitless mode for 1 min with the PTV injector (Agilent Technologies) maintained at the temperature of 250 °C and equipped with a 1.5 mm i.d. (figure 2) multibaffled liner (Agilent Technologies). Chromatographic separation was performed on a 30 m × 0.25 mm, *d*f 0.25 μm SLB-5 ms capillary column (Supelco) using the following temperature program from 50°C to 250 °C at 10°C/min. The transfer line and source were maintained at the temperatures of 280 and 150 °C, respectively. Preliminarily, full scan EI data were acquired to determine appropriate masses for selected-ion monitoring mode under the following conditions: ionization energy, 70 eV; mass range, 40-250 amu; scan time, 3.6 scan/s; electron multiplier voltage, 2024 V. The mass spectrometer was finally operated in time-scheduled SIM mode by recording the current of the following ions: from 0 to 5.5 min *m/z* 43, 57 and 86 for hexane and *m/z* 63, 121 and 122 for benzodioxole; from 5.5 to 7.5 min *m/z* 91, 92 and 134 for BMK and from 7.5 to 20 min *m/z* 104, 131 and 162 for safrole. For all the investigated analytes, the corresponding ion ratios were used for confirmation purposes. A dwell time of 100 ms was used for all the ions. Signal acquisition and data handling were performed using the HP Chemstation (Agilent Technologies).

D.5 METHOD EVALUATION

Detection (yD) and quantitation (yQ) limits were calculated according to EURACHEM guidelines[10] as signals based on the mean blank ($\bar{y}_b$) and the standard deviation of blank responses (s_b):

$y_D = \bar{y}_b + 2t\, s_b$ $\qquad$ $y_Q = \bar{y}_b + 10\, s_b$

where t is the t-Student value (one-tailed distribution) at the confidence level chosen (95%) and degrees of freedom (d_f). $\bar{y}_b$ and s_b were determined by performing six blank measurements. The concentration values corresponding to the LOD and LOQ were obtained from the corresponding signals y_D and y_Q through a proper calibration plot.

D.6 REFERENCES

[1] Soncini, P.; Bonsignore, S.; Dalcanale, E.; Ugozzoli, F. *J. Org. Chem.* **1992**, *57*, 4608-4612.

[2] Bianchi, F.; Mattarozzi, M.; Betti, P.; Bisceglie, F.; Careri, M.; Mangia, A.; Sidisky, L.; Ongarato, S.; Dalcanale, E. *Anal. Chem.* **2008**, *80*, 6423-6430.

[3] SADABS Bruker AXS; Madison, Wisconsin, USA, 2004; SAINT, Software Users Guide, Version 6.0; Bruker Analytical X-ray Systems. In Software Users Guide, Version 6.0; Bruker Analytical X-ray Systems, Madison, WI, 1999. Sheldrick, G. M.; SADABS v2.03: Area-Detector Absorption Correction. University of Göttingen, Germany, 1999.

[4]A. Altomare, M. C. Burla, M. Camalli, G. L. Cascarano, C. Giacovazzo, A. Guagliardi, A. G. G. Moliterni, G. Polidori, R. Spagna, *J. Appl. Crystallogr.,* **1999**, *32*, 115-119.

[5]G. M. Sheldrick, G. M.; *SHELXL97. Program for Crystal Structure Refinement*, University of Göttingen: Göttingen, Germany, **1997**;. G. M.Sheldrick, *Acta Crystallogr*., **2008**, *A64*, 112-122.

[6] WinGX 1.80.05, Farrugia, L. J. *J. Appl. Crystallogr*., **1999**, *32*, 837-838

[7] *SQUEEZE* - v.d Sluis, P.; Spek, A. L. *Acta Crystallogr., Sect A,* **1990**, *46*, 194-201

[8] Mercury CSD 3.1 Development, Bruno, I. J.; Cole, J. C.; Edgington, P. R.; Kessler, M. K.; Macrae, C. F.; McCabe, P.; Pearson, J.; Taylor, R. *Acta Crystallogr.* **2002**, *B58*, 389-397.

[9] UCSF Chimera, version 1.4.1, Pettersen, E. F.; Goddard, T. D.; Huang, C. C.; Couch, G. S.; Greenblatt, D. M.; Meng, E. C.; Ferrin, T. E. *J. Comput. Chem.* **2004**, *25*, 1605-1612.

[10] The Fitness for Purpose of Analytical Methods: A Laboratory Guide to Method Validation and Related Topics, EURACHEM Guide, 1st English Edition 1.0-1998, LGC (Teddington) Ltd., http://www.eurachem.ul.pt/